



Republic of Iraq

Ministry of Higher Education & Scientific Research

University of Kerbala

College of Engineering

Mechanical Engineering Department

**Studying the effects of modified fin geometries on the
performance of triple _square channel thermal storage unit**

A Thesis Submitted to the Council of the College of the Engineering/University of
Kerbala in Partial Fulfillment of the Requirements for the Master Degree in
Mechanical Engineering

By:

Zainab Abdel Karim Salem

Supervisors

Prof. Dr. Mohammed Wahhab Aljibory

Asst. Prof. Dr. Farhan Lafta Rashid

April 2024

Shawwal 1445

بِسْمِ اللَّهِ الرَّحْمَنِ الرَّحِيمِ

تَرْفَعُ دَرَجَاتٍ مِّنْ نَّشَأٍ

وَقَوْقَ

كُلِّ ذِي عِلْمٍ

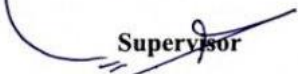
عَلِيمٍ

صدق الله العلي العظيم . يوسف - الآية (76)

Examination committee certification

We certify that we have read the thesis entitled " **Studying the effects of modified fin geometries on the performance of triple _square channel thermal storage unit** " and as an examining committee, we examined the student "**Zainab Abdel Karim Salem**" in its content and in what is connected with it and that, in our opinion, it is adequate as a thesis for the degree of Master of Science in Mechanical Engineering.

Supervisor


Signature: 

Name: Prof. Dr. Mohammed

Wahhab Aljibory

Date: 9/5/2024

Supervisor

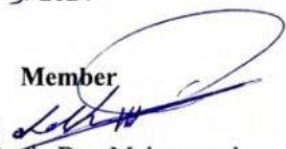
Signature: 

Name: Asst. Prof. Dr. Farhan

Lafta Rashid

Date: 9/5/2024

Member


Signature: 

Name: Prof. Dr. Mohammed

Hussein Ahmed

Date: 9/5/2024

Member

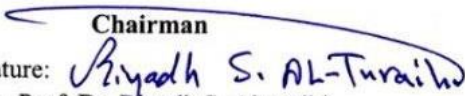
Signature: 

Name: Asst. Prof. Dr. Haider

Nadhom Aziz

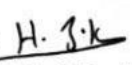
Date: 9/5/2024

Chairman

Signature: 

Name: Prof. Dr. Riyadh S. Alturaihi


Date: / /2024

Signature: 

Name: Asst. Prof. Dr. Hayder Jabar Kurji

Head of the Department of Mechanical
Engineering

Date: 9/5/2024

Signature: 

Name: Asst. Prof. Dr. Haider

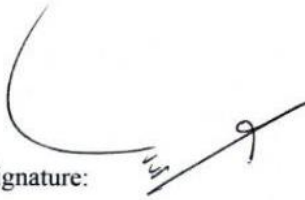
Nadhom Aziz

Dean of the Engineering College

Date: 9/5/2024

Supervisor certificate

We certify that the thesis entitled "**Studying the effects of modified fin on the performance of triple_ square channel thermal storage unit** " was prepared by **Zainab Abdel Karim Salem** under our supervision at the Department of Mechanical Engineering, College of Engineering, University of Kerbala as a partial of fulfilment of the requirements for the Degree of Master of Science in Mechanical Engineering.



Signature:

Prof. Dr. Mohammed Wahhab Aljibory

Date: ~~27~~ 3/ 2024



Signature:

Asst .Prof. Dr. Farhan Lafta Rashid

Date: 27/ 3/ 2024

Linguistic certificate

I certify that the thesis entitled "**Studying the effects of modified fin geometries on the performance of triple _square channel thermal storage unit,**" which has been submitted by **Zainab Abdel Karim Salem,** has been proofread, and its language has been amended to meet the English style.

Signature:



Name: *Asst. Prof. Dr. Samir Ali*

Amin

Title: *Linguistic Reviewer*


University of Alfarahidi

College of Technical Engineering

Date: 27 / 2 / 2024

Undertaking

I certify this research work titled "**Studying the effects of modified fin geometries on the performance of triple _ square channel thermal storage unit**" is my own work. The current work has not been presented elsewhere for assessment. Where material has been used from other sources, it has been properly acknowledged / referred.

Signature: 

Zainab Abdel Karim Salem

Date: 27/3/2024



Dedication

To the Creator of the tablet and the pen, the Creator of the atom and the breeze, and the Creator of everything from nothing

To the one who conveyed the message and fulfilled the trust... and advised the nation. to the Prophet of Mercy and the Light of the Worlds

To the pure Sadat and his most trustworthy bride...the people of the House of Prophethood

To the desire of my heart and the one closest to me from my soul who is hidden from sight and lurking in the eye of insight, to the rest of the greatest the owner of the era and the time (may God Almighty hasten his relief)

I dedicate this success to myself

To my supervising professors, Prof. Dr. Muhammad Wahab and Asst. Prof. Dr. Farhan Lafta, for all the valuable guidance and information they provided me that contributed to enriching my thesis in its various aspects.

To that sweetheart with a pure heart. To the one whom the Most Merciful has recommended to me in righteousness and kindness, to the light of my days and the glow of my life, to the one whose prayers always include my name, the friend of my days... my tender mother.

To the source of my strength and pride. I have always pledged this success to him. Here I am, dedicating it to you... my beloved father

To my support and the smile of my days, to those whom God strengthened my support, so they were the best helper, my sisters (Ghusoon

and Noor), my brothers (Jalal and Muhaimin), and my dear sister's husbands (Thamer Nehme and Haider Muhammad).





Acknowledgments

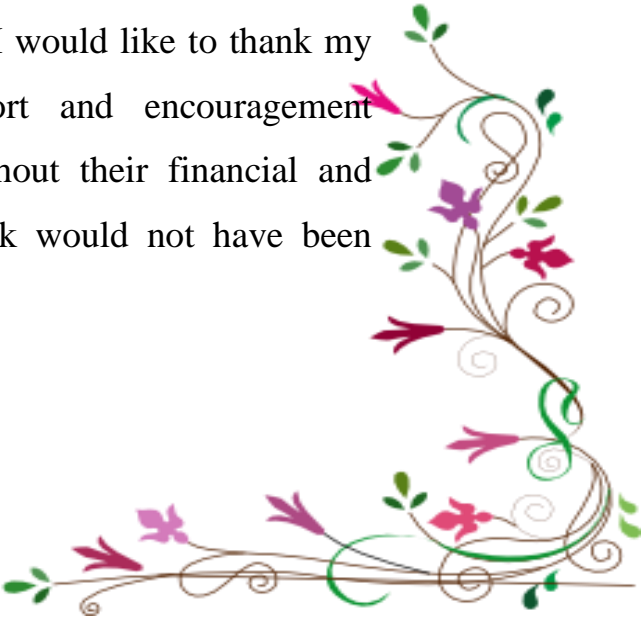
Firstly, I would like to express my sincere thanks and gratitude to God (Glory be to Him) for the guidance through this work and for all the blessings that He has bestowed upon me.

Thanks go to my supervisors, Dr. Mohammad Wahab Aljibory and Dr. Farhan Lafta Rashid, for their advice, encouragement, and supervision.

Thanks also go to the head and crew of mechanical engineering and the staff of Tahrir Preparatory School for Boys for all the assistance they provided.

Special thanks to my mother and my sisters who stood with me in all my steps to complete this research and help me build the system.

Finally, and most importantly, I would like to thank my family for their continuous support and encouragement throughout the study period, as without their financial and personal sacrifices, the research work would not have been possible.



Abstract

In energy storages system, it considered that the latent heat thermal energy to be highly significant than the sensible energy owing to its large storage energy densities in a unit mass at almost fixed thermal energy. The recent work uses internal and external fins to discuss a technique for enhancing heat transfer during the melting of phase change materials (PCM) in a triple-square channel heat exchanger (TSCHE). A 3-D numerical model is evolved employing FLUENT 2021 software. Pure conduction and natural convection are considered in the simulation. In the first case of the work, it was studied numerically by using RT42 paraffin wax, with copper triple-square channel. Finding the fins number, length of fin, mass flow rates, and phase change material (PCM) geometry in TSCHE is to study the influence of time for a comprehensive PCM melting. The study focused on the cases of fins, specifically Case A (without fins), Case B (with 4 fins), Case C (6 fins), and Case D (8 fins), all of which had a length of 42 mm. Also, case E (4 fins), case F (6 fins), and case G (8 fins) have a length of 47.6 mm and, the computational outcomes manifested that the case G (geometry of the PCM 8-cell) performed a shorter time to complete the melting of PCM, with a total melting time reduced to 29.2%. At the second case, the study was conducted numerically and experimentally: Paraffin wax RT64 is used, the system was made of stainless steel 304, the effect of volumetric flow rate, without and with using a fin. To validate the suggested model, experiments were carried out. The results of the simulation match those of the experimental part. The use of fins improved heat transfer during the paraffin wax melting process and thus reduced the melting time when using the same volumetric flow of (4, 8,

and 16) l/min, respectively, the total enhancement of 29.68 %, 36.97%, and 48.7%. After that, the maximum difference was determined to identify the differences between the experimental and numerical results for the flow rates of HTF (4, 8, and 16) l/min which were (4, 8, and 9) %, so the maximum difference was 9% for flow rate 16 l/min.

Table of Contents

Examination committee certification	3
Supervisor certificate.....	4
Linguistic certificate.....	5
Undertaking	vi
Dedication	vii
Acknowledgments	viii
Abstract.....	ix
Table of Contents	xi
List of Tables.....	xiv
List of Figures	xv
List of Abbreviations.....	xix
List of Latin Symbols	xx
Chapter One: INTRODUCTION	1
1.1 Background.....	1
1.2 Latent Thermal Energy Storage Systems	1
1.2.1 Paraffin waxes	4
1.2.2 Measurement Technique of the Melting Temperature and Enthalpy of the Paraffin wax.....	6
1.3 Heat Transfer Enhancement Techniques of PCMS (Solid-Liquid) 7	
1.3.1 Extended surface.....	8
1.4 Thermal Energy Storage Type.....	11
1.5 Application of Triple-Tube Heat Exchangers Powered by PCMS 12	
1.6 Scope and Objective of This Work	14

1.7	Outline of Thesis	14
Chapter Two: LITERATURE REVIEW		15
2.1	Numerical Researches	15
2.2	Experimental Researches.....	25
2.3	Numerical and Experimental Researches.....	31
Chapter Three: NUMERICAL MODELING and SIMULATION		47
3.1	Introduction	47
3.2	Numerical Simulation.....	47
3.2.1	Simulation of numerical model	48
3.3	Design Considerations.....	49
3.3.1	Computational model building	49
3.4	Assumptions	54
3.5	Governing Equations	55
3.5.1	Enthalpy–porosity method.....	56
3.6	Setup and Solution.....	58
3.6.1	Boundary conditions and operating parameters	58
3.7	Mesh independency	63
3.8	Validation	64
3.9	Closure.....	65
Chapter Four: Experimental Work.....		66
4.1	Introduction	66
4.2	Designing and Constructing the Rig	66
4.3	Experimental Setup.....	66
4.4	Rig Building Steps.....	68
4.5	The Mechanism of Working.....	74
4.6	Measurement Instrumentations	74

4.6.1	Temperature measurement	74
4.6.2	Flow rate measurement.....	75
4.7	Calibration	76
4.8	Repeatability	77
Chapter Five: Results and Discussion.....		78
5.1	Numerical Results.....	78
5.1.1	Volumetric flow rate of HTF effect on the melting rate	79
5.1.2	Effect of the fins numbers upon the rate of melting.....	81
5.1.3	Effect of the length of fin upon the fraction of melting	84
5.1.4	Effect of the geometry of PCM unit in TSCTSU.....	85
5.2	Optimization	92
5.2.1	Effect of the volumetric flow rate of HTF and fins geometry on melting rate of PCM.....	93
5.2.2	Effect of the PCM unit geometric in the TSCTSU	98
5.3	Experimental Results.....	102
5.3.1	Effect of Volumetric Flow rate of HTF with and without Fins 102	
5.4	Comparison of Numerical Results with Published Literature Results	105
Chapter Six: Conclusions And Future Work		109
6.1	Conclusions	109
6.2	Recommendations for Future Research	110
References		111

List of Tables

Table 1.1: The thermal properties of Paraffins (Reproduced as it's from Zhang et. al [2]).	5
Table 2.1: Summary of Literatures Review	39
Table 3.1: Geometrical dimensions of the thermal energy storage.	51
Table 3.2: Mesh settings and information.....	53
Table 3.3: Mesh count per each case.	53
Table 3.4: Properties of Steel, Copper and Water. [41].....	59
Table 3.5: Properties of RT42 and RT64HC. [41].....	60
Table 3.6: Differences between different levels of mesh refinement. ..	63
Table 5.1: The properties of paraffin wax and copper. [41]	79
Table 5.2: Number and length of the fins for TSCTSU.....	82
Table 5.3: The cell geometry variation for TSCTSU.....	85
Table 5.4: Percentage of the time of melting for various cases of TSCTSU.....	87
Table 5.5: The properties of paraffin wax and stainless steel 304. [41]	93

List of Figures

Figure 1.1: The schematic diagram of the PCM phase change transition (Re-produced as it is from[1]).	2
Figure 1.2: PCMs' classification.	4
Figure 1.3: Techniques for Improving Heat Transfer in the LHTES System.....	8
Figure 1.4: Rectangular Fin.....	9
Figure 1.5: Triangular Fin.	10
Figure 1.6: Cylindrical Fin.	10
Figure 1.7: Trapezoidal Fin.....	10
Figure 1.8: Parabolic Fin.....	11
Figure 1.9: Application of triple-tube heat exchanger powered by PCM: (a) The energy saving of domestic hot water system, (b) CSP applications, (c) Condensation heat recovery, and (d) Liquid desiccant air conditioning system.	13
Figure 2.1: Different cases considered in their study.....	17
Figure 2.2: Schematic representation of the annular tube heat exchanger (HT: Hot tube, IT: Insulated tube).....	18
Figure 2.3: Schematic representation of the investigated cases.....	19
Figure 2.4: (A) 3D model of the shell and tube TES with embedded fins (B) A two-dimensional illustration of the studied model with boundary conditions. (C) A mesh sample.....	19
Figure 2.5: 3D configuration of LHTESS with fins.....	20
Figure 2.6: Two-dimensional view of LTESS (right) and 3D view (left).	22
Figure 2.7: Different cases in the article.	22

Figure 2.8: Latent heat thermal energy storage (LHTES) unit: (a) ascending conical; (b) cylinder; and(c) descending conical.....	24
Figure 3.1: Models and fin configurations.....	48
Figure 3.2: The 3D geometric model of thermal energy storage.....	52
Figure 3.3: The schematic of the created three-dimensional mesh of thermal energy storage.....	54
Figure 3.4: Boundary conditions.....	59
Figure 3.5: The schematic diagram of the flow chart steps of computational model constructed via employing ANSYS-FLUENT software	62
Figure 3.6: PCM temperature vs. time for different meshes.....	64
Figure 3.7: Verification of the numerical results.....	65
Figure 4.1: (A) The schematic of investigational setup and (B) The physical setup of investigational facility	67
Figure 4.2: Locations of thermocouples.....	68
Figure 4.3: (a) Supplying the required parts, (b & c), the stages of cutting, crimping, and the final shape of the channels, and (d) Fins form.....	70
Figure 4.4: Channels manufacturing steps with installing the fins.....	71
Figure 4.5: Wax casting process.....	72
Figure 4.6: Final form of TSCTSU	72
Figure 4.7: Preparing the water source and connecting it to the pump, heater and TSCTSU	73
Figure 4.8: Cover the device with insulator and operate it.....	73
Figure 4.9: (A) Temperature Recorder. (B) Thermocouple Type (k)Type Lutron BTM-4208SD	75
Figure 4.10: Flow Meter Type LZM.....	76
Figure 4.11: The calibration of water flow meter	77

Figure 5.1: Liquid fraction of PCM RT 42 vs. melting time for (5, 8 and 10) l/min of HTF at 70°C / numerically.	80
Figure 5.2: RT42 PCM temperature vs. melting time for (5, 8 and 10) l/min of HTF at 70°C / numerically.....	81
Figure 5.3: The effect of fins on the liquid fraction of RT42 PCM with melting time (min) / numerical.	83
Figure 5.4: The effect of temperatures of HTF on the RT42 PCM with melting time (min) / numerical.	83
Figure 5.5: Influence of the length of fin upon the time of melting for Cases D and G to RT42 PCM with the time (min)/numerical	85
Figure 5.6: The melting fraction for RT42 PCM with melting rate for all enhancement cases / numerical.....	86
Figure 5.7: The melting fraction of RT42 PCM for case (A without fins) with melting time (numerical).	87
Figure 5.8: The fraction of the RT42 PCM field melting for case (B with 4 fins and length 42 mm) with melting time / numerical.	89
Figure 5.9: The fraction of the RT42 PCM field melting for case (C with 6 fins and L42 mm) with melting time / numerical.....	89
Figure 5.10: The fraction of the RT42PCM field melting for case (D with 8 fins and L42 mm) with melting time / numerical.....	90
Figure 5.11: The fraction of the RT42PCM field melting for case (E with 4 fins and L 47.6 mm) with melting time/ numerical.....	91
Figure 5.12: The fraction of the RT42 PCM field melting for case (F with 6 fins and L 47.6mm) melting time / numerical.....	91
Figure 5.13: The fraction of the PCM field melting for case (G with 8 fins and L 47.6 mm) / numerical.	92

Figure 5.14: Liquid fraction of PCM RT64 vs melting time for (4, 8, 16, and 24) l/min of HTF / numerical.....	94
Figure 5.15: RT64 PCM temperature vs. time for (4, 8, 10 and 24) l/min of HTF / numerical.	95
Figure 5.16: Studied planes.	96
Figure 5.17: Sections of different case studies: (a) without fins, and (b) the 47.6 mm length of fins.	96
Figure 5.18: Melting rate of RT64 PCM for without fins and eight of fins cases with melting time / numerical.	97
Figure 5.19: RT64 PCM average temperature until full melting with time for the with and without fins cases / numerical.	98
Figure 5.20: Liquid fraction for RT64 PCM with different time steps of without fins case at 16 (l/min) at z=0/ numerical.	99
Figure 5.21: The temperature distribution of RT64 PCM with different time steps of without fins case at (16 l/min) at z=0 / numerical.	100
Figure 5.22: The 47.6 mm fins case (8 RT64 PCM geometry sections)- Liquid fraction with different time steps at z=0 / numerical.	101
Figure 5.23: Temperature of RT64 PCM field with different time steps at z = 0 / numerical.	102
Figure 5.24: The rate of HTF volumetric flow without the influence of fins upon the time of RT64 PCM melting/ experimental.....	103
Figure 5.25: The rate of HTF mass flow without the influence of fins upon the time of PCM melting/ experimental.	104
Figure 5.26: Comparison of Numerical results with Al-Abidi et al. [41] results / numerical.....	106
Figure 5.27: Comparison of experimental and numerical results for the present work without and with using fins for flow rate 16 l/ min.	107

List of Abbreviations

Abbreviation	Description
CFD	Computational Fluid Dynamics
CFF	Copper Foam Fin
DSC	Differential Scanning Calorimetry
FST	Full Solidification Process Time
HTF	Heat Transfer Fluid
HXs	Heat Exchangers
LHESS	Latent Heat Energy Storage System
LHTS	Latent Heat Thermal Storage
nanoIPCM	Nanoparticle Improved Phase Change Material
PCM	Phase Change Material
CSP	Concentrating Solar Power
RSM	Response Surface Methodology
SHTES	Sensible Heat Thermal Energy Storage
STESSs	Sensible Thermal Energy Storage Systems
TCES	Thermochemical Energy Storage
TES	Thermal Energy Storage
TSTLHS	Triple Square Tube Latent Heat Storage
THE	Triple Tube Heat Exchangers
LHS	Latent Heat Storage
TSCTES	Triple Square Channels Thermal Energy Storage
L	Length of fin

List of Latin Symbols

Symbol	Description	Units
α	Thermal Diffusivity	m^2/s
P_r	Prandtl Number = $\frac{c_p \mu}{K}$	--
R_e	Reynold Number = $\frac{\rho v l}{\mu}$	--
m	Mass Flow Rate of HTF	kg/s
ϕ	Nanoparticle Volume Fraction	
A	Aspect Ratio	--
e	Eccentric Distance Between the Center of Inner and Outer Tube	--
HCV	Higher Calorific Value	(J/kg)
LCV	Lower Calorific Value	(J/kg)
Ste	Stefan Number	--
T _{in}	Inlet (HTF)Temperatures	°C
ρ	Fluid Density	kg/m^3
f	Melt fraction	--
h	Average heat transfer coefficient	$\text{W} \cdot \text{m}^{-2} \cdot \text{k}^{-1}$
k	Thermal conductivity	$\text{W} \cdot \text{C}^{-1} \cdot \text{k}^{-1}$
L	Latent heat of melting	$\text{kJ} \cdot \text{kg}^{-1}$
T	Temperature	°C
W_o	Width of outer channel	mm

W_m	Width of middle channel	mm
W_i	Width of inner channel	mm
g	Gravitational acceleration	m/s^2
f	Liquid fraction	--
V	Velocity of liquid PCM	m/s

Chapter One: INTRODUCTION

1.1 Background

The energy protection is the highly engaged area of exploration in the present period. Alternate energy sources must be added to the current energy mix to meet the rising demand for energy and diminishing supply of fossil fuels. Thermal energy comes from nature in the solar energy form, which being free, abundant, doesn't pollute, can be used easily, and lasts forever. Latent Heat Thermal Energy Storage (LHTES), Sensible Heat Thermal Energy Storage (SHTES), and Thermochemical Energy Storage (TCES) are the three types of thermal energy storage. Latent thermal energy storage entails changing a material's phase while maintaining a constant system temperature, such as going from a solid to a liquid state or vice versa. In contrast, only the material's temperature increases in Sensible Thermal Energy Storage Systems (STESSs) to store heat. Thermal energy is stored by chemical processes in the Thermo-Chemical Energy Storage (TCES) devices, and it's recovered through the reverse chemical reactions utilization [1].

1.2 Latent Thermal Energy Storage Systems

Latent Thermal Energy Storage Systems (LTESSs) based on Phase Change Materials (PCM) have the capacity to store significant amounts of heat at relatively low operating temperatures, making them an appropriate solution to thermal energy management issues. Figure (1.1) shows that the thermal energy being stowed in the PCMs as a sensible and latent thermal heat during the charging (heating) and discharging (cooling) processes. Due to this,

LTESSs are used in numerous engineering applications, such as solar air collectors, electronics product heating and cooling systems, thermal storage of building structures and refrigeration, drying technology, building equipment, like the cold storage, hot water for national utilization, and waste heat retrieval regimes[1].

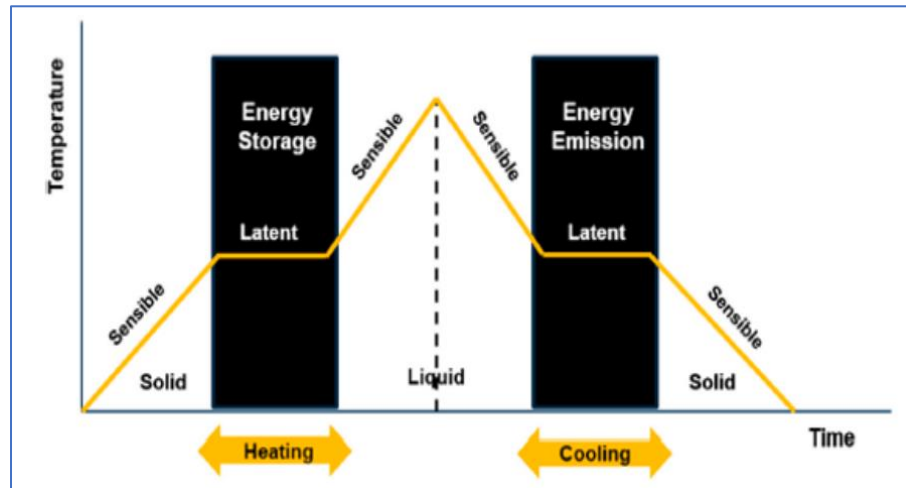


Figure 1.1: The schematic diagram of the PCM phase change transition (Re-produced as it is from[1]).

Typically, Heat Transfer Fluid (HTF) serving as a material for heat exchanging the between a PCM and a heat source, is used for storing the thermal energy. Most frequently, HTF uses a shell and tube heat exchanger to transfer heat to PCMs. However, the majority of PCMs have poor thermal conductivity, which makes move heat inside the PCM difficult. For effectively storing as well as extracting the thermal energy in such regimes, the heat transfer improvement becomes crucial. Regarding thermal energy storage, PCMs have garnered a lot of attention recently[1].

PCMs in LTESS systems use phase transitions, like solid-to-solid liquid to gas, solid to gas to store energy via exerting heat equals to their phase conversion temperature. While the solid-solid phase transition can also result

in thermal energy storage, it has a slow rate and low energy storage density[2]. This is why PCMs with a solid-liquid transition are preferred due to their small volumetric change, ease of handling, and high thermal energy density[1]. However, for PCMs to be used in actual applications, they need to possess specific properties, such as a solid-liquid phase transition, high thermal conductivity, chemical stability, non-flammability, and thermal stability[2]

There are :

1. Thermal characteristics, including a suitable melting point, a high phase transition enthalpy and specific heat capacity, and a high thermal conductivity.
2. Physical characteristics: No phase separation, little volumetric change, and high density.
3. Chemical characteristics: Ultimate chemical stability, absence of corrosion, compatibility with the container, absence of poisonous or combustible elements, and absence of pollution.
4. Kinetic characteristics: Low level of supercooling, a fast enough rate of crystallization, and a phase change that can be reversed.
5. Economical: Plenty of resources, good recycling, affordable prices, and simple accessibility. But as of this writing, no PCM is known that fulfills all of the aforementioned criteria.

Despite the benefits of solid-liquid PCMs, a PCM that meets all the mentioned requirements has not been discovered yet, and there are still some issues that need to be addressed. For example, solid-liquid PCMs are prone to problems, such as liquid leakage, limited thermal conductivity, phase separation, and supercooling [2]. This highlights the need for developing methods to improve the properties of PCMs when combined. PCMs are

classified into three types based on their melting temperatures [1]: Inorganics, organics, and eutectics (mixes), as depicted in figure (1.2).

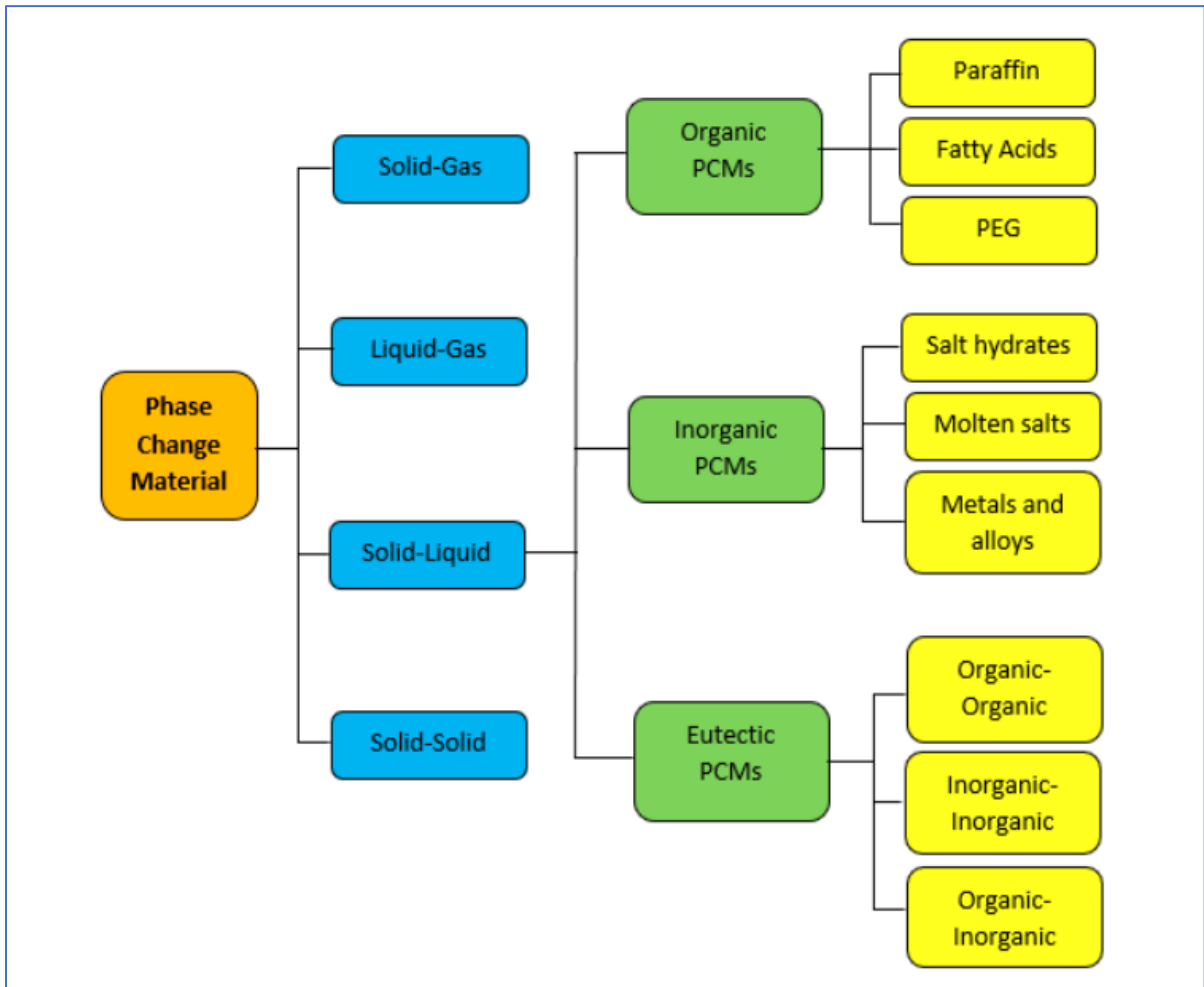


Figure 1.2: PCMs' classification.

1.2.1 Paraffin waxes

They're chemically created n-alkane mixes designated by the symbol $C_n H_{(2n+2)}$. They come from the byproducts of processed crude oil. Paraffin may be employed for low temperature applications since its phase transition temperatures, which are shown in Table (1.1), are typically between (18 and 71)°C [3].

Paraffins have desirable properties, like chemical stability, low vapor pressure, no phase separation, self-nucleation, and high latent heat density; however, their main drawbacks include moderate flammability, liquidity, and low thermal conductivity, making their use challenging [4].

Table 1.1: The thermal properties of Paraffins (Reproduced as it's from Zhang et. al [2]).

Phase change temperature (°C)				Density (kg/l)					
PCMs	Melting	Congeaing	Heat of Fusion (kJ/kg)			Solid	Liquid	Thermal Conductivity (W/ (m.K))	
RT 21	18-23	22-19	155			0.88	0.77	0.2	
RT 22 HC	20-23	23-20	190			0.76	0.7	0.2	
RT 24	21-25	25-21	160			0.88	0.77	0.2	
RT 25	22-26	26-22	170			0.88	0.76	0.2	
RT 26	25-26	26-25	180			0.88	0.75	0.2	
RT 28 HC	27-29	29-27	250			0.88	0.77	0.2	
RT 31	27-33	33-27	165			0.88	0.76	0.2	
RT 35 HC	29-36	36-31	160			0.86	0.77	0.2	
RT 42	38-43	43-37	165			0.88	0.76	0.2	
RT 44 HC	41-44	44-40	250			0.8	0.7	0.2	
RT 47	41-48	48-41	165			0.88	0.77	0.2	
RT 50	45-51	51-46	160			0.88	0.76	0.2	
RT 54 HC	53-54	54-53	200			0.85	0.8	0.2	
RT 55	51-57	56-57	170			0.88	0.77	0.2	
RT 60	55-61	61-65	160			0.88	0.77	0.2	
RT 62 HC	62-63	62	260			0.85	0.84	0.2	
RT 64 HC	63-65	64-65	250			0.88	0.78	0.2	
RT 65	58-65	65-58	150			0.88	0.78	0.2	
RT 69 HC	68-70	69-67	230			0.94	0.84	0.2	
RT 70 HC	69-71	71-69	260			0.88	0.77	0.2	

1.2.2 Measurement Technique of the Melting Temperature and Enthalpy of the Paraffin wax.

Differential scanning calorimetry (DSC) is the method currently utilized to calculate the melting temperature and enthalpy of the PCM. The difference between the amount of heat needed to raise the temperature of a sample and a reference is assessed using the thermal analytical method known as DSC.

Throughout the experiment, the sample and reference are both kept at virtually identical temperatures. The fundamental idea behind this method is that to keep both the sample and the reference at the same temperature throughout a physical change, such as a phase transition, more or less heat must be transferred to the sample than to the reference. Whether the process is exothermic or endothermic determines whether less or more heat must be transferred to the sample. For instance, as a strong example melts into a fluid, it will require more intensity streaming to the example to expand its temperature at a similar rate as the reference. This is because the sample absorbs heat during the endothermic phase transition from solid to liquid. Similarly, less heat is required to raise the sample's temperature during exothermic processes like crystallization. Differential scanning calorimeters can measure the heat absorbed or released during such transitions by observing the difference in heat flow between the sample and the reference. A heat flux curve versus temperature or time is the outcome of a DSC experiment. Two distinct conventions exist: Depending on the technology used in the experiment, exothermic reactions in the sample are represented by peaks that are either positive or negative [5].

1.3 Heat Transfer Enhancement Techniques of PCMS (Solid-Liquid)

Any LHTS application necessitates the methods of heat transfer improvement. To improve the heat transfer in latent heat thermal storage, various strategies have been proposed for enhancing the paraffins' thermal conductivity such as:

- Metallic fillers
- Metal matrix structures
- Finned tubes in a variety of thermal storage systems
- Aluminum shavings

Figure (1.3) provides a summary of several approaches for improving heat transmission. Nanoparticles as well as the metal foams are hard to manufacture in a governed way, so these methods are generally not cost-effective. Therefore, the simplest and most cost-effective method for the LHTES system is geometrical optimization. Experimental and numerical (theoretical) methods can be used to study and analyze these heat transfer augmentation techniques [1].

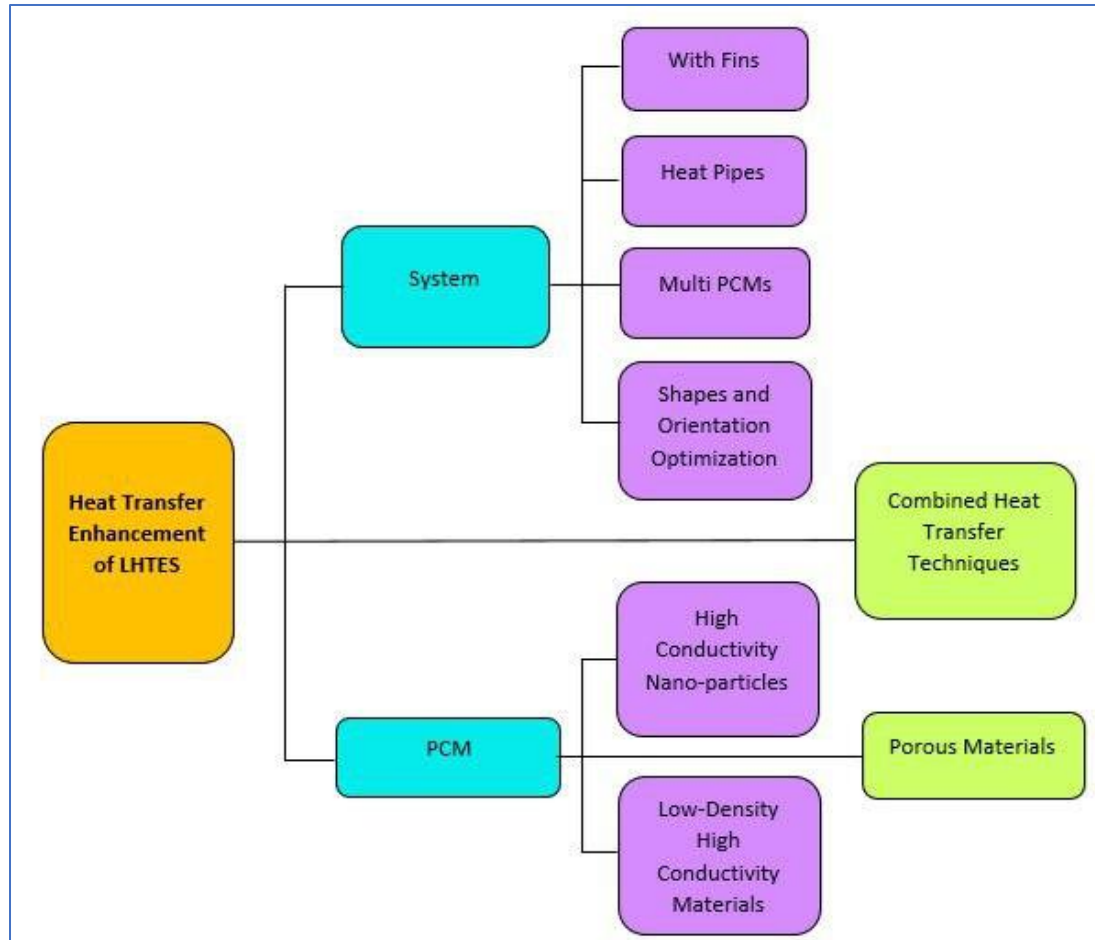


Figure 1.3: Techniques for Improving Heat Transfer in the LHTES System.

1.3.1 Extended surface

In thermal engineering, it is crucial to remove excessive heat from system components. To achieve this, improving heat transport is a key topic. There are two ways to enhance the heat transfer from surfaces, namely, increasing the surface's heat transfer area or increasing the heat transfer coefficient between the surface and its surroundings. One of the most commonly used methods is to attach fins to walls and surfaces in order to increase the area of heat transfer. Fins, also known as extended surfaces, are frequently employed in heat-exchanging devices to improve the heat transfer

between a primary surface and the surrounding fluid through conduction, convection, and radiation [6].

It has long been customary to use expanded surfaces to effectively and efficiently dissipate heat to increase the functionality and lifespan of the equipment. It offers a workable, affordable, and dependable answer to the demand for heat removal problems in thermal management. It also makes no noise or disturbance. To improve the heat transfer surface area, expanded surfaces are one of the best engineering approaches. Materials utilized for fins are frequently low-emissivity and high-thermal-conductivity materials, such as copper and aluminum, which provide minimal radiation in most of cases[7]. Different fin types have been employed, ranging from those with relatively simple geometries to those with complex geometries. Several of the typical fin geometries including rectangular (Figure 1.4), triangular (Figure 1.5), cylindrical (Figure 1.6), trapezoidal (Figure 1.7), and parabolic (Figure 1.8) are shown. However, rectangular fins are frequently used due to their ease of fabrication. As a result, research on fin is extremely pertinent and justifiable [6].

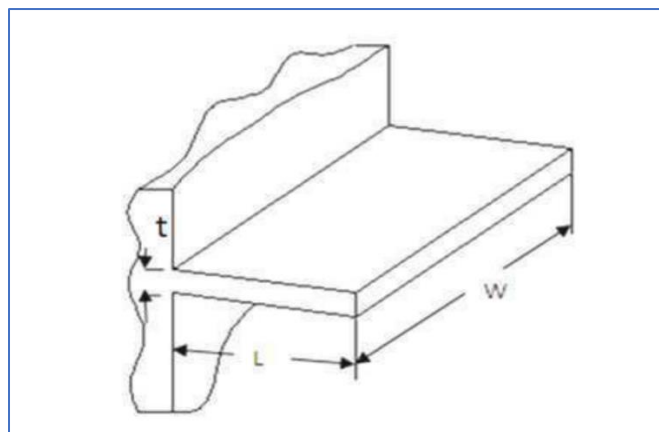


Figure 1.4: Rectangular Fin.

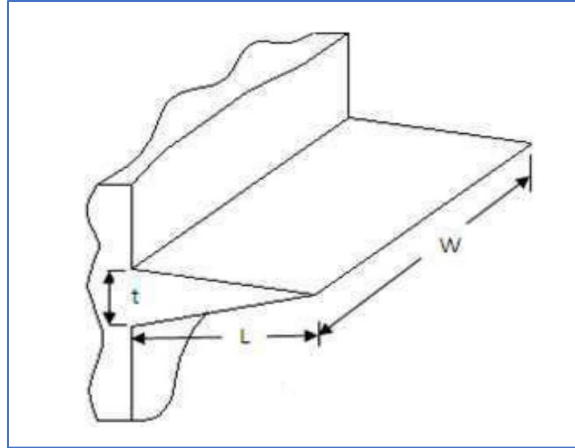


Figure 1.5: Triangular Fin.

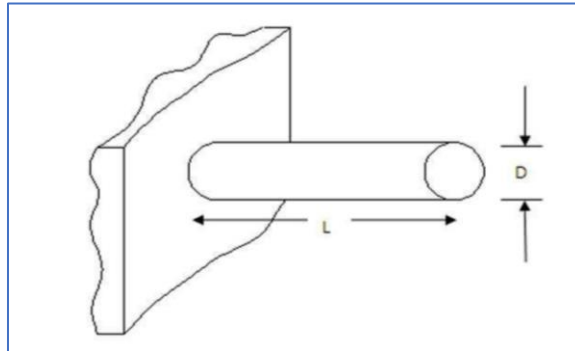


Figure 1.6: Cylindrical Fin.

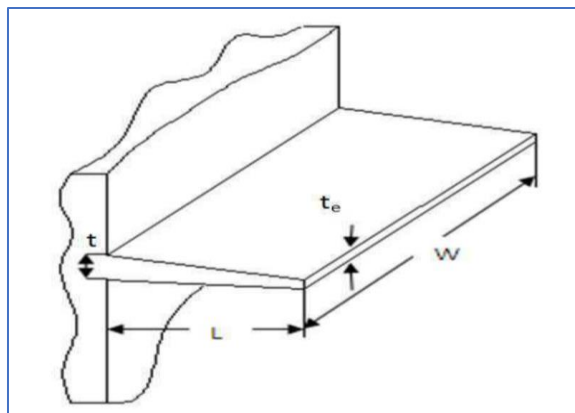


Figure 1.7: Trapezoidal Fin.

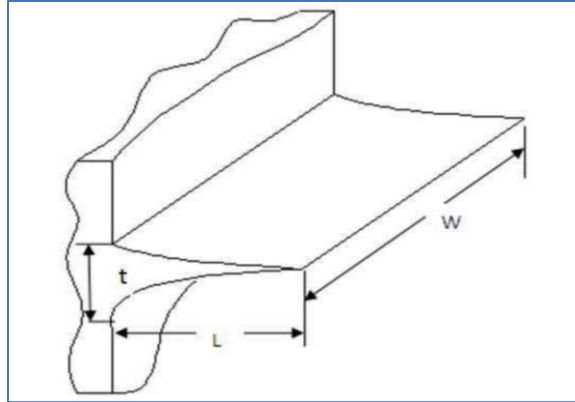


Figure 1.8: Parabolic Fin.

The design of contemporary thermal systems aims to develop heat exchangers that are smaller and more effective. Improving energy transfer through heat and reducing energy loss from inefficient use has become an increasingly important responsibility for thermal system designers due to the worldwide increase in energy demand. To meet this objective, heat transfer surfaces with high heat transfer coefficients and high area compactness are required. Fins have been traditionally used as heat transfer enhancement devices. Therefore, it is important to design fins that can remove the most heat with the least amount of material while also considering how simple the fin form is to manufacture[7].

1.4 Thermal Energy Storage Type

To store and distribute heat, latent heat thermal energy storage (LHTES) systems use a thermal exchange structure and a PCM, where the thermal storage systems are heat exchangers. Heat exchangers (HXs) have different models, among which triple -tube heat exchangers (TTHE) are one of the double tube heat exchangers under investigation. It has been reported that triple tube heat exchangers are more effective than double tube heat exchangers for optimal heat transfer in concentric heat exchangers. An

overview of experimental, theoretical, and analytical research on different popular heat storage containers, such as rectangular, sphere-shaped, annulate, and cylindrical enclosures [8] will be reviewed in the chapter two.

1.5 Application of Triple-Tube Heat Exchangers Powered by PCMS

During the times of power crisis, declining fossil fuel reserves, and growing environmental concerns, solar thermal storage in latent heat can act as a clean heat option [9]. However, solar thermal energy has certain drawbacks. It is an irregularly available resource [10], as there is no sun irradiation at night and limited solar irradiation on overcast or rainy days. To make the best use of solar energy, LHTES must be incorporated [11 ,12]. Solar parabolic-trough collectors are a type of solar thermal equipment that can be used in a variety of applications, such as:

- Air-cooling systems for buildings.
- Food drying processes.
- Refrigeration systems.
- Desalination, power plants, and manufacturing processes. Figure (1.9) provides a few examples

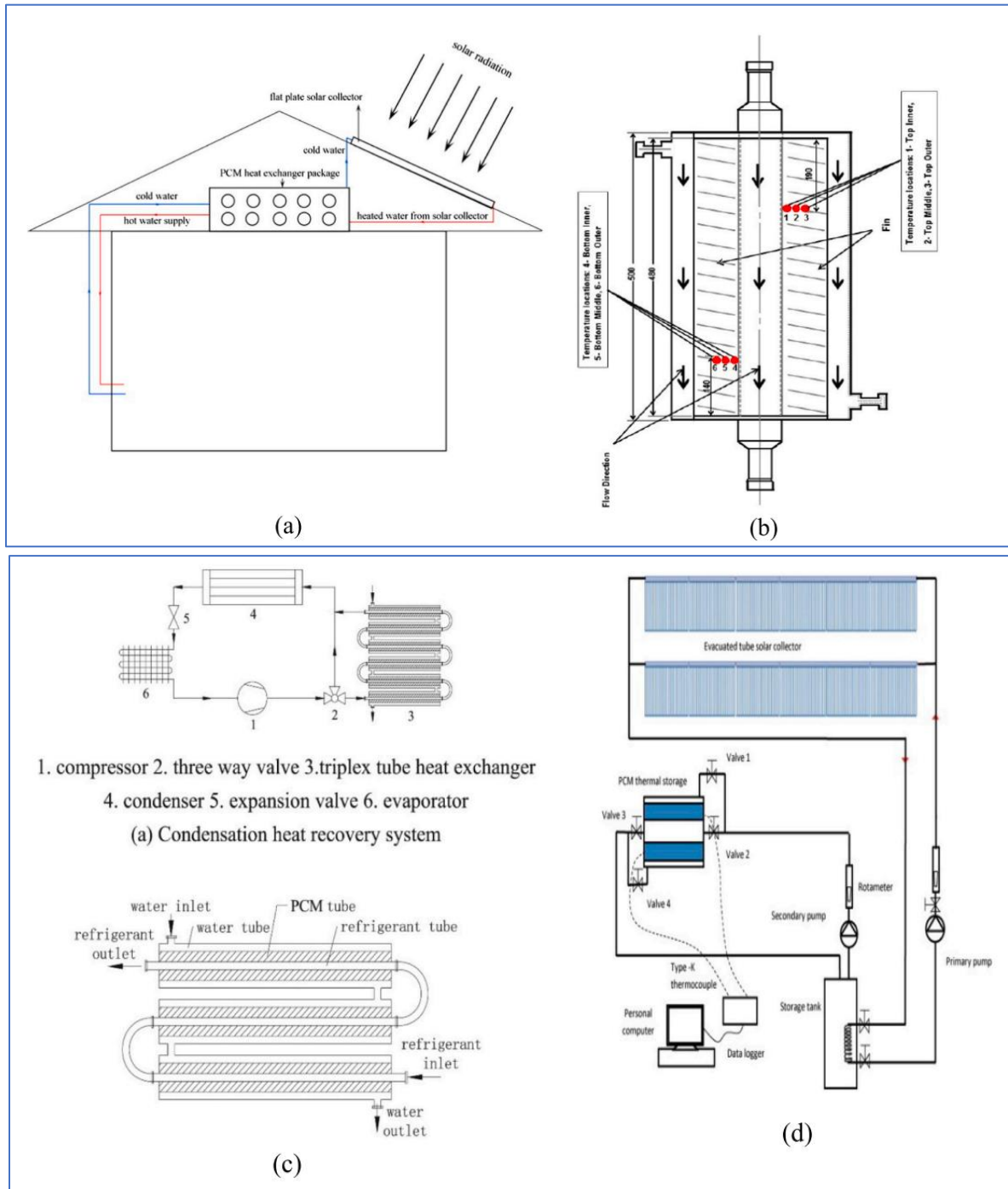


Figure 1.9: Application of triple-tube heat exchanger powered by PCM: (a) The energy saving of domestic hot water system, (b) CSP applications, (c) Condensation heat recovery, and (d) Liquid desiccant air conditioning system.

1.6 Scope and Objective of This Work

This thesis investigates the possibility of decreasing PCM melting time in a unique Triple Square Tube Latent Heat Storage (TSTHS) arrangement with fins, where the HTF flows in one direction (gravity direction). This setup would enhance the natural convection during the PCM charging. Another goal is to examine the thermal performance of some fins to each channel and improve their size and position under various HTF thermal and flow conditions. Also, a theoretical model is to be developed for predicting the best state of discharge and the best state of fins and to validate the model experimentally.

1.7 Outline of Thesis

The rest of the thesis can be summarized for each chapter as below:

- Chapter 2 provides a literature review on numerical and experimental studies of TTHX with PCM and the characterization of fins.
- Chapter 3 introduces the numerical work on TTHX. The effects of operational conditions (HTF flow rate, HTF inlet temperature, flow direction of HTF) on the charging are studied.
- Chapter 4 presents the experimental work on TTHX.
- Chapter 5 discusses the main results of the study.
- Chapter 6 summarize the conclusion and gives recommendations for future research.

Chapter Two: LITERATURE REVIEW

The world has been grappling with the problem of pollutants resulting from various sources, such as cars, factories, and electrical stations, which has prompted a shift towards clean energy sources, like solar energy, wind energy, and other renewable energies. Effective use and conservation of solar energy and waste heat require capturing thermal energy, for which the PCMs can be employed as SLHSSs. While there have been limited experimental studies comparing the effectiveness of these systems, it has been found that the latent heat storage systems can store higher energy density with a smaller temperature differential between storing and distributing heat as compared to sensible energy storage systems.

2.1 Numerical Researches

Seddegh et al. [13] carried out a combined conduction and convection heat transfer model to be used in evaluating and comparing the thermal behavior of vertical and horizontal shell-and-tube energy storage systems employing phase change materials (PCMs). The temperature change, solid-liquid interface, phase distribution, total melting, and solidification time during the charging and discharging operations of PCMs are all studied using the model, which is first assessed using published experimental data that is accessible in the literature. According to the results of the simulation, convective heat transfer during the charging process for the horizontal orientation strongly influences the melting of the solid PCM's upper portion while having less of an impact on the melting of the solid PCM's bottom half. According to the results, the orientation that is horizontal has superior thermal

performance when charging, particularly when charging part load energy. In addition, the results demonstrated that increasing the temperature of the hot heat transfer fluid (HTF) inlet significantly shortens the total charging time for both orientations. However, the charging and discharging procedures are not significantly affected by increasing the flow rate.

Hong et al. [14] discussed a numerical simulation of thermal energy storage using latent heat in a two-dimensional rectangular cavity with thermally active components. The study varied the cavity's aspect ratio from (0.5 to 2), the number of heat sources on the heated wall from (1 to 4), and the inclination angle from 0 to 90°. The results showed that when the inclination angle is 90°, the aspect ratio has a significant impact on the thermal behavior. It suggests that using discrete heat sources for thermal energy storage is a promising and efficient approach, with a potential reduction of over 40% in thermal storage time when the inclination angle is set to 0, the aspect ratio is 0.5, and there are four heat sources. The study also discussed the different stages of the melting process in the cavity.

Eslamnezhad and Rahimi [15] investigated numerically the enhancement of heat transfer method using rectangular fin to melt the phase-change material in a triplex tube heat exchanger. A two-dimensional numerical model using fluent software was chosen, and conduction and natural convection were taken into account in their simulation. The arrangement of the rectangular fins along the triplex tube heat exchanger is one of the most influential factors in the process of melting which has been studied, and also the best type of this arrangement to increase the efficiency of heat exchanger and reduce the time of melting of the phase-change material has been suggested in the form of different proposed models.

Saeed et al. [16] carried out a study for a pear-shaped TES system to discuss two main thermal improvement techniques (Fins and the Nano-Enhanced Phase Change Material (NePCM) utilization). The TES unit is furnished with fins and filled with n-octadecane PCM that has been combined with Al_2O_3 nanoparticles. To achieve the best heat transmission and accelerate the melting of PCM, several Al_2O_3 concentrations (like 0, 3 and 6 vol%), forms of fin (two-fin, T-shaped fin, and Y-shaped fin, a), and fin materials (Steel, Al, and Cu) were adjusted. By comprehending the temperature contours, liquid fraction, Bejan number, average Nusselt number, average unit temperature, and average liquid fraction, the performance was discussed. The findings showed that the time of melting reduced via (14%) and (32%), correspondingly, when Al_2O_3 the alumina (Al_2O_3) nanoparticles (6%) as well as the Cu fins being used as opposed to pure PCM with steel 302 fins. Moreover, adding a copper fin in a Y shape to a pear-shaped unit is the greatest option for speeding energy storage. The supremacy of the irreversibility of heat transfer irreversibility above the irreversibility of fluid friction results from the usage of steel 302 fins. See figure (2.1).

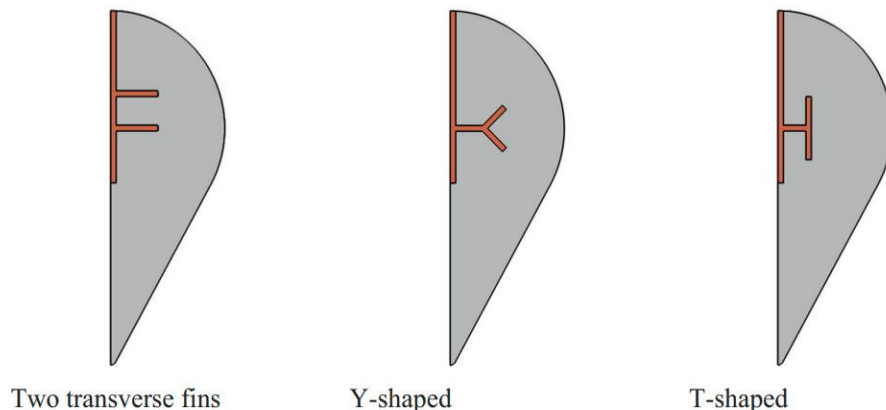


Figure 2.1: Different cases considered in their study.

Nesrine et al. [17] investigated how the orientation of the fins in a horizontal, 2-finned annular tube HX affects the transfer of heat when n-eicosane, a PCM, utilized in the thermal storage systems. When the system's angle altered from 0° (vertical fins) to 90° (horizontal fins), the consequence of the orientation of fins upon the rate of melting, natural convection, and thermal conduction, was explored. And, the results indicated that the conduction heat transfer dominates at the beginning of the melting process. Because the arrangement of the fins prevents the natural convection from taking place, the transfer of heat in the horizontal fins being highly active, whereas the PCM's higher half melts, as well as less active as the PCM's lower half melts during the melting process. However, throughout the entire melting process, the vertical fins' capacity for heat transfer and convection is nearly constant. In comparison, the vertical fin system achieves superior heat transfer performance; compared to the case for the horizontal fins, there was a 250% decrease in total melting. See figures (2.2) and (2.3)

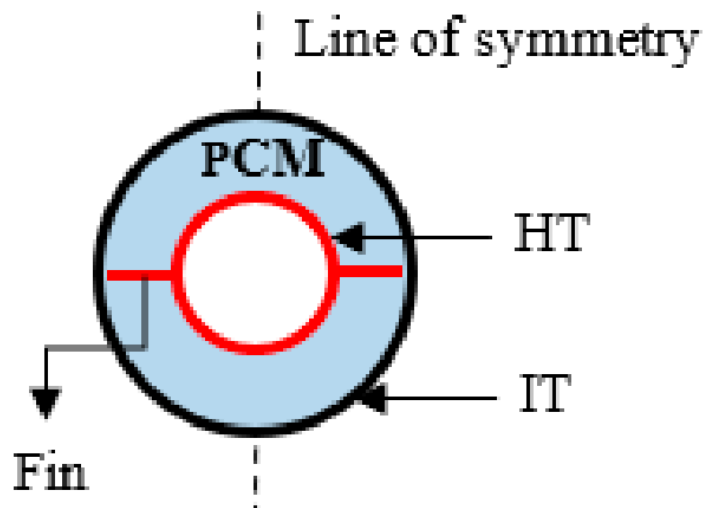


Figure 2.2: Schematic representation of the annular tube heat exchanger (HT: Hot tube, IT: Insulated tube).

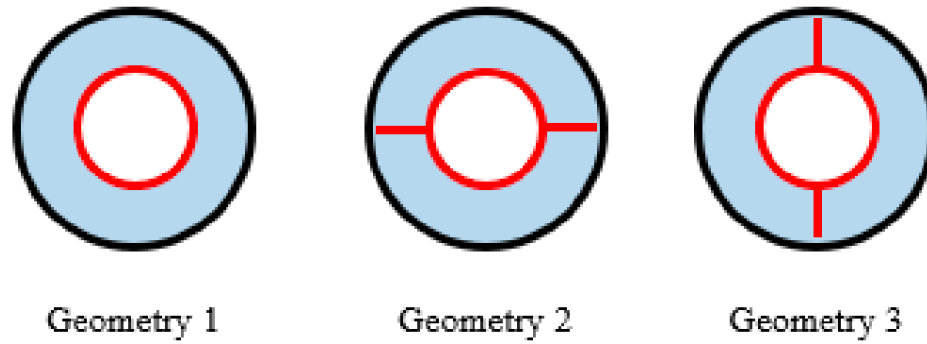


Figure 2.3: Schematic representation of the investigated cases.

Ahmed et al. [18] carried out a numerical simulation on the model of the melting procedure of NePCM within an annular thermal storage system. And, the TES regime comprises a cylindrical tube with three fins and a wavy shell wall. The outcomes were shown for different inward cylinder positions (right-left-all over), internal chamber pivot point ($0 \leq \alpha \leq 3\pi/2$), as well as the nano-added substances focus ($0 \leq \phi \leq 0.04$). Also, the results also revealed that the NePCM melting process was sped up by the elevated values of the concentration (0.4) of nano-additives, the larger tube rotational angle ($3\pi/2$) values, and the tube positioning into the lower location. See figure (2.4)

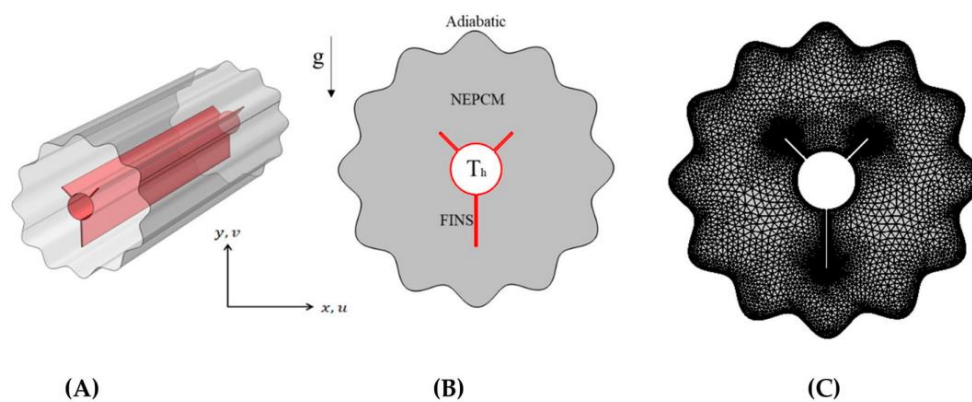


Figure 2.4: (A) 3D model of the shell and tube TES with embedded fins (B) A two-dimensional illustration of the studied model with boundary conditions. (C) A mesh sample.

Hosseinzadeh et al. [19] obtained that via combining hybrid nanoparticles ($\text{MoS}_2\text{-Fe}_3\text{O}_4$) and new fin shape into a triplex-tube storage, a better PCM solidification rate can be achieved. The researchers utilized a computational model that regards the natural conduction as well as confirmed it versus preceding investigational data. Authors calculated and reported the effects of different volume fractions of nanoparticle, parameters of radiation parameters, and form factors upon the liquid-solid interfaces evaluation, rate of phase change, and time of solidification procedure on the entire process of solidification. The outputs demonstrated that the utilization of the aforementioned methods leads to better PCM solidification. The results also indicated that the factor of radiation possesses an important influence upon the rate of phase change, contributing to (74.58%) of the complete Solidification Process Time (FST). In addition, the researchers designed optimal factors for optimizing the FST in the triplex-tube LHTESS employing approaches of Taguchi and RSM. Furthermore, as a novelty, a precise relationship for the FST with a higher exactness was evolved, see figure (2.5).

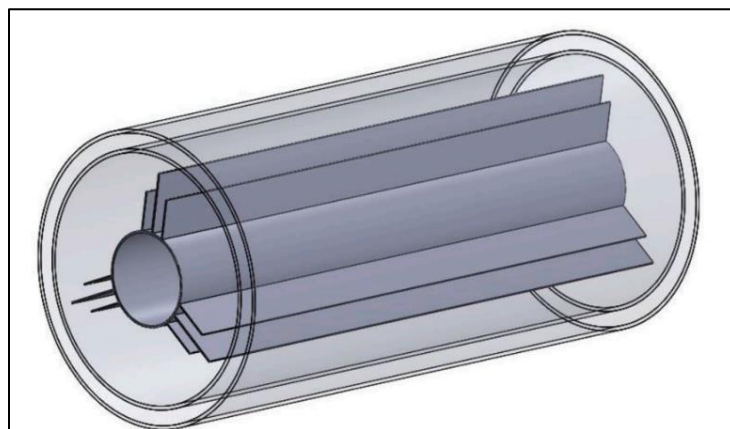


Figure 2.5: 3D configuration of LHTESS with fins.

Maneengam et al. [20] introduce a numerical investigation for the melting influences upon the convection of a phase change material in hexagonal containers with hot cross sections. Based on the number of heated suites, four cases were taken into account: C1 (two-horizontal fins), C2 (two-vertical fins), C3 (four fins), and C4 (eight-heated parts). The results showed the following: The distributions of temperature, velocity and Bejan number increase when the heated wings are increased due to the improvement of buoyancy –convection phenomenon .In addition, the case of C4 depicted that the molten region is confined to the majority of the flow range. At lower temporal values, isotherms, velocities, and liquid fraction are observed near the heated inner portions, while the temporal progression leads to the formation of a suitable temperature and melting of the hexagons of the flow. The concentration of the NP dynamic viscosity of the mixture is increased, so the velocities decrease with the growth of the φ (entropy) with the passage of time resulting from viscous dissipation becomes more important than the irreversibility resulting from the heat transfer. The results obtained are recommended to use two heated fins design in LHTSS to obtain the highest heat transfer rate. It is also recommended to use 6% concentration of NP (nanoparticles) to reduce the occurrence of irreversibility in heat transfer within LHTSS. See figures (2.6) and (2.7).

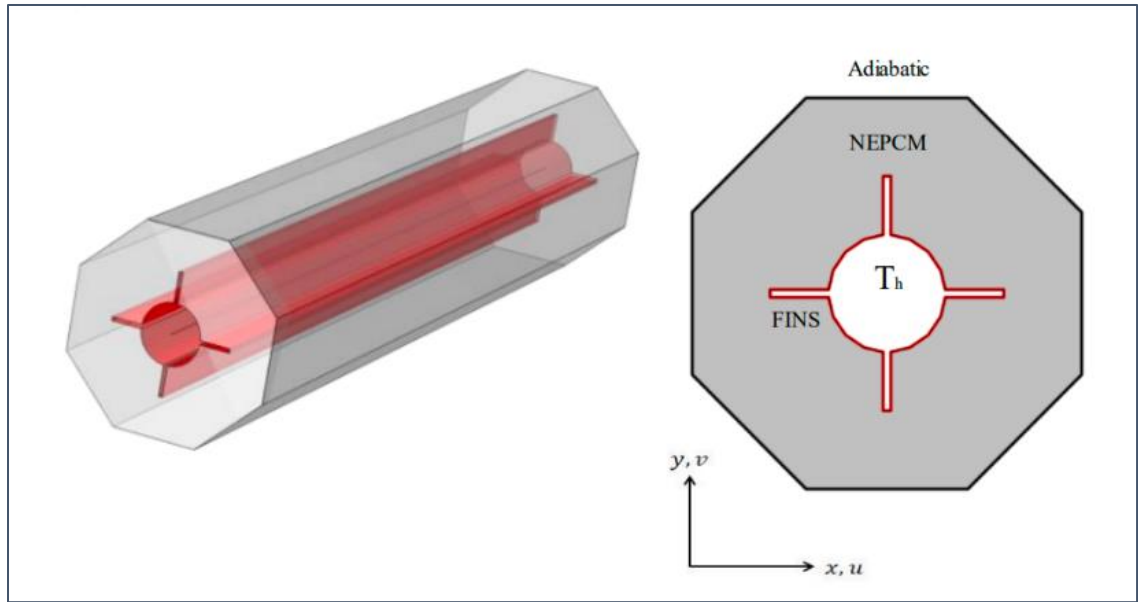


Figure 2.6: Two-dimensional view of LTESS (right) and 3D view (left).

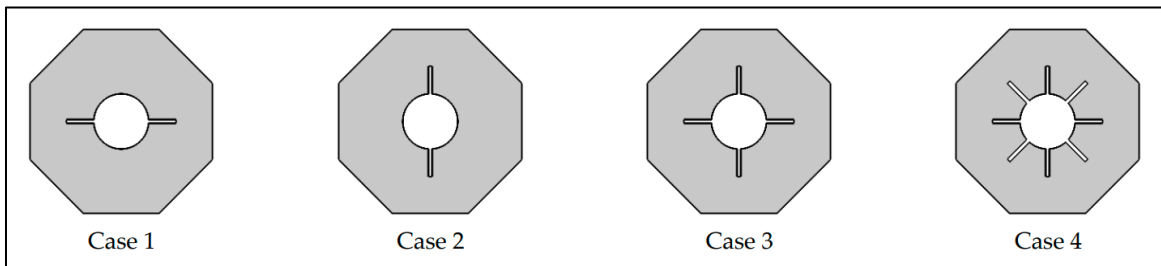


Figure 2.7: Different cases in the article.

Sun et al. [21] proposed the use of circular fins having a staggered spreading in order to perform enhanced rates of thermal response for a PCM vertical technique of a triple-tube HX, where the heat transfer fluid includes (2) opposed streams of flow. Due to the heat diffusion lack into the various PCM unit components being not similar, therefore, various fin configurations, sizes of fin, and boundary conditions of the flow of HTF were discovered by utilizing melting computational investigations in the PCM triple-tube regime. The results indicated that it is possible to increase the rate of thermal charge and the rate of melting by 59.1% and 37.2% in the case of staggered distribution, as well as in the case of inline distribution, the rate of melting

and the rate of thermal charge has increased by 33.7% and 50.4%. In addition, natural convection played a greater positive role when longer, thinner fins were used in the storage unit's perpendicular direction; as a result, melting rates were accelerated. Where it was found with the dimensions of the fin, which was the fusion rate, was increased by 23.6% compared to the Basic Box.

Huang and Yao [22] conducted a new type of longitudinal trapezoidal fin structure, and various comparative studies. The advantages of introducing the Fibonacci sequence in the longitudinal fin arrangement were demonstrated by studying the fin arrangement. Furthermore, the temperature changes at specific points were studied, and the geometrical parameters of the fin were optimized by the method of the response surface. The most important conclusions were obtained. And, outcomes revealed that adding new longitudinal trapezoidal fins are able to enhance the PCM solidification performance in the LHTES. The solidification time of the PCM will be reduced compared to the traditional quadrilateral fin by 45%. The height and width of the fins show the way the response surface has significant effects on the solidification performance of the PCM, and they are also greatly improved through the elongation of the fin angle. Among these factors the most obvious effect is the fin height of the LHTES system. The solidification time of a tube is greatly affected by the temperature of the cold fluid of the inner tube. In addition, the results showed that the difference in temperature between the inner wall and PCM exceeds 20 K, whereby a faster cooling rate can be obtained.

Ghalambaz et al. [23] work for the phase change latent heat thermal energy storage (LHTES), a conical shell-tube design with irregular fins was

considered. Nano-enhanced phase change material (NePCM) was used to fill the shell. As the geometrical design parameters, the shell's cone aspect ratio and the fin's aspect ratio were used. Copper, graphite oxide, alumina, and other nanoparticles were the subjects of the investigation. The findings revealed that the kind and concentration of nanoparticles were second to the shell-aspect ratio and fin aspect ratio as the most crucial design factors. At their best, both ascending and descending designs can result in the same melting rate. The melting rate might increase by up to 18.5% with the best LHTES design. A simple tube filled with 4.5% alumina-Bio-PCM and 1.5% copper-Bio-PCM had a cone aspect ratio of 1.17 and was the best design for ascending (descending) design. See figure (2.8).



Figure 2.8: Latent heat thermal energy storage (LHTES) unit: (a) ascending conical; (b) cylinder; and(c) descending conical.

Zarei et al. [24] numerically investigated a triplex-tube used as a Thermal Energy Storage (TES) regime. And, the triplex-tube used fin-improved PCMs. The system's geometry was enhanced by the addition of metallic (copper) fins to increase the heat transfer area. In order to determine the best design for minimizing the solidification time and achieving the

supreme performance improvement for the TES regime chosen for the present investigation. The effects of the existence, copper fins sizes, and configuration were investigated. Also, the outcomes uncovered that the best execution had a place with balances with a blend design, with a connection point of 90° and the length and width of 28 mm and 1 mm, individually. Compared to the system without fins, this configuration could cut the amount of time needed for solidification to be complete by around 42%. Also, it was presumed that raising the balance length can provide its beneficial outcome to improve the TES framework presentation till an ideal point just, whereas expanding the width revealed a different impact. In addition, the angles between the fin direction and the surface of the tube were examined, and it was determined that 90° was the most suitable angle for the TES case chosen for this study. Additionally, applying fins to the surface of the exterior or interior tube or using the mixture technique had no discernible influence, but applying the fins to the exterior surface of the tube had a detrimental effect on how well the TES system performed in comparison to not applying them.

2.2 Experimental Researches

Pandiyarajan et al. [25] used a thermal energy storage tank to store the available excess energy, and a shell and finned tube HX to be incorporated into an IC engine arrangement for extracting the heat from the exhaust gas. Using cylindrical phase change material (PCM) capsules in a TES tank of a (20 MJ) capacity, a combined sensible and latent heat storage system for thermal energy storage designed, fabricated, and tested by integrating them with a diesel engine of 7.4 kW capacity. Results showed that the system recovers nearly 10–15% of the total heat that would otherwise be wasted. At full load, the heat exchanger can extract approximately 3.6 kW of heat. By

decreasing the exhaust gas temperature below 100°C, it is possible to recover the heat which is liberated from the fuel along with the exhaust gas during the burning of fuel (HCV–LCV).

Modi et al. [26] conducted experimental studies involved analyzing the thermal performance of four solid finned tubes with varying fin heights (10, 20, 25, and 30 mm), three perforated finned tubes with different hole sizes (4, 8, and 12 mm), and four different angular positions (0°, 30°, 60°, and 90°). Their findings indicated that angular positions of 0° and 30° showed a high rate of average temperature rise during charging, while it had no substantial effect on discharging. They also found that the optimal fin height for the melting process was 65% of the annulus, while the solidification process did not exhibit the optimal fin height. Although perforation improved the thermal performance marginally, for the same fin volume, small diameter holes were recommended over large holes. This is because the perforated fins with hole diameters of 4 mm and 8 mm reduced the pre-melting time by 12.65% and 3.16%, respectively, when compared to solid fins.

Karami and Kamkari [27] experimentally tested a vertical shell and tube latent heat energy storage heat exchanger with perforated fins to see how it improves the thermal performance. The results were compared to those of unfanned and solid finned heat exchangers as the base cases. The shell side contains a phase-change material in the form of lauric acid, and water flows through the inner tube. To facilitate a visual comparison of the melting processes, transparent Plexiglas tubes were used for the heat exchanger shells. Copper was used to make the fins and tubes under different inlet water flow rates (0.5 and 1 l/min) and temperatures (55 and 65 °C). Also, the experimental results demonstrated that the perforated finned heat exchanger's

time-averaged Nusselt number is approximately 30% higher than that of the solid finned heat exchanger. Additionally, the perforated finned heat exchanger has a total melting time that is approximately 7 % than that of the solid finned heat exchanger.

Awarmol and Pise [28] mentioned that the experimental study's main goal is to measure and evaluate the increase of natural convection heat transfer of a perforated fin array with various perforation diameters (4–12 mm) and inclination angles (0–90°). Geometry and direction are the factors for this natural convection cooling using finned surfaces. The steady-state heat transfer from arrays of solid fins and perforated fins was studied in this work. Perforated fins with a 12 mm perforation diameter and a 45-degree orientation angle were used to boost the heat transfer coefficient. This resulted in a 32% increase in heat transfer coefficient over a solid fin array while conserving approximately 30% in material mass.

Kamkari and Shokouhmand [29] presented an experimental study of the PCM melting in a transparent rectangular enclosure without and with horizontal incomplete fins. And, the enclosure walls were thermally insulated on the other sides and heated isothermally from one side. For finned and unfinned enclosures, experiments were conducted at the wall temperatures of (55, 60 and 70°C) for ($3.6 \times 10^8 \leq Ra \leq 8.3 \times 10^8$). The melting procedure visualization as well as the field of temperature was directly achieved. The quantitative and qualitative information about the phenomena of melting were determined employing digital photos of the immediate melt front developments and the records of temperature at the enclosure vertical mid-plane. During the melting process, melt fractions, heat transfer rates, and Nusselt numbers were derived from the experimental data. According to the

findings of the experiments, while the surface-averaged Nusselt number decreased, the number of fins increased the total heat transfer rate and decreased the melting time. The ratio of melting enhancement and the efficiency of the fins as a whole augmented with the fins number as well as reduced with the temperature of wall. After reaching certain maximum values, melting enhancement ratios decreased over time, indicating that partial fins are more advantageous during the initial melting phase.

Kamkari and Groulx [30] carried out an experimental investigation to examine the effect of inclination angle on the PCM melting in finned rectangular enclosures and to visualize the melting process. In the side-heated enclosures with varying numbers of fins, the lauric acid melting process was assessed at inclination angles of 90° (vertical), 45° , and 0° (horizontal). The enclosure was constructed from clear acrylic material with the exception of one side that was covered in an aluminum plate to heat it isothermally in order to view the melting process. Reduced inclination angles were found to increase the melting rate for the finned and unfinned enclosures alike. When compared to the 0-fin vertical enclosure, heat transfer was improved by 56% and 115% in the 3-fin vertical and 0-fin horizontal enclosures, correspondingly. According to this thermal behavior, inclining the enclosure rather than adding fins to the vertical enclosure can be a more efficient way to increase the melting rate. The 3-fin horizontal enclosure had the fastest rate of heat conduction and, as a result, the shortest melting time among the several examples was examined.

Kamkari et al. [31] studied the dynamic thermal conduct of the PCM melting in a rectangular enclosure at different angles of inclination. As a phase change material (PCM) with an elevated Prandtl no. ($Pr \approx 100$), lactic acid was

used. While one side of the enclosure was heated isothermally, the other walls were thermally insulated. And, the fractions of melt, the Nusselt nos. as well as the rates of local interfacial heat transfer at the solid–liquid interface were determined by combining the melt pictures' image processing with registered temperatures. The findings demonstrated that the inclination of enclosure possesses an important impact upon the PCM's heat transfer rate and melting time as well as the formation of natural convection currents. As the tendency point is diminished from 90° to 0° , the convection flows in the fenced in area increments and tumultuous stream structures show up. And, the Benard convection cells creation into the PCM in form of liquid is indicated by the wavy solid–liquid interface line that appears when melting begins in the horizontally inclined enclosure. For similar hot wall temperatures, a lessening in tendency point prompts an extensive improvement in the energy transfer from the nook's hot mass to the phase change material (PCM). And, it is obtained that the intensity moves upgrade proportion for the flat fenced in area is multiple times higher than that of the vertical enclosure.

Salem et al. [32] stated that in a vertical shell-tube HE configuration, the LHTESS' efficiency characteristics were practically tested. Water streams in the cylinders that are organized as roundabout layers at specific radii in the shell, which is involved by natural paraffin stage change material (RT60). The tests use semi-circular tubes rather than fully circular ones and take into account the impacts of the tube area ratio, layer radius ratio, number of tube layers, and distribution of the tubes (inline/staggered). During the charging and discharging phases of these studies, hot water (65 to 75°C) is used, and cold water (25°C) is utilized. The main results of this study are that the charging time is reduced by 7.2%, 7.3%, 17.6%, and 11% when semicircular

tubes are used instead of complete ones, the area ratio is increased from 2.4% to 4.3%, and the same number of tubes is distributed in two layers instead of one. The charging/discharging effectiveness improved by 8.1%/2.6%, 7.4%/3.3%, 19.7%/5.7%, and 8%/4.5% in accordance with these augmentations. Moreover, the charging efficacy is increased by 5.3% when a staggered distribution of the tubes is used rather than an inline one. Finally, a set of experimental correlations is created to forecast the storage system's charging efficiency.

Lv et al. [33] designed and constructed a pilot-scale latent heat storage system with four groups of tubes embedded with various fins—longitudinal, H-shaped, spiral, and without fins—that was loaded with 5674.7 kg of medium-temperature phase change material (PCM). During the charging system, the smooth cylinder had the most elevated outlet temperature, trailed by the cylinders with longitudinal, H-formed, and winding blades, demonstrating that the twisting balances had the best intensity move execution while the smooth's was awful. The thermal energy storage unit's temperature differential was greater in the vertical direction than it was in the horizontal direction. Additionally, the thermal insulation performance test revealed that because the latent heat system was charged from top to bottom, the temperature of PCM in the higher portion declined more slowly than that in the lower part. In addition, the longitudinal, H-shaped, spiral, and unfinned tubes had accumulative energies of 500.67, 541.57, 567.35, 432.56 MJ, 21.39, 23.14, 24.24, and 18.48 kW, respectively, after charging for 6.5 hours. The latent heat storage system had a calculated charging efficiency of 66.48%.

Zou et al. [34] used comparative experiments to compare the thermal efficiency of LTESU integrated with Copper Foam Fin (CFF), Sensible

Thermal Energy Storage Unit (STESU), and Latent Thermal Energy Storage Unit (LTESU). There was no apparent thermal stratification, and the investigational outcomes demonstrated that the rate of STESU's thermal varying was greater than that for else units. Although there being a noticeable thermal stratification, the LTESU possessed the lowermost rate of thermal change. And, the solid-liquid interface upon the cross-section of LTESU took the shape of an inverted triangle during the thermal charging process. The lower portion of the PCM was a dead zone that was unable to alter its phase and did not take part into the thermal discharging and charging. And, even yet, the thermal efficacy of LTESU outperformed by 18.7%. Also, the capacity of thermal charging, the capacity of thermal discharging, and the thermal efficacy could all be increased by 51.1%, 55.9%, and 10.8%, respectively, by integrating with CFF.

Majeed et al. [35] used water as a HTF, and the investigational scrutiny was carried out upon a vertical LHTES equipped with a phase change material (PCM) in this work. The impact of including a permeable metal froth was explored to charge process. Trial perceptions manifested the frothed TTHX possessed a better rate of softening above the non-frothed TTHX. And, with the porous metal foam addition, the time amount required for the charging process decreased for both TTHX configurations. The copper froth impact was critical for the frothed TTHX. Also, the decrease into the entire time of softening for the non-frothed and frothed TTHX was (43%) for a similar temperature (69°C) of HTF.

2.3 Numerical and Experimental Researches

Vogel & Thess [36] used a benchmark experiment to evaluate the precision of numerical melting models that are controlled by natural

convection. In order to quantify the phase state and velocities using particle image velocimetry and shadowgraph imaging, respectively, a rectangular box packed with a model liquid (n-octadecane) was symmetrically heated from the two sides. Two separate techniques were used in the numerical method to calculate fluid flow, temperature, and phase state. And, the initial is a comprehensive model that utilizes changeable thermophysical characteristics as well as the fluid volume technique for allowing the expansion of volume into a second phase of air that one solves into the (2) dimensions. Also, the second is a condensed model employing the Boussinesq approximation and constant thermophysical characteristics, which is solved in either two or three dimensions. The authors make a systematic comparison between the fluid model's detailed volume and the simplified Boussinesq model in the first section of the work. It was discovered that, for the certain group of factors ($Pr=52$, $Ste=0.092$, $A=4$, and $Ra=2108$), there is a discrepancy of less than 4% between the simplified and detailed models to predict the global amounts, like the fraction of the phase of liquid and the rate of the entire flow of heat, while there is a difference of up to 20% between the velocities. In the second piece of the work, the researchers thought about the reenactments of the improvement on Boussinesq model in three aspects with the benchmark explore. It was discovered that while the velocity magnitudes are significantly overestimated, the simulation correctly foresees the fraction of the phase of liquid and the temperatures with ($< 4\%$) deviations.

Kumar and Verma [37] conducted numerical and experimental investigations on the melting properties of lauric acid into a horizontal shell and finned tube-type storage unit. The goal of the current study is to enhance the rate of the melting of a PCM while maintaining the conduction influences

by using minimal fin lengths that span (36%) of the concentric arrangement's annular length. An effort was made to include a finned tube in the capacity holder in order to increase the rate of intensity transfer between the PCM and HTF at (3) distinct unpredictable positions ($e=12, 18$ and 24 mm) of a finned (HTF) tube from the concentric external cylinder center ($e=0$ mm). Numerical calculations yield results that are consistent with experimental findings. Examining the improvement in PCM's melting rate, it was discovered that the maximum eccentric annulus has a melting rate that is 21% higher than the concentric configuration. This is because the increased dominance area for natural convection effects also makes PCM's temperature distribution more uniform. The bottom annulus's fin arrangement, which has a 60° angle between the fins, successfully achieves the eccentric behavior for improving melting performance. It was shown that a rise in Stefan number accelerates the PCM melting regardless of the inner tube's eccentric location, and an eccentric annulus stores heat at a rate that is 18.7% greater than a concentric annulus.

Qaiser et al. [38] stated that the multiple heat transfer tubes and altered shell designs are the subject of experimental and numerical investigations in this paper to improve the transfer of heat into a horizontal LTESS. In the steel shells and copper tubes that carry water as the heat transfer fluid (HTF), stearic acid was used as a phase change material. As the Base Case, a single Y-fin HTF tube was divided into two to five tubes in various configurations to maintain the PCM's constant mass. When compared to the Base Case, the mean rates of heat transfer improved via (33.6%) and (23.7%), respectively, via the vertical double tube as well as triple tube V-configurations. Additionally, the comprehensive times of melting decreased via (21.7%) and

(21.7%). Furthermore, it was suggested to modify the design of the elliptic and triangular shells for double and triple tube configurations, respectively. In comparison to the Base Case of the Y-fins single tube layout, the two configurations increased the mean rate of heat transmission via (85%), which shortens the total PCM melting time by 50%. In contrast with the base case, an expansion in the temperature of the HTF of (5.6%) further developed the typical Nusselt no. via above (37%) for the two cases. In addition, the relationships between the mean Nusselt no. and the melting Fourier no. and were established.

Z. Mahmoud et al. [39] presented that in a phase change material (Paraffin RT-35) triple-tube HX in which (2) heat-transfer fluids flow in the reverse directions throughout the internal and external tubes, and this study describes the way the circular fins with a staggered spreading and a changeable locations can be used to address the rates of low thermal response. An experimentally verified computational fluid-dynamic model was used to numerically examine and optimize various circular fin configurations, dimensions, and orientations under various heat-transfer fluid flow conditions. The outcomes showed that the liquefying rate, contrasted and the finless' base instance can be further developed via (88%) as well as the rate of intensity charging via (34)%, if the blade direction being descending vertical lengthways the PCM shell's right half and left side. Also, the findings indicated that adopting longer fins with thinner thicknesses in the storage unit's vertical orientation has advantages. The fins' size is changed from $2 \times 7.071 \text{ mm}^2$ (thickness x length) to $0.55 \times 25.76 \text{ mm}^2$ (thickness x length), which decreases the time of melting via 22% as well as boosts the rate at which the heat is charged by 9.6%. The necessity of identifying the optimal

Reynolds numbers and heat-transfer fluid intake temperatures to maximize the melting improvement prospective of the circular fins having downward-upward fin locations was also proven by this work.

Joulin et al. [40] compared numerical and experimental results for a PCM that is conditioned in a parallelepipedic polyefin envelope for passive solar wall applications. By squeezing the samples with a real setup consisting of heat flux sensors and thermocouples mounted on two vertical aluminum exchanger plates, the experimental results were obtained. Using a two-dimensional application of Fluent and a custom one-dimensional Fortran code, numerical predictions were made. Both methods laid out a very high level of agreement (65%) with experimental findings about the melting process. However, both numerical codes were unable to effectively forecast the phase shift process during solidification; the maximum relative error was 57% (with an average of 8%).

Al-Abidi et al. [41] explored numerically a heat transfer improvement strategy for PCM melting in a triplex tube heat exchanger (TTHX) leveraging internal and external fins. It was discovered that the time it takes for the phase change material (PCM) to completely melt the PCM is influenced by the Stefan number, fins no., fins length, and material of TTHX. And, the proposed model was validated through experiments. The results of the simulation match those of the experiment. Case G's (8-cell PCM unit geometry) computational results indicated that the total melting time reduced to 34.7%, resulting in a shorter melting time.

Muhammad et al. [42] used experimental data to create and validate a two-dimensional model of an existing vertical flow, 1 MWh, high temperature thermal storage unit. A parametric report was performed to assess

the key plan boundaries and their impact on the temperature profile and charge effectiveness. The charge efficiency was found to range from 77 to 94 percent. The output temperature and flow rate for a constant power output were presented in the numerical model for this pilot scale model at an industrial level of (330 MWh) storage, taking into account the residual input heat from the solar thermal collectors.

Liu et al. [43] improved the solidification performance of a shell and tube LHTES apparatus by suggesting of an innovative longitudinal triangular fin. First, the two alternative arrangements of novel fins (Fin-B and Fin-C) were contrasted with the standard rectangular fin (Fin-A) in terms of their solidification characteristics (solid fractions, temperature distribution, and solidification time). And, the novel longitudinal triangular fins are able to considerably enhance the performance of the solidification of the PCM into LHTES, as well as the Fin-C possessed better efficacy of heat transfer and supreme performance of solidification among the (3) kinds of fins, in accordance with the additional research results upon the influences of fin's geometrical factors, original temperature, and materials of fin upon the performance of the solidification. When compared to conventional rectangular Fin-A, the solidification time of Fin-C-I significantly decreased by 38.30%. Characteristically, the time of solidification was reduced by either declining the first temperature or raising the thermal conductivity as well as the heights of fin. In any case, the base width impact of a three-sided blade upon cementing execution can be dismissed. The recommended temperature difference between the PCM and inner wall was greater than 20 K to achieve a faster cooling rate.

Abdulateef et al. [44] used Fluent 15 software was used to numerically investigate the heat-transfer enhancement using various longitudinal fin configurations employing both a PCM and a nano-PCM in a large triplex-tube heat exchanger (TTHX). By spreading 10% to 25% alumina (Al_2O_3), the results demonstrated that the pure PCM's 0.2 W/m K thermal conductivity can be distinctly improved. In this way, the softening time diminished to (12%, 11% and 17%) for interior, interior outside, and outer fins, correspondingly, contrasted and the PCM instance with no nanoparticle. When compared to TTHXs with internal and internal-external fins-nano-PCM, the model with external fins-nano-PCM embedded in to a large TTHX improved the thermal performance by 14% and 11%, respectively, making it the highly effective model to achieve the whole melting of PCM in 188 minutes. For the PCM and nano-PCM, the simulation results were confirmed and in good agreement with the results of the experiments.

Rashid et al.[45] this study examines several more factors that influence the solidification enhancement of phase change materials (PCMs). These variables include the effect of employing various fin geometries, the temperature of the thermal fluid, heat exchanger length and pipes' diameters, the velocity of the coolant, the length and thickness of fins, fins' intensity, and the geometries of PCM units. Discussions center on findings and recommendations from earlier research. According to the outcome of this work, the solidification enhancement of PCM suggests plans for further research initiatives.

Aljibory et al.[46] In this study, heat transfer and fluid flow features were numerically and experimentally studied in a circular steel passage of length 50 cm with an outer diameter of 40 mm and inner diameter of 37 mm under a

constant surrounding temperature of 673 K for Reynolds numbers $Re=10,800$, 12,900, and 15,700, in order to simulate a gas turbine blade cooling passage. Turbulence was simulated using ANSYS - FLUENT (version 16.1), and the (k- ϵ) turbulence model was utilized. The rib constructions (of 5×10 mm equilateral triangular cross-section) were fixed inside the circular passage and diverged by 5 cm. The results of temperature and velocity distribution along the circular passage's centerline for the smooth passage were compared with those of a circular passage fitted with these enclosed ribs. An improvement in the rate of heat transfer, especially at $Re=12,900$, was observed in the tube with ribs, with a rate of heat transfer increase of 84.3% compared to the smooth case; the ribbed tube was also observed to have a greater performance factor for turbulent flow.

Summary of literatures review is depicted in Table (2.1).

Table 2.1: Summary of Literatures Review

Reference	Configuration	Studied parameters	Highlighted results/findings
Seddegh et al. (2016) [13] Type of Study: Numerical	Vertical and horizontal shell-and-tube on PCM RT(50)	The temperature change, total melting, and solidification time during the operations.	Convective heat transfer during horizontal charging significantly affects melting in the upper part of solid PCM but has a lesser impact on the lower half.
Hong et al. (2018) [14] Type of Study: Numerical	Two-dimensional rectangular cavity with thermally active components	Varies the cavity's aspect ratio from 0.5 to 2 and the inclination angle from 0 to 90°.	When the inclination angle is 90°, the aspect ratio has a significant impact on thermal behavior
Eslamnezhad & Rahimi (2017) [15] Type of Study: Numerical	Rectangular-finned triplex tube heat exchanger.	Triplex heat exchangers with fins.	The arrangement of the rectangular fins along the triplex tube heat exchanger is one of the most influential factors in the process of melting
Saeed et al. (2022) [16] Type of Study: Numerical	Pear-shaped with several Al ₂ O ₃ concentrations fin forms and fin materials.	Temperature contours, liquid fraction, Bejan number, average Nusselt number.	The melting time is reduced by 14% and 32%, respectively, when 6% of Al ₂ O ₃ nanoparticles and copper fins are used as opposed to pure PCM with steel 302 fins.

Reference	Configuration	Studied parameters	Highlighted results/findings
Nesrine et al. (2021) [17] Type of Study: Numerical	Two-finned annular tube heat exchanger with (PCM).	The consequence of the fins' orientation on melting rate, thermal conduction, and natural convection is explored.	The vertical fin system achieves superior heat transfer performance; Compared to the case for the horizontal fins, there was a 250% decrease in total melting.
Ahmed et al. (2022) [18] Type of Study: Numerical	Cylindrical tube with three fins.	Different inward cylinder positions, ($0 \leq \alpha \leq 3\pi/2$), and ($0 \leq \phi \leq 0.04$)	NePCM melting process was sped up by high values of the nano-additives concentration (0.4), larger values of the tube rotation angle ($3\pi/2$), and positioning of the tube in the lower position.
Hosseinzadeh et al. (2021) [19] Type of Study: Numerical	Triple-tube storage with novel fin configuration.	Solidification rate of PCM with a combination of hybrid nanoparticle (MoS ₂ - Fe ₃ O ₄)	Radiation parameter has a significant impact on the phase change rate, contributing to 74.58% of the full solidification process time (FST).
Maneengam et al. (2022) [20] Type of Study: Numerical	Hexagonal containers.	The number of heated suites.	The distributions of temperature, velocity and Bejan number increase when the heated wings are increased due to the improvement of buoyancy – convection phenomenon.
Sun et al. (2021) [21] Type of Study: Numerical	Triple-tube vertical heat exchanger with asymmetrical round fins.	Staggered circular fins' effect.	The insertion of circular fins with a staggered distribution had a significant impact on the time savings during the melting process.
Huang & Yao. (2021) [22] Type of Study: Numerical	New trapezoidal longitudinal fin	Fin arrangement.	The solidification time of the PCM was be reduced compared to the traditional quadrilateral fin by 45%.

Reference	Configuration	Studied parameters	Highlighted results/findings
Ghalambaz et al. (2021) [23] Type of Study: Numerical	Conical shell-tube with irregular fins was and NePCM	The shell's cone aspect ratio and the fin's aspect ratio and type of nanoparticles.	A simple tube filled with 4.5% alumina-Bio-PCM and 1.5% copper-Bio-PCM had a cone aspect ratio of 1.17.
Zarei et al. (2020) [24] Type of Study: Numerical	The triple-tube with fins	The effects of the presence, configuration, and dimensions of copper fins	Reduce the time required for complete solidification by approximately 42% when compared to the system without fins.
Pandiyarajan et al. (2011) [25] Type of Study: Experimental	Shell and finned tube heat exchanger to be integrated with an IC engine.	Cylindrical phase change material (PCM) capsules in a TES tank.	Recovers nearly 10–15% of the total heat that would otherwise be wasted. At full load, the heat exchanger can extract approximately 3.6 kW of heat.
Dutil et al. (2023) [26] Type of Study: Experimental	Four solid tubes with longitudinal fins	Different heights of fins, with various hole sizes and different angles.	Angles of 0° and 30° revealed a rapid rise in average temperature while charging, the best fin height was discovered to be 65% of the annulus and fins with hole sizes of 4 mm and 8 mm reduced pre-melting time by 12.65% and 3.16%, respectively, compared to solid fins
Karami & Kamkari (2020) [27] Type of Study: Experimental	Heat exchanger with perforated fin	The melting process of PCM under different inlet water flow rates and different temperatures.	The perforated finned heat exchanger's time-averaged Nusselt number is approximately 30% higher than that of the solid finned heat exchanger.
Awasarmol & Pise (2015) [28]	Heat exchanger with perforated fin	Perforated fin array with varying inclination degrees and perforation diameters.	A 32% improvement in heat transfer coefficient compared to solid fin arrays while simultaneously reducing material usage by almost 30% by mass.

Reference	Configuration	Studied parameters	Highlighted results/findings
Type of Study: Experimental			
Kamkari & Shokouhmand (2014) [29] Type of Study: Experimental	Rectangular enclosure with or without fins	Nusselt numbers, melt fractions, and heat transfer rates during melting	Increasing the number of fins enhanced the overall heat transfer rate and shortened the melting time, whereas the surface-averaged Reduced Nusselt number
Kamkari & Groulx (2018) [30] Type of Study: Experimental	Rectangular enclosures with different inclination angles fins.	Liquid fractions and heat transfer rates.	The 0-fin horizontal and 3-fin vertical enclosures improved heat transmission by 115% and 56%, respectively, as compared to the 0-fin vertical enclosure.
Kamkari et al. (2014) [31] Type of Study: Experimental	Various inclination angles in rectangular enclosure	Melt fractions, Nusselt numbers, and heat transfer rates.	The PCM's melting time and heat transfer rate are greatly influenced by the enclosing inclination.
Salem et al. (2023) [32] Type of Study: Experimental	Vertical shell-tube heat exchanger	The different cases of tube layers.	The charging time is reduced by 7.2%, 7.3%, 17.6%, and 11% when semicircular tubes are used instead of complete ones, the area ratio is increased from 2.4% to 4.3%, and the same number of tubes are distributed in two layers instead of one.
Lv et al. (2023) [33] Type of Study: Experimental	Four groups of tubes implanted with different fins.	Melting rate with different fins	The spiral fins had superior heat transfer, resulting in the highest outlet temperature, while the smooth tube exhibited the lowest performance.

Reference	Configuration	Studied parameters	Highlighted results/findings
Zou et al. (2023) [34] Type of Study: Experimental	Thermal Energy Storage Unit.	(LTESU), (STESU), and the LTESU combined with CFF.	Compared to STESU, LTESU has an 18.7% greater thermal efficiency. The thermal charging capacity, thermal discharging capacity, and thermal efficiency may all rise by 51.1%, 55.9%, and 10.8%, respectively, with the integration of CFF.
Majeed et al. (2022) [35] Type of Study: Experimental	Vertical LHTES with PCM	Impact of including a porous metal foam on the process of charging.	For the foamed and non-foamed TTHX, the total melting time was reduced by 43% at the same 69 °C HTF temperature.
Vogel & Thess (2019) [36] Type of Study: Numerical & Experimental	Rectangular box with a model fluid	Fluid flow, temperature, and phase state.	The liquid phase percentage and temperatures are predicted by the simulation with variances less than 4%.
Kumar & Verma (2020) [37] Type of Study: Numerical & Experimental	finned tube and horizontal shell.	The melting rate of PCM at various locations of the inner tube at angles.	A higher Stefan number accelerates PCM melting, and an eccentric annulus's heat storage rate is 18.7% more than that of a concentric annulus.
Qaiser et al. (2022) [38] Type of Study: Numerical & Experimental	Circular shell within three circular HTF tubes.	The impact of tube configurations and orientations	The PCM's melting rate by 27.2% and the LTESU's energy storage capacity by 3.72% in comparison to the basic model.

Reference	Configuration	Studied parameters	Highlighted results/findings
Z. Mahmoud et al. (2021) [39] Type of Study: Numerical & Experimental	Circular fins in triple-tube heat exchanger	Circular fin designs, sizes, and orientations.	When the fin orientation is downward-upward along the left and right sides of the PCM shell, the melting rate can be increased by 88% and the heat charging rate can be increased by 34% when compared to the basic case of finless.
Joulin et al. (2011) [40] Type of Study: Numerical & Experimental	A parallelepipedic polyefin envelope-conditioned PCM.	Comparison of a PCM's experimental and numerical findings	For the melting process, both numerical approaches demonstrated extremely excellent agreement with experimental findings ([less-than-or-equals, slant]5%).
Al-Abidi et al. (2013) [41] Type of Study: Numerical & Experimental	inside and outside fins in a (TTHX)	The (PCM) unit shape, TTHX material, Stefan number, fin length, fin thickness, and fin number.	In case G (8-cell PCM unit shape), the PCM melted faster, resulting in a 34.7% reduction in the overall melting time.
Muhammad et al. (2023) [42] Type of Study: Numerical & Experimental	A TES system built on a rock bed.	Analyses the main design factors and how they affect the charge efficiency and temperature profile.	The charging efficiency was shown to be between 77% and 94%.
Liu et al. (2019) [43] Type of Study: Numerical & Experimental	Longitudinal triangular in shell and tube (LHTES)	The fins' dynamic temperature response and the effects of their geometrical parameters.	Fin-C exhibited the best solidification performance and improved heat transfer efficiency. By lowering the starting temperature or raising the thermal conductivity and fin heights, the solidification period was shortened.
Abdulateef et al. (2017) [44] Type of Study: Numerical & Experimental	TTHX with longitudinal fins employing both a PCM and a nanoPCM	Spreading 10% to 25% alumina (Al ₂ O ₃)	The model with exterior fins-nano-PCM incorporated in a large TTHX enhances thermal performance by 14% and 11%, respectively, compared to TTHXs with internal and internal-external fins-nano-PCM. This makes it the most effective model for attaining total PCM melting in 188 minutes.

Reference	Configuration	Studied parameters	Highlighted results/findings
Rashid et al.(2023) [45] Type of Study: Numerical & Experimental	Various fin geometries	The temperature of the thermal fluid, heat exchanger length and pipes' diameters and the velocity of the coolant.	According to the outcome of this work, the solidification enhancement of PCM suggests plans for further research initiatives.
Aljibory et al. (2018) [46] Type of Study: Numerical & Experimental	Circular steel passage	Triangular cross-section) were fixed inside the circular passage and diverged by 5 cm.	An improvement in the rate of heat transfer, especially at $Re=12,900$, was observed in the tube with ribs, with a rate of heat transfer increase of 84.3% compared to the smooth case; the ribbed tube was also observed to have a greater performance factor for turbulent flow.
The present work	TSCTSU with internal and external longitudinal fins	Various fins case and material	The melting rate is enhancement when using the external and internal longitudinal fins in TSCTSU.

The primary focus of this study was on the internal and external thermal performance of a TSCTSU (Triplex Square Channel Thermal Storage Unit). The effect of mass flow rates on PCM melting and the procedure of PCM charging beneath the non-steady and steady heat transfer fluid-inlet temperatures were the issue of experimental and numerical study for various PCM kinds.

According to the literature survey, despite the numerous research on melting enhancement in triple-tube energy storage unit, no prior results on the problem of improving melting enhancement in this system for the laminar fluid flow range are accessible to the authors' knowledge. As a result, this research aims to see how fins affect the heat transfer in the wax. The influence of several relevant factors, like velocity of HTF, material of storage unit and cases of fins will be investigated.

Chapter Three: NUMERICAL MODELING and SIMULATION

3.1 Introduction

The charging process of an LHS system is numerically modeled and simulated in this chapter. The goal of numerical analysis is to comprehend the operation of the thermal system. Ansys-Fluent is an application of commercial software that uses computational fluid dynamics models to understand the research. This uses the enthalpy approach to account for the melting phenomena. Numerical analysis is done for the thermal behavior of the LHS system. The LHS system has been enhanced with fins on inner and middle tubes (of varying numbers), and its PCM has also been subjected to various inlet and mass flow rates. The goal of this chapter is to anticipate a thermal energy storage design performance.

3.2 Numerical Simulation

Horizontal LHS with fins geometries are created using commercially available software Ansys Design Modeler to solve the continuity, momentum, and energy equations in order to investigate and examine heat transfer fluid flow, and PCM melting time and temperature in the thermal energy storage. Geometries are appropriately meshed, and the mesh size is decided after grid sensitivity test. These meshed geometries are then solved using Ansys-Fluent.

This analysis is executed for triple square channels latent heat storage to visualize the outcome of operating/geometric parameters such as inlet temperature of HTF and mass flow rates during the charging process.

Also, analysis is extended to LHS with different fin geometries. The simulated results are validated with experimental ones. The simulation is done for both RT42 and RT64 PCMs. The RT42 material was implemented and simulated in different seven cases with different fin configuration and arrangements. The RT64 was investigated in only no fins (case A) and eight fins parting the PCM into separate portions (case G). Figure (3.1) illustrates the different configurations investigated in this work.

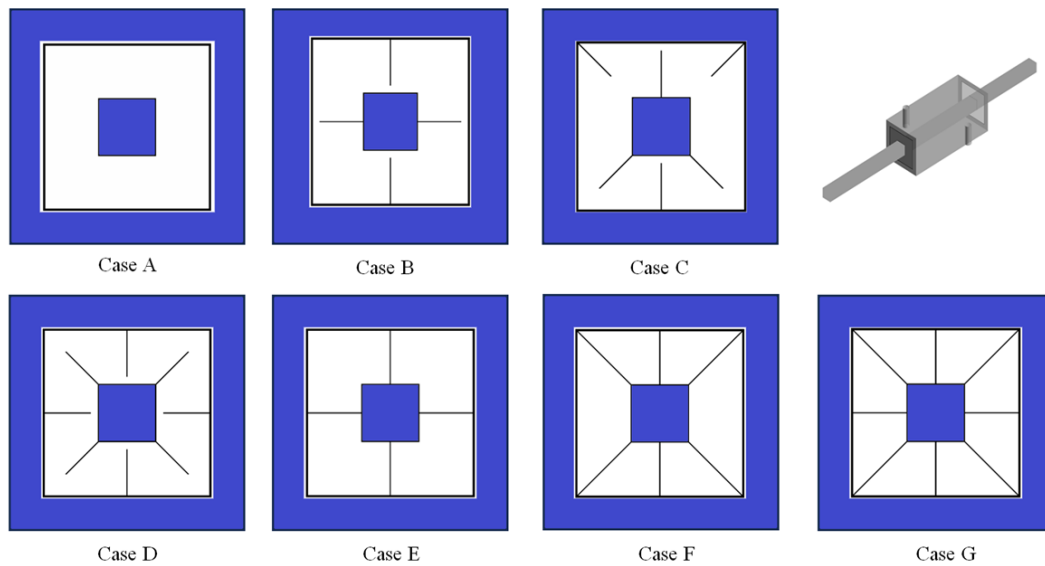


Figure 3.1: Models and fin configurations.

3.2.1 Simulation of numerical model

Engineers can use CFD techniques to examine complicated fluid flows that cannot be solved analytically. Numerical approaches may be used to address three fundamental notions of that regulate the physical fluid in diverse engineering systems: Momentum, mass, and energy conservation. The definition of governing equations with convenient assumptions may be done by using an integral of a mathematical equation or a partial term of a differential equation. Most of the time when dealing with fluid mechanics

problems, CFD discretizes these equations into an algebraic form and solves them numerically in time or space at a discrete point to provide unique fluid flow values and heat transmission, regardless of the complexity of boundary conditions of flow geometry.

3.3 Design Considerations

Refer to the factors and aspects that engineers and designers take into account when designing a system, product, or process. These considerations are essential for ensuring that the design meets the desired objectives, functions effectively, and is safe, reliable, and cost-effective. Using the hydraulic diameter law, the dimensions of the triple-square channels were calculated based on the dimensions taken from the [41]. Where were the inner tube radius (r_i) is 25.4 mm with 1.2 mm thickness, the middle tube radius (r_m) is 75 mm and the outer tube radius (r_o) is 100 mm; with 2 mm thickness [41].

3.1

$$D_h \text{ for } W_o = \frac{4 \times 200}{4 \times (200)^2} = 200 \text{ mm}$$

$$D_h \text{ for } W_m = \frac{4 \times 150}{4 \times (150)^2} = 150 \text{ mm}$$

$$D_h \text{ for } W_i = \frac{4 \times 50.8}{4 \times (50.8)^2} = 50.8 \text{ mm}$$

3.3.1 Computational model building

Fluent is based on finite-volume approach, which has the same sequence required for analysis as other discretization approaches:

1. Geometric design
2. Mesh generation
3. Specification of material properties

4. Defining the boundary conditions
5. Using an appropriate solver to solve the model
6. Post-processing

In the simulation of the present model, the above will be followed. In the case of modeling, those steps will be followed. For every engineering issue to be solved, the following key parameters that influence numerical solution are specified as:

- A- **Modeling Geometry:** It is an express used to describe a fluid's physical shape and the direction that it flows.
- B- **Boundary condition:** This is an essential aspect of the model because it defines the sections of the surface that make up the actual geometry, such as inlet and outlet parts for fluid flow.
- C- **Mesh generation:** The process of dividing a complete component into multiple components refers to this. ANSYS FLUENT will use networking according to the form of the structure and the degree of complexity.
 - **Geometry designing:** SolidWorks has been employed for modeling the 3D domain of triple square channels thermal energy storage (TSCTES) with and without fins before transferring them to Ansys Design Modeler regimes being modeled with control volumes constructed around every grid. This section presents both simple and complex geometric shapes. The first choice for designing the test model is the x-y plane. The test model's three-dimensional structure is then obtained by applying an extrude order, which has been used as a preprocessor for Fluent in the ANSYS workbench program. The test models'

geometrical dimensions match those for the investigational setup, as given in the Table (3.1). Also, the three-dimensional geometrical models of the three systems are depicted in figure (3.2).

Table 3.1: Geometrical dimensions of the thermal energy storage.

Parameters	Dimensions
Outer channel	(200×500×2) (mm)
Middle channel	(150×480×2) (mm)
Inner channel	(50.8×1400×1.2) (mm)
Fins	(47.6×480×1) (mm)
Thickness of insulation	(70) (mm)
Air mass flow rate	(4,5,8,10,16 and 24) kg/s

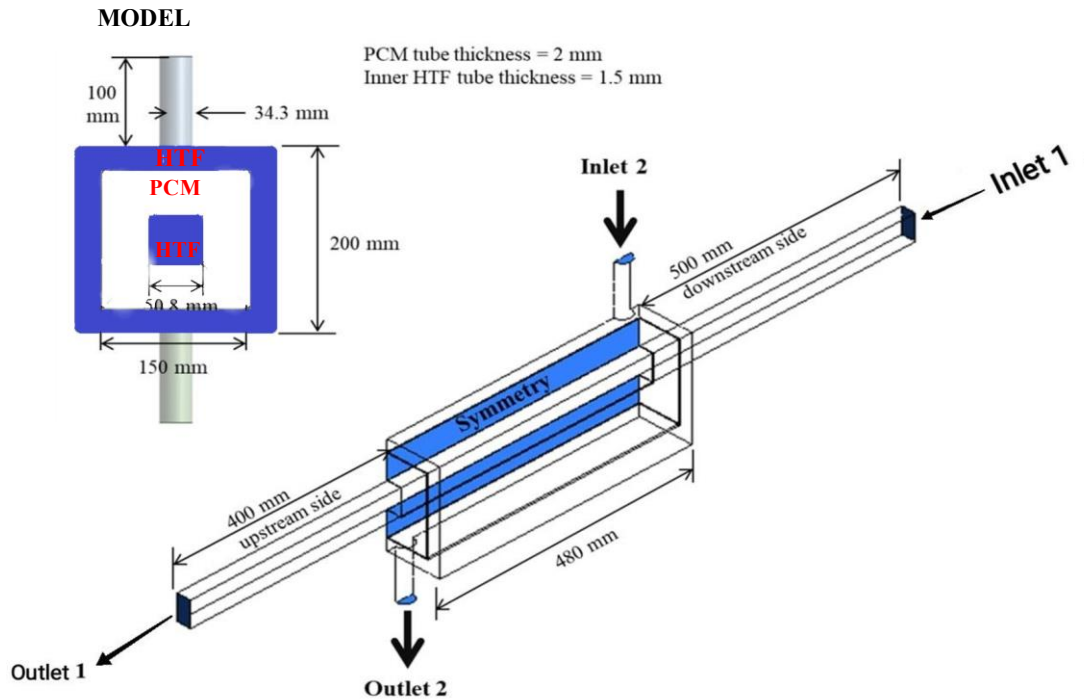


Figure 3.2: The 3D geometric model of thermal energy storage.

- **Meshing:** Meshing is the process of breaking up a geometry into several parts and nodes. As a result, the load may be spread evenly over the geometry when it is applied. The time needed to provide an accurate answer grows as the number of nodes and elements rises (for example, elements get smaller). The use of fine-sized hexahedral elements is utilized to create a high-quality mesh for each channel wall and fin. Fluent simulations require the right computational mesh for the domain beneath the analysis to be generated. Therefore, the size of mesh in domain has to be gradually augmented to a degree where the addition of more control volumes does not significantly alter the theoretical findings produced. Also, the numbers of nodes and elements in the present investigation are listed in Table (3-2).

Table 3.2: Mesh settings and information.

Methods	Edge sizing and multizone methods
Number of elements	See Table 3-3
Number of nodes	See Table 3-3
Growth rate	1.2
Bounding box diagonal	1.6813 m
Average surface area	1.6721e-2 m ²
Minimum edge length	1.2e-3 m

The following Table 3-3 shows the number of elements and nodes as per each configuration. The schematic of generated 3D mesh of thermal energy storage is depicted in figure (3.3).

Table 3.3: Mesh count per each case.

Case	A	B	C	D	E	F	G
Elements #	290550	252330	320460	341310	324165	290598	355034
Nodes #	1242096	1097168	1384485	1486860	1397891	1252953	1548385

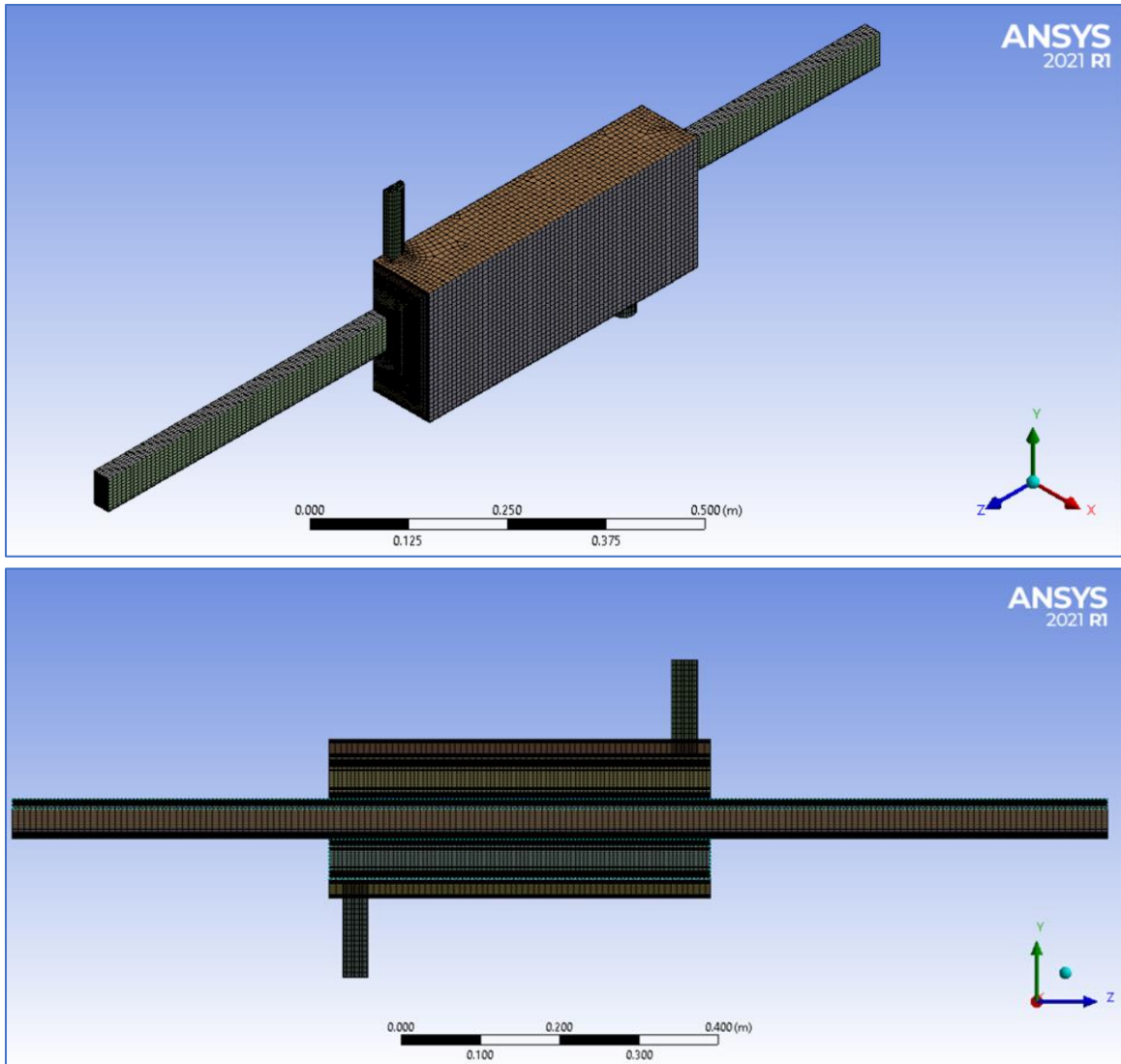


Figure 3.3: The schematic of the created three-dimensional mesh of thermal energy storage.

3.4 Assumptions

The following assumptions are made:

- The channel domain is filled completely with the PCM (paraffin wax RT-42 and RT-64).
- Melting of the PCM is homogenous, incompressible and Newtonian fluid. Also, the PCM flow is considered laminar and unsteady.

- c. There is no gain or loss of heat (the exterior surface of the LHS unit can be regarded thermally insulated).
- d. The perfect contact is between fins and base channels.
- e. The viscous dissipation is considered to be negligible.
- f. The solid in the mushy region is homogeneously distributed.
- g. The ambient temperature is 28 °C (301 K).
- h. Reference temperature is 15 °C (288) K and reference pressure is 101325 Pa.
- i. During melting, the effect of natural convection is considered.
- j. The properties of PCM are supposed to remain constant excluding the density variation with the temperature where the buoyancy forces are based Boussinesq approximation.

3.5 Governing Equations

The respective governing equations employed for thermal energy storage are as follow[47]:

I. Continuity equation:

$$\frac{\partial \rho}{\partial t} + \nabla \cdot \rho \vec{V} = 0 \quad (3.2)$$

II. Momentum equation:

The momentum equations are derived from Newton's Second Law of Motion, which involves balancing the forces that act upon the element of fluid. Such forces are equivalent to the product of fluid element mass and acceleration.

$$\rho \frac{\partial \vec{V}}{\partial t} + \rho (\vec{V} \cdot \nabla) \vec{V} = -\nabla P + \mu (\nabla^2 \vec{V}) - S_u \quad (3.3)$$

III. Energy equation:

The 1st thermodynamics law illustrates how the applied work and heat transport through an area result in an exchange of energy for that system. Incompressible flows have a constant density, so the energy equation can be written as follows:

$$\frac{\partial}{\partial t}(\rho H) + \nabla \cdot (\rho \vec{v} H) = \nabla \cdot (k \nabla T) \quad (3.4)$$

Where ρ, μ, \vec{v} and k are the density, viscosity, fluid velocity and the thermal conductivity of PCM, respectively.

The body force term in momentum equation is modeled by considering the Boussinesq approximation based on a reference density (ρ_{ref}) and temperature (T_{ref}), and the thermal expansion coefficient (β). The effect of natural convection on the phase change process of PCM is due to its density change (s_D) and Earth's gravity (s_g) as follow as: -

$$\mathbf{s}_u = \mathbf{s}_D + \mathbf{s}_g \quad (3.4 a)$$

$$\text{and } \mathbf{s}_D = \mathbf{g} \beta \rho_{ref} T_{ref} (\mathbf{T} - T_{ref}) \quad (3.4 b)$$

$$\text{also, } \mathbf{s}_D = \frac{-1}{\rho} \left(\frac{\partial \rho}{\partial T} \right) \mathbf{P} \quad (3.4 c)$$

3.5.1 Enthalpy–porosity method

In order to solve the PCM melting problem, the enthalpy-porosity approach was employed. The methodology is based on the liquid fraction, which compares the liquid volume to the overall volume of the storage container. The domain of the storage unit will be separated computationally into three regions: solid, liquid, and mushy zone. The enthalpy-porosity technique treats the mushy (partially solidified) area as a porous material.

Each cell's porosity is fixed to equal one to its liquid percentage. In totally solidified areas, the porosity is zero. The solid-liquid contact region is known as the mushy zone, and it serves as a barrier between the two phases. Porosity is represented by a liquid fraction f , as stated in [48], [49].

$$f = \begin{cases} 0, & \text{if } T \leq T_s \\ \frac{T-T_s}{T_l-T_s} & \text{if } T_s \leq T \leq T_l \\ 1, & \text{if } T \geq T_l \end{cases} \quad (3.5)$$

The terms T_s and T_l refer to the solidus and liquidus temperatures of PCM, respectively. The local temperature is represented as T .

The total enthalpy (H) is the sum of sensible enthalpy (h) and latent enthalpy (ΔH) and may be represented using equations:

$$H = h + \Delta H \quad (3.6)$$

Where ,

$$h = h_{ref} + \int_{T_{ref}}^T C_p dT \quad (3.7)$$

Where h_{ref} is the sensible enthalpy of PCM at T_{ref} , C_p is the specific heat at constant pressure, and L is the latent heat of PCM.

The S source term, often known as the Darcy term in momentum equation (3-2), is a crucial treatment method for the mushy zone.

$$S_D = \frac{(1-f)^2}{f^{3+\varepsilon}} V A_{mush} \quad (3.8)$$

To prevent division by zero, the ε constant ε is set at 0.001. Also, the mushy zone constant A_{mush} is a constant value ranging from 10^4 to 10^7 [50], referring to the melting front's shape.

3.6 Setup and Solution

3.6.1 Boundary conditions and operating parameters

The inlet boundary conditions are identified as the inlet water temperature and the inlet mass flow rate of water. The outlet is subjected to the application of the outflow boundary condition. At first, the PCM is thought to be a solid state and has a temperature of 311.15 K to make sure that melting begins as the simulation begins. However, the HTF temperature is represented by the constant temperature of the channel wall, which is 353.15 K, individually. To formalize the TSCTSU's limits, one can do the following:

$$\text{At } w = w_i \rightarrow T = T_{HTF} \quad (3.9)$$

$$\text{At } w = w_o \rightarrow T = T_{HTF} \quad (3.10)$$

The three models' initial temperatures will be:

$$\text{At time} = 0 \rightarrow T = T_{ini} \quad (3.11)$$

The momentum, continuity, and energy equations are non-linear partial differential equations, subjected to the following initial and boundary conditions. The initial conditions of PCM and HTF temperatures are kept 311.15 and 343.15 K, respectively. Boundary and initial conditions are shown in Figure (3.4), while the details of material properties are given in Tables (3.4) and (3.5). A symmetry boundary condition is defined to reduce the computational grid and required solution time. An outflow boundary condition is used on the outlet for backflow prevention on the outlets. The interfaces between the solids and liquids are manually applied.

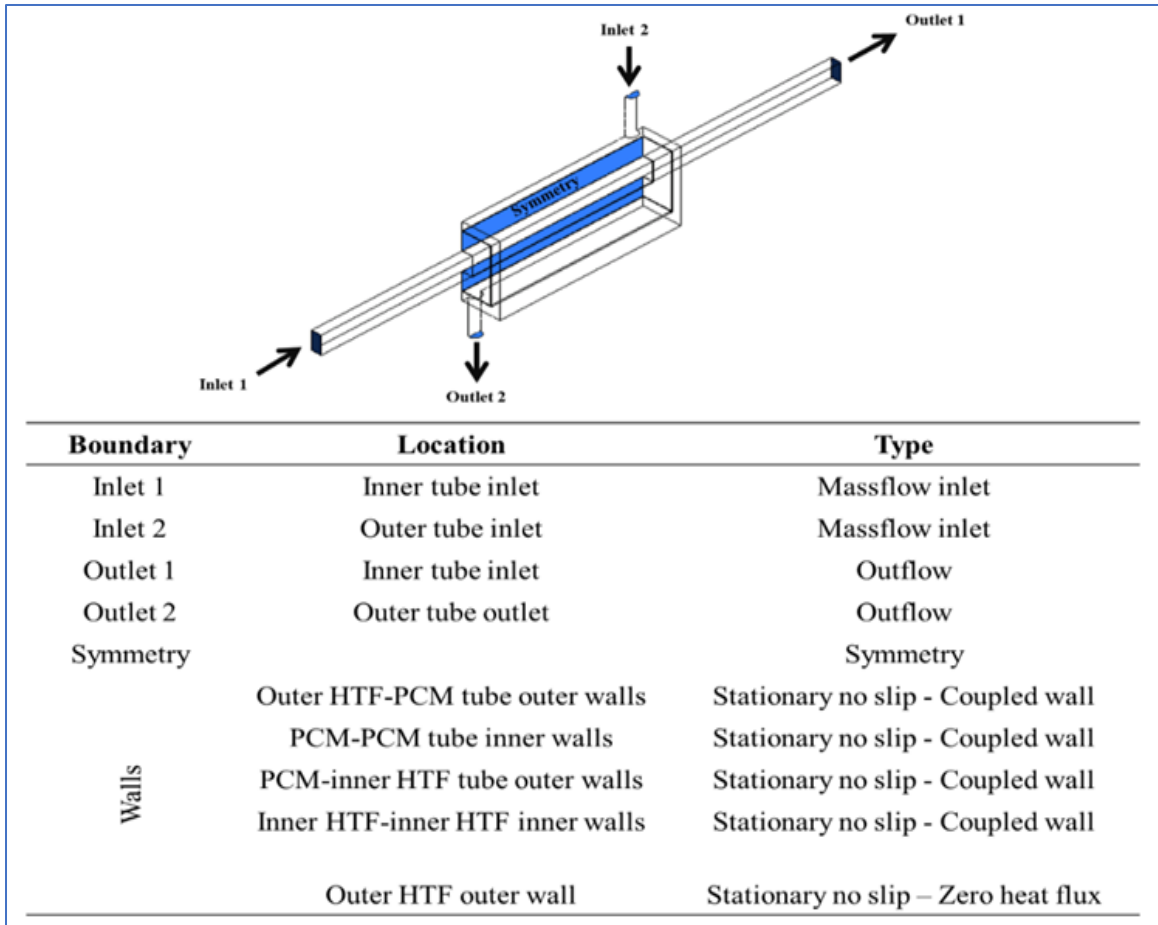


Figure 3.4: Boundary conditions.

Table 3.4: Properties of Steel, Copper and Water. [41]

Material properties	Steel	Copper	Water
Density (kg/m^3)	8030	8978	998.2
Specific heat (J/kg K)	502.48	381	4182
Thermal conductivity (W/m K)	16.27	387.6	0.6
Viscosity μ (kg/m.s)	-	-	0.001

Table 3.5: Properties of RT42 and RT64HC. [41]

Properties	RT42	RT64HC
Density (kg/m ³)	760	780
Specific heat, C_p (J/kg.K)	2000	2000
Thermal conductivity, k (W/m.K)	0.2	0.2
Viscosity, μ (kg/m.s)	0.02351	0.0035
Thermal expansion coefficient, α (1/K)	0.0005	0.000545
Pure solvent melting heat (J/kg)	165000	250000
Solidus temperature (K)	311.15	334.15
Liquidus temperature (K)	315.15	337.15

- **Setting of Simulations:** Input parameters (solver settings) tell the methodology for solving the Ansys-Fluent program how to compute the solution required. The technique for thermal analysis utilizing an ANSYS (Fluent) program must be specified. In the current work, the unsteady state has been chosen. The first stage in the solution methodology is the ways of solution. The fluid in the thermal energy storage is examined using the workbench Fluid Flow (Fluent), which also addresses the issue of heat transmission. The program is used to simulate the situation mentioned above, and this involves defining the boundary conditions and giving the software the necessary data, such as the properties of the wax and the water, among other things.
- The gravitational acceleration is set to 9.81 m/s^2 to guarantee the presence of body forces and buoyancy as density changes.

However, the simulation where the interfaces between more than a phase, or where there are changes/variations in density, and gravitational acceleration, must be considered. A pressure-based solver is used with least-square cell-based gradient, PRESTO! pressure formulation, QUICK momentum formulation, second order upwind energy, and first order upwind turbulent kinetic energy and specific dissipation rate.

- The operational reference conditions are kept as default at 288 K and 101325 Pa, gravity in -Y direction, without specifying operating density. The Boussinesq model is used to formulate the density change over time with the change in temperature depending on the thermal expansion coefficient. Regarding the viscous model and according to the classification of each case of flow rate based on the Reynolds number calculations into laminar or turbulent, the laminar or SST k-omega models are used with low Re-correction. See figure (3.5)
- Appendix (A) explains in detail the steps for working on the ANSYS FLUENT program.

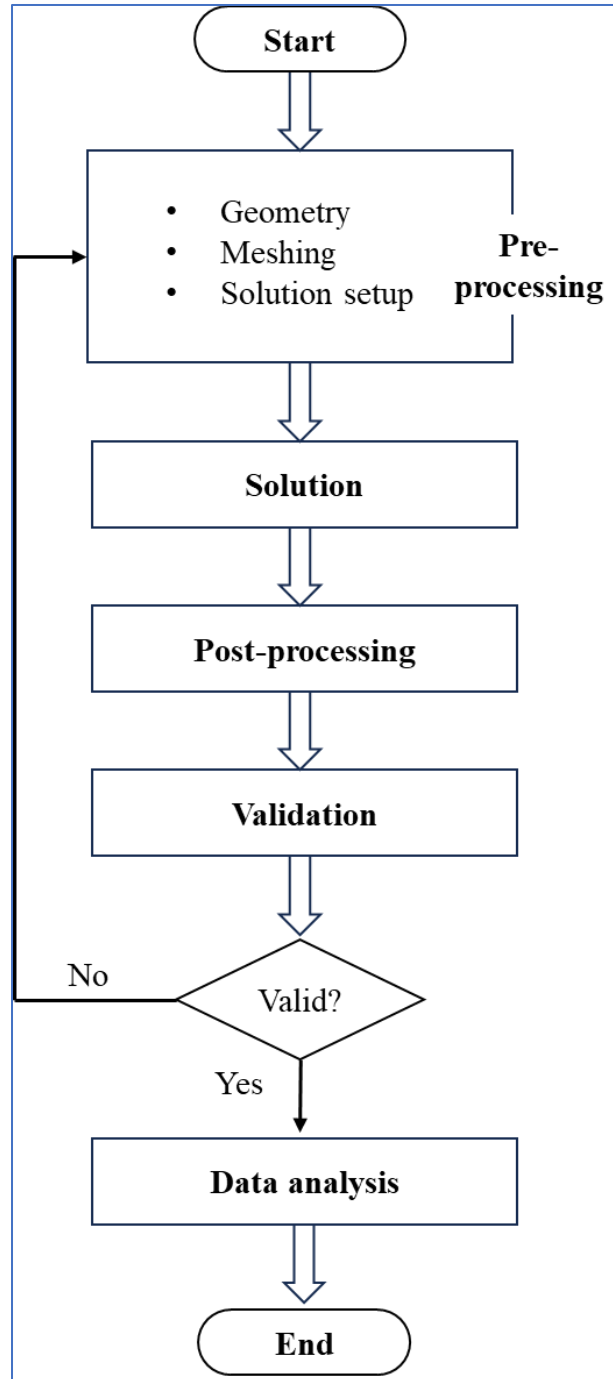


Figure 3.5: The schematic diagram of the flow chart steps of computational model constructed via employing ANSYS-FLUENT software

3.7 Mesh independency

In numerical simulations, it is crucial to define the mesh count, i.e., the number of cells at which the numerical solution is brought to stability, or the results are slightly changing in a permeable limit. This is called as well mesh independency/convergence study which aims to determine if the solution and convergence are mesh independent or not. However, this is more suitable for steady-state simulations where only the final result is of interest. In this transient/time-changing simulation, three different increasing meshing are used for the baseline finless case by increasing the number of divisions in the HTFs as well as PCM each time taking into account the longitudinal/axial length of the hexagonal cells.

The following Table (3.6) and Figure (3.6) reveal the differences between the different test cases, respectively.

Table 3.6: Differences between different levels of mesh refinement.

Mesh count	Temperature at 15 min. (K)
159839	315.66
266261	315.97
434750	316.46

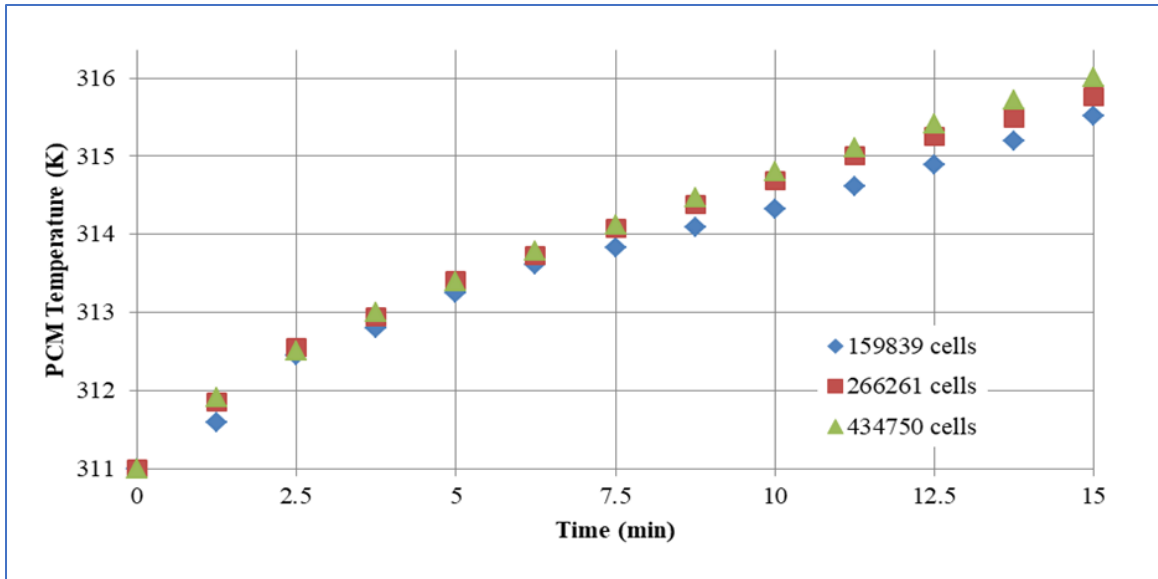


Figure 3.6: PCM temperature vs. time for different meshes.

It is noticeable that the maximum difference between any two cases is less than 0.5 K which is relatively acceptable. Thus, a different mesh is used for each case individually depending on its geometry due to the existence of fins. The chart above shows that there is more convergence in the most of the results between the 266261 and 434750 cases.

3.8 Validation

The numerical outcomes of Mat et al. [51] were applied to the code to validate it. The impact of fins affixed to the PCM zone (RT58) inners and outer surfaces in a triple-tube TES unit was investigated experimentally in the work by Mat et al. Three (500 mm) long copper tubes in a circle made up the device. The walls of the middle and outer tubes were 2 mm thick, while the walls of the inner tube were 1.2 mm thick. The PCM was housed in the middle tube, which was also used for circulating the water acting as the HTF into the other two tubes. Furthermore, the mentioned study's beginning and boundary conditions were employed in the current study's validation. Figure (3.7)

compares the results of the two investigations. This graph shows that the trust is at an extremely high level about 98%. These comparisons attest to the accuracy of the procedure.

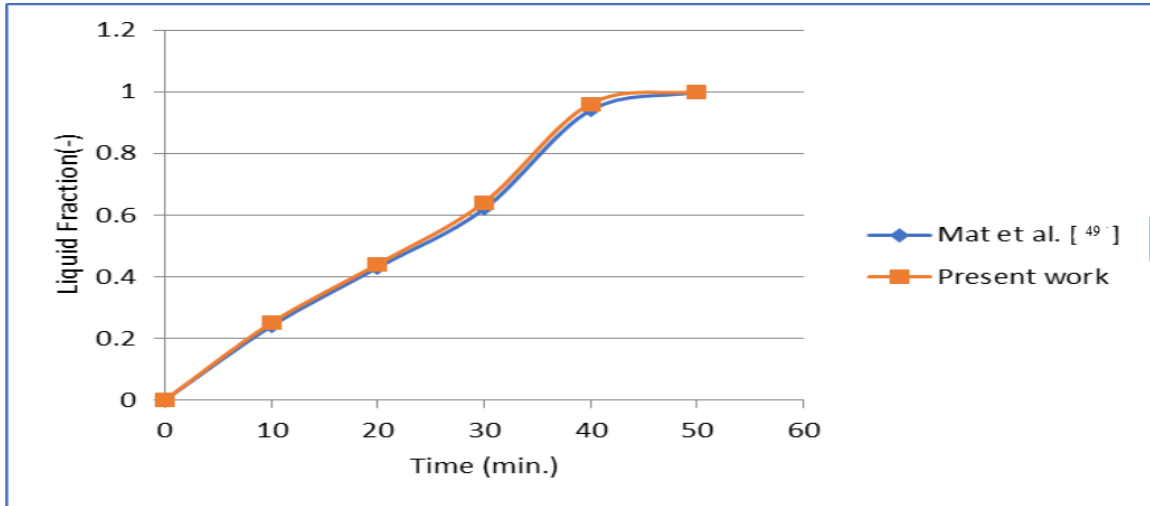


Figure 3.7: Verification of the numerical results.

3.9 Closure

The LHS contains melting processes that are successfully simulated. Simulations are conducted for a horizontal concentric square channel with an LHS and an LHS with external and internal longitudinal fins. The problem is defined, and the assumptions are made. An enthalpy-porosity technique is used for modeling the melting process. Horizontal square channel LHS, LHS with longitudinal fin, and PCM are simulated using commercial CFD code.

Chapter Four: Experimental Work

4.1 Introduction

This chapter presents a detailed description of the design and building of an investigational setup for studying the optimum model performance of a triple-square channel thermal energy storage unit using paraffin wax) RT64) with and without fins. All practical experiments and system construction were conducted in the laboratories of the Mechanical Engineering Department - College of Engineering - University of Karbala.

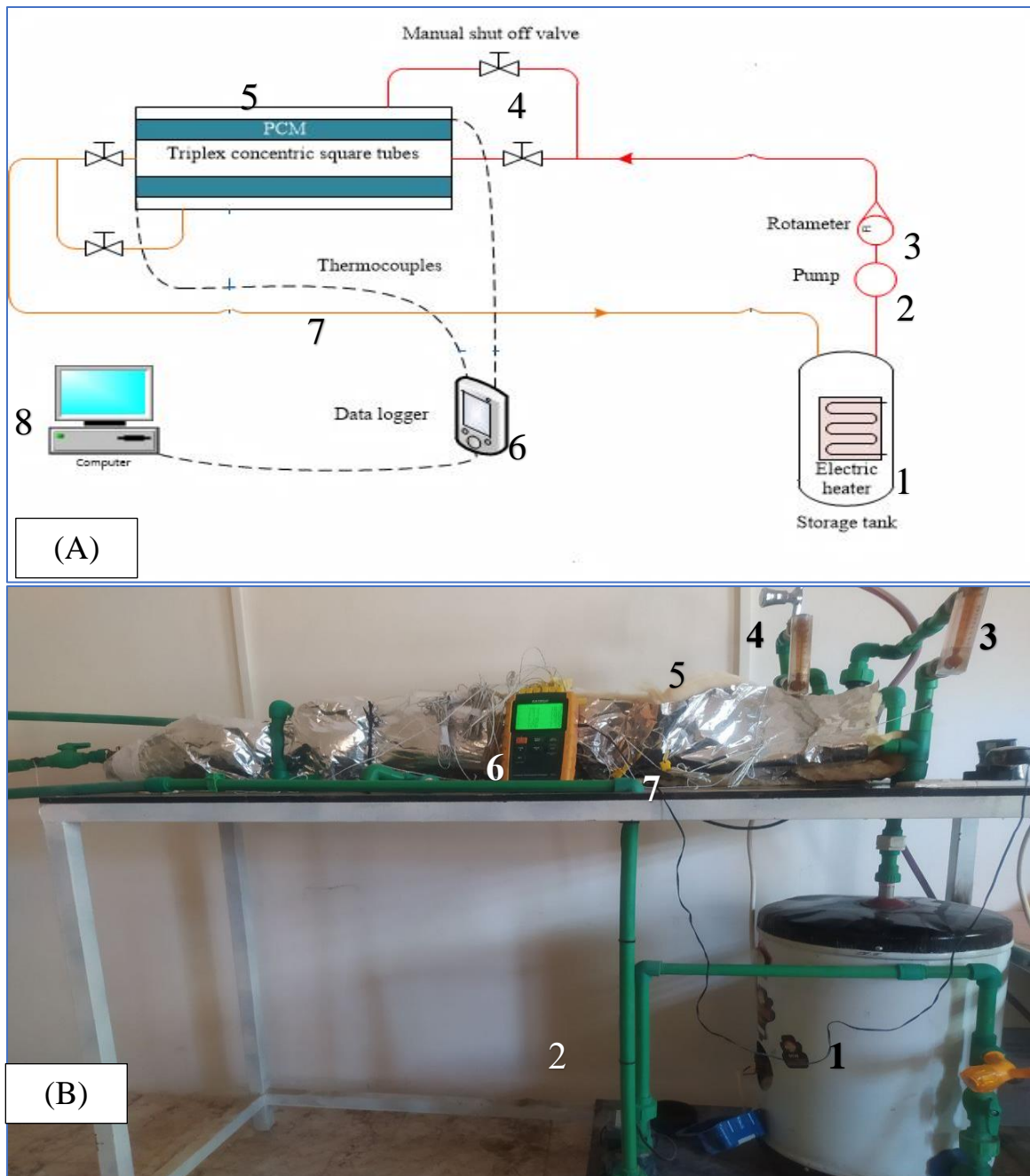
4.2 Designing and Constructing the Rig

The sections below provide a description of the experimental procedures which are carried out as follows:

1. The prototype of the thermal energy storage system was designed and manufactured after reviewing the previous literature. The previously unused triples square channels were proposed.
2. Some equipment was purchased, the necessary calibration was performed in the laboratories of the Quality Control and Measurement Unit in Baghdad, after which it was installed and equipped in the Laboratory of the Department of Mechanical Eng. at the University of Kerbala, College of Engineering, and the experimental work was conducted.
3. Ensuring the accurate manufacturing of the test rig, and making sure there is no leakage through the test rig parts.

4.3 Experimental Setup

The Base Case TSCTSU's a schematic diagram and experimental apparatus are shown the Figure (4.1).



(A)

(B)

Figure 4.1: (A) The schematic of investigational setup and (B) The physical setup of investigational facility

It comprises a hot water reservoir (1), a pump for circulating the hot water (2), a rotameter (3), and manually operated valves for controlling the flow (4) the water was utilized as an HTF. Also, shell and tube type LTESS with internal

and external longitudinal fins (5), data logger (6), thermocouples (7) and personal computer (8). For ensuring the totally developed flow at the LTESS inlet, the length of HTF tube was prolonged sufficient at the inlet. The HTF tube was supplied with hot water using a 400 W pump, which provides different flow rates. Likewise, the PCM temperature was measured at various cross sections via putting fifteen thermocouples (K-type) with an error in a (± 1 K) range at a (10 mm) distance from the shell, as shown in Figure (4.2). By adding two more thermocouples to the heat storage system's outlet and inlet, it is possible to measure the temperature drop across the LTESS.

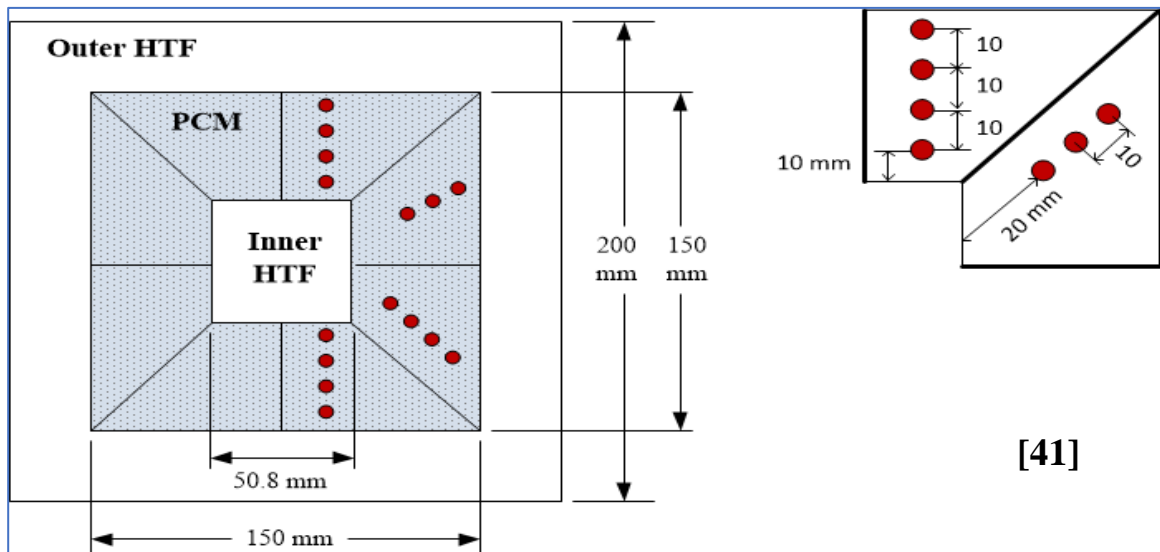


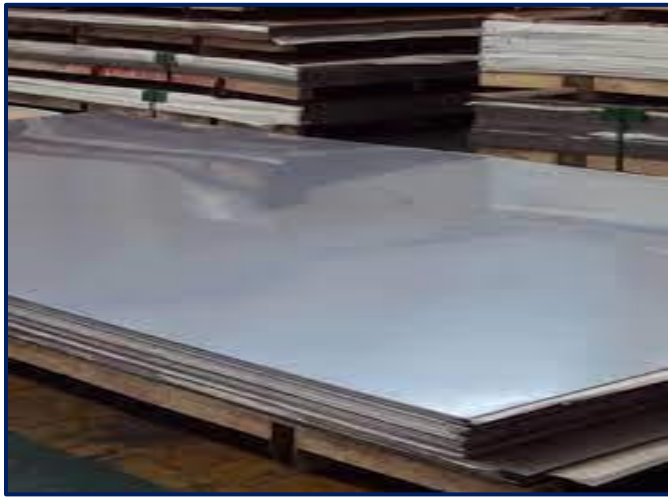
Figure 4.2: Locations of thermocouples.

4.4 Rig Building Steps

1. Purchasing three sheets of stainless steel (304) with a thickness of (1, 1.2, and 2) mm from the local market in Baghdad, as depicted in figure (4.3a).
2. Getting a 25 Kg of paraffin wax (RT64) from the Dora refinery.
3. Cutting and crimping the panels in a square shape with the agreed measurements and dimensions, where the inner channel (w_i) is 50.8 mm wide and 1.2 mm thick, while the outer channel (w_o) is 200 mm wide,

and the middle channel (w_m) is 150 mm wide. All tubes are 2 mm thick to ensure a good thermal conductivity as well as improve the heat transfer between HTF and PCM, as shown in figure (4.3b & 4.3 c).

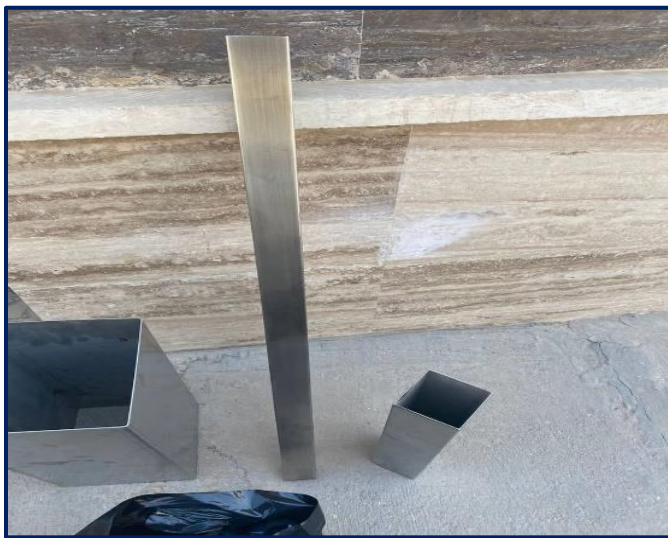
4. Cut 8 slices of stainless steel 304, representing the number of fins dimension (47.6×480) mm, as shown in Figure (4.3d).
5. Welding all channels one inside the other, where the system includes with and without fins. Distributing and installing thermocouples inside the middle channel to measure the melting point of the wax in specific locations, as revealed in Figure (4.2). In the case of fins, four fins are installed inside the middle channel and four others are fixed on the surface of the inner channel for creating a discrete geometry of PCM unit for filling with PCM, as shown in figure (4.4).
6. Pouring the wax into the middle channel, as shown in Figure (4.5).
7. Welding the sides of the channels in order to close them, as displayed in Figure (4.6). The volume occupied by the PCM was 0.00725707 m^3 . Converting these values to mass, depending on the PCM density, there was 5.66 kg of material stored in the equipment.
8. Connecting two flowmeters to the water entry of the external and internal channel. Then, preparing the water pipes of the system for the entry and exit of water, and they are connected to the pump and the electric heater, as shown in figure (4.7).
9. Covering the PCM thermal energy storage with 70 mm thick glass wool insulation to reduce the heat losses and achieve an adiabatic surface, as illustrated in figure (4.8).



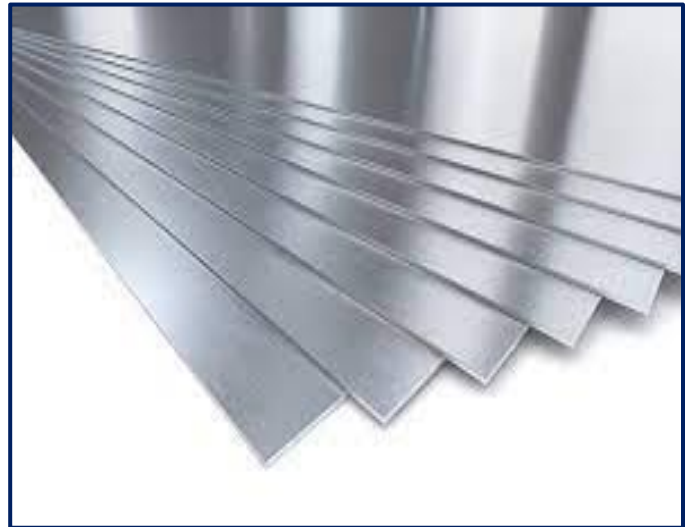
(a)



(b)



(c)



(d)

Figure 4.3: (a) Supplying the required parts, (b & c), the stages of cutting, crimping, and the final shape of the channels, and (d) Fins form.



Figure 4.4: Channels manufacturing steps with installing the fins.



Figure 4.5: Wax casting process.



Figure 4.6: Final form of TSCTSU



Figure 4.7: Preparing the water source and connecting it to the pump, heater and TSCTSU



Figure 4.8: Cover the device with insulator and operate it.

4.5 The Mechanism of Working

The experiment was carried out during the months (May, June, July), where different mass flow rates were studied (5, 8, 16, 24) l/min in cases with and without fins at a temperature of 80 degrees Celsius. At the beginning, the pump is operated to ensure that the flow meters are working and set to the required mass flow rate. The electric heater is turned on and its thermostat is set to a temperature of 80 degrees Celsius for half an hour, after which the pump is turned on to heat the material inside the thermal storage system for a quarter of an hour, and then the pump is turned off while the heater remains working with the use of the data logger and thermocouples installed inside it to monitor the temperature of the water entering the system.

When the required temperature is reached, the heater is turned off, the pump is turned on, and a period of five minutes waiting for the flow to stabilize within the system. Also, the temperatures for the entry and exit of the water and the temperature of the thermocouples fixed with paraffin wax is recorded to determine the time required for the complete melting of the wax every ten minutes. When the wax becomes completely liquid, the pump and the rest of the parts are turned off.

4.6 Measurement Instrumentations

The experimental work includes a variety of measuring instruments, as listed below:

4.6.1 Temperature measurement

Thermocouples and temperature recorder sensors were used for monitoring the variation of temperature through the TES regime operating.

I. Temperature recorder

The thermocouples reading was recorded using a Digital Temperature Recorder (Lutron BTM-4208SD, SD memory card, 12 channels), as depicted in figure (4.9 A). The data may be stored on an SD memory card and then transferred to a spreadsheet. A prediction's accuracy of this device is $\pm(0.4\%+0.5)^{\circ}\text{C}$.

II. Thermocouples

The twin wire thermocouples (K-type), Nickel Cr/Ni aluminum wires were insulated by elevated temperature glass, as revealed in the Figure (4.9 B). These instruments were utilized for measuring the particular locations' temperature into the inlet, outlet, and middle channel of wax system. The accuracy of device is $\pm 0.25^{\circ}\text{C}$.

4.6.2 Flow rate measurement

Two of the flow meters, kind LZM (1-18) litter/min, were used for measuring the rate of the flow of water, as evinced in the Figure (4-10).

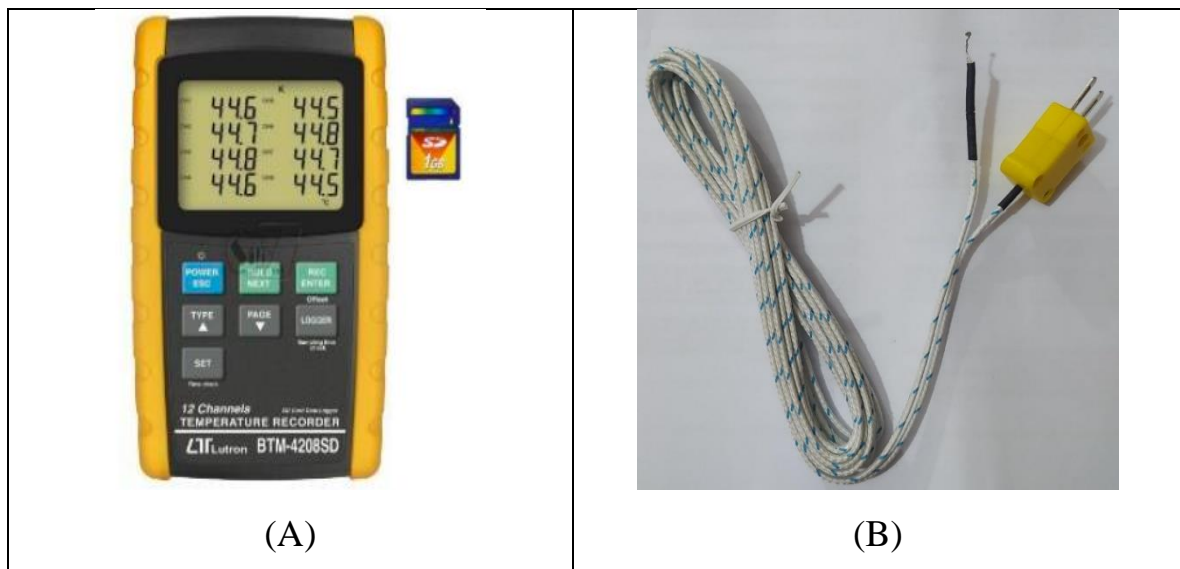


Figure 4.9: (A) Temperature Recorder. (B) Thermocouple Type (k) Type Lutron BTM-4208SD



Figure 4.10: Flow Meter Type LZM.

4.7 Calibration

The Renewable Energy Directorate of the Ministry of Science and Technology as well as the Central Organization for Standardization and Quality Control Metrology/Physics Section calibrated the following measuring equipment:

- Thermometer type Lutron BTM-4208SD.
- Thermocouples.

The results of the calibration of the thermocouple device are given in Appendix (B).

A graduated cistern filled with water that was released from the experimental setup at a certain flow rate was used to calibrate the flow meter that was employed for measuring the rate of the flow of water. The time of the water reached a specific point in the balloon was recorded. The operation should then be carried out three times, and Figure (4.11) shows how the mean values were expressed in a curve using the readings of flow meter. Also, in Appendix

(C), the cooling water flow rate measurement's uncertainty calculation is displayed.

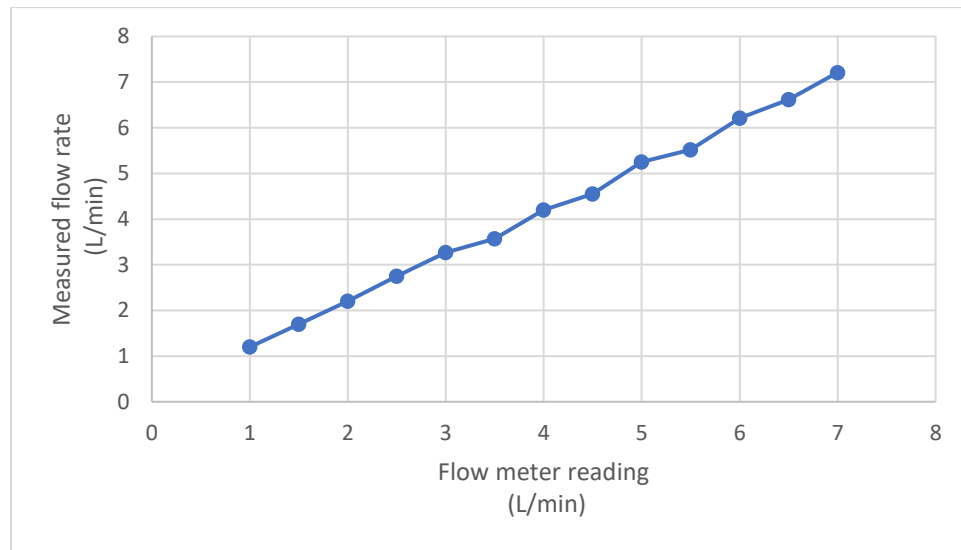


Figure 4.11: The calibration of water flow meter

4.8 Repeatability

The variance caused via an instrument or a difference observed if the similar worker measures the similar part several times is known as repeatability. Furthermore, when many operators measure the same component with the same equipment, a repeatable variation happens.

To ensure that the 1 test could be reproduced, it was performed in this experiment with the same setup. Equation from [52] may be used to compute the Pm standard deviation:

$$\sigma = \sqrt{\frac{1}{M} \sum_{i=1}^M (X_i - \bar{X})^2} \quad (4.1)$$

Where: x_i : The element, \bar{x} : The mean, σ : The standard deviation and M: The measurements number. In the Appendix (C), Table (C-1) evinces the Pm standard deviation with a virtuous data repeatability introduced.

Chapter Five: Results and Discussion

The present chapter contains four sections: The 1st one introduces the numerical outcomes of the distribution of temperature, mass flow rate effect and effect of fins. The second section is the optimization for type of wax and material of system. The third section manifests the investigational outcomes of the chosen optimal case of fins determined in a governed atmosphere in the laboratory of the Mechanical Department laboratory at the College of Engineering/University of Kerbala. Finally, a comparison has been conducted between the present work with published literature and the experimental and numerical results into section four.

5.1 Numerical Results

This work studies the effect of fins on the performance of a triple-square channel thermal storage unit. Then, the most effective fin length on the wax melting time will be chosen and designed practically. In this section, HTF's temperature distribution and different mass flow rates of HTF (water) will be studied in different internal and external longitudinal fin cases in a triple-square channel thermal storage unit. The first case: This section will explore the effects of varying numbers and different lengths of fins on the melting process of a thermal energy storage system that uses PCM. Identifying the most efficient pattern will be analyzing different cases for the fins using the same conditions and materials used in Al-Abidi [41]. It's important to mention that the entire volume of the whole fins will remain constant for ensuring that the same volume of PCM is utilized in the system. The second case: After determining the best

condition of the fins, it was studied numerically, using stainless steel instead of copper to manufacture the system.

Case One:

1. Using paraffin wax RT42 with a melting point of 42 °C.
2. The system was made of copper.
3. Study different lengths and numbers of longitudinal fins.
4. Table (5.1) shows the properties of paraffin wax and copper.

Table 5.1: The properties of paraffin wax and copper. [41]

Properties	RT42	Copper
Density ρ [kg/m^3]	760	8978
Specific heat capacity C_p [$J/kg.K$]	2000	381
Thermal conductivity k [$W/m.K$]	0.2	387.6
Dynamic viscosity μ [$kg/m.s$]	0.02351	-
Thermal expansion rate β [$1/K$]	0.0005	-
Latent heat L [J/kg]	165000	-
Melting Temperature T_m [K]	311.15_315.15	-

5.1.1 Volumetric flow rate of HTF effect on the melting rate

The effect of various HTF volumetric flow rates upon the procedure of PCM melting was studied. Figures (5.1) and (5.2) reveal that the melting rate and PCM temperature increase due to the flow of a 70°C HTF flowing over it for the different flow rates. These charts depict the average temperature and liquid fraction over time for the (5, 8, and 10) l/min of HTF volumetric flow rates. In this study, the simulation for 15 minutes using a time step of 0.5 minute showed that the volumetric flow rate increases the needed period for melting as

well as increases the total temperature due to higher heat gain into the PCM. Due to the increased mass flow rate, a higher velocity through the cross-sectional area exists.

Consequently, the Reynolds number increases, the Nusselt number, and the heat transfer coefficient increases. Results of (8 and 10) l/min are converging and almost identical. Only a 1.1% mass fraction is the difference between the (10 and 8) l/min. The value of the mass fraction is identical for approximately the first five minutes and starts to diverge as the charging time increases. Therefore, the best volumetric flow rate was 10 l/min because it gave the shortest melting time for paraffin wax compared to mass flow rates (4 and 8) l/min.

In summary, the mass flow rate of the surrounding fluid plays a crucial role in determining a solid material's melting rate, particularly in convective heat transfer cases. Higher flow rates generally lead to faster melting rates by enhancing heat transfer, maintaining larger temperature differentials, and reducing the thermal boundary layer thickness.

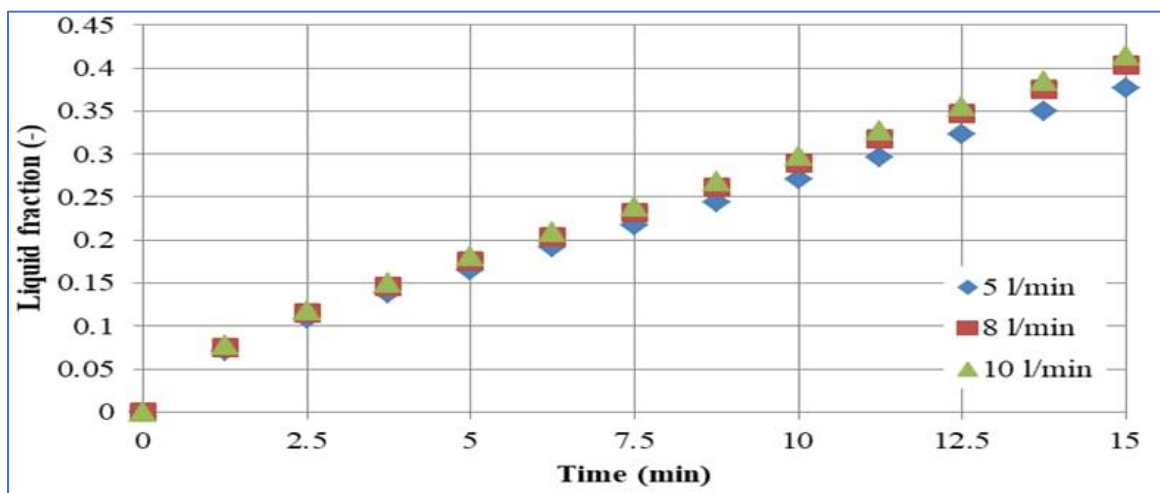


Figure 5.1: Liquid fraction of PCM RT 42 vs. melting time for (5, 8 and 10) l/min of HTF at 70°C / numerically.

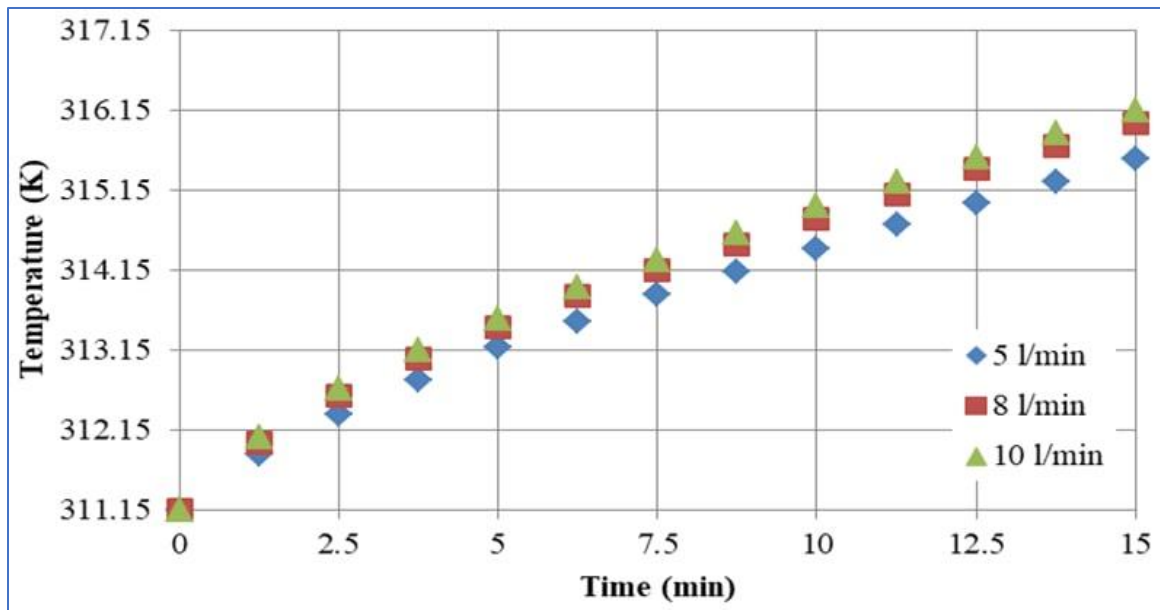


Figure 5.2: RT42 PCM temperature vs. melting time for (5, 8 and 10) l/min of HTF at 70°C / numerically.

5.1.2 Effect of the fins numbers upon the rate of melting

The optimal volumetric flow rate of the HTF on the system (10 l/min.) was subsequently utilized for various fin cases. Table (5.2) shows the various cases where the (3) various fins numbers. being utilized on the PCM unit side, upon the internal and external channels. And the fins number was varied in the three cases, while the length of the fins remained constant at 42 mm.

The combination of fins with the LHESs plays a crucial role in enhancing the efficacy of thermal unit via increasing the thermal exchange surface area. Additionally, the highly thermally conductive copper fins utilization has a significant impact on improving the mean thermal conductivity of the unit. The fins work as thermal delivery agents from the internal and external sides to the PCM's deep parts. However, it can also hinder the natural convection heat transfer by creating obstacles against the molten PCM circulation. And, the fins' cross-sectional areas for the whole cases being the similar ($20,160 \text{ mm}^2$), for

guaranteeing the similar PCM volume use, as well as the whole fins being in a horizontal direction.

Table 5.2: Number and length of the fins for TSCTSU

Case	A	B	C	D
No. of fins	-	4	6	8
Fin length (mm)	-	42	42	42
Fin thickness (mm)	-	1	1	1

Figure (5.3), it can be observed that liquid fraction development for cases (A–D) throughout the melting procedure. And, the initial charging procedure takes place rapidly in the 1st 500 seconds owing to the conduction heat transfer with the solid PCM. Once the liquid fraction reaches 95%, a plateau is observed in the curve shape across the all cases owing to the natural convection dominance at such stage. Based on observations, it can be concluded that the phase-changing process is slowest in case A when there are without fins, while the fastest melting process occurs in case D, which has the highest surface area.

Based on Figure (5.4), it can be seen that the average temperature experiences increase in the initial 300 seconds due to the thermal conduction effect. The natural convection is created in the melted PCM close the walls zone, as well as the fins existence causes a decrease in the PCM warming rate. Among all cases, Case D, with the uppermost fins no., shows the uppermost value of mean temperature due to its highest surface area. Thermal equilibrium is reached within 3000 seconds in this case. However, the melting process in Case A is the slowest as compared to all other cases, and thermal equilibrium is achieved in 3500 seconds, which is 14.6% slower than in Case D.

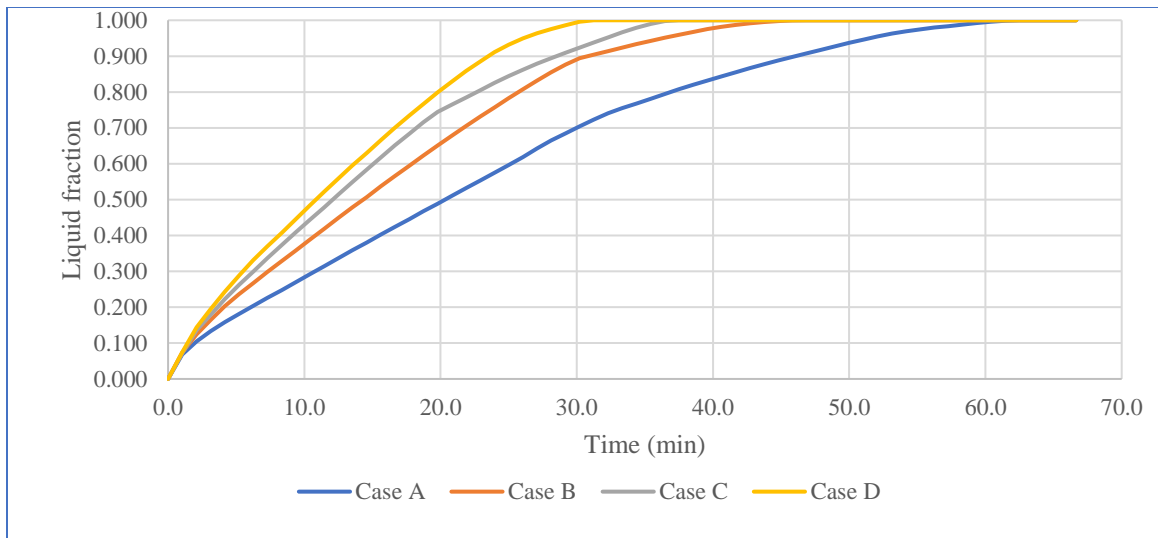


Figure 5.3: The effect of fins on the liquid fraction of RT42 PCM with melting time (min) / numerical.

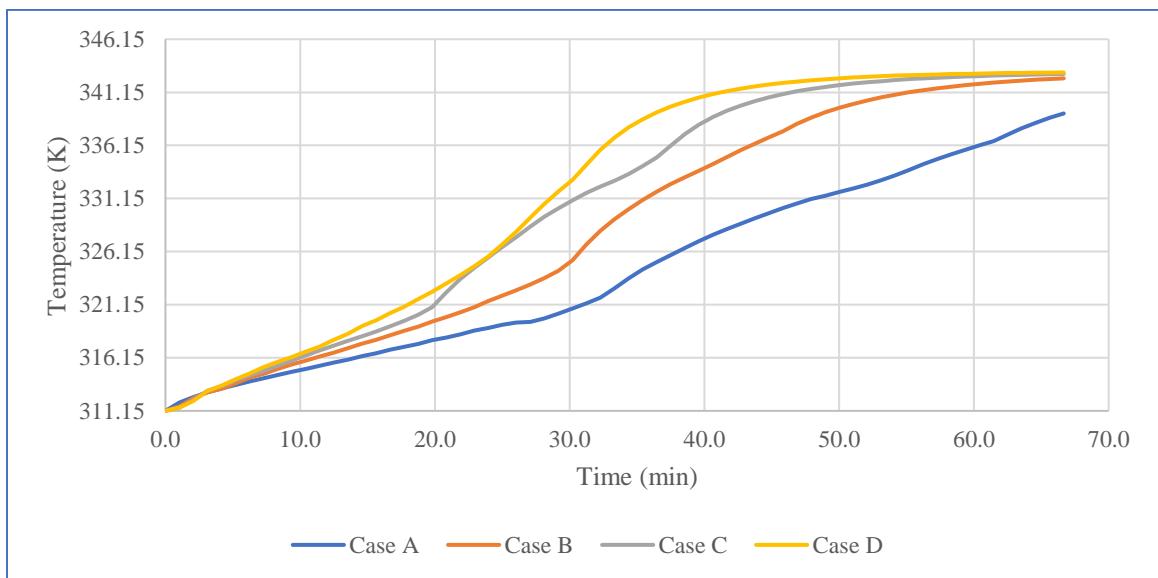


Figure 5.4: The effect of temperatures of HTF on the RT42 PCM with melting time (min) / numerical.

The data in Table (5.3) indicates that as the fins numbers increases, the PCM melting time decreases. Specifically, Cases B, C and D had complete melting times that were 45.8%, 37.5%, and 31.3% of that of the TSCTSU without fins (Case A), respectively. The number of fins had a significant impact

on the melting fraction at any given time, with a greater effect observed for a larger fins number. Such factor plays a critical role in the procedure of PCM melting as the fins prolong the area of heat transfer as well as conduct the heat straight to the surfaces of PCM.

5.1.3 Effect of the length of fin upon the fraction of melting

To study the dimensionless fin length (l) influence upon the heat transfer as shown in Table (5.3), after that the fin numbers were fixed at $N = 8$, and the HTF temperature was set at $T_w = 70^\circ\text{C}$. Figure (5.5) was used to describe the results, using longer fins for each fin arrangement leads to an increase in the Surface area exposed to heat transfer and better melting propagation in the annulus by increasing thermal penetration depth into PCM. The melting time can be saved by 31.3% and 29.2% for the case with D and G, respectively, when the length of the fin increases from (42) to (47.6) mm. However, the time required to melt PCM completely is 1750 s and 1875 s respectively.

The study shows that the increase in fin length leads to melting enhancement, which significantly augments the surface contact between the hot fins and PCM, resulting in the enhancement of the heat conduction process. Additionally, as the length of the fin increases, the gap between the shell and the fin decreases. This allows heat to be transferred to the shell more quickly, since the thermal resistance between the fins and (inner and outer) channels decreases, as recorded by the temperature of the inner and outer channels. Longer fins provide a greater surface area for heat exchange. This increased surface area allows for more efficient heat transfer from the environment to the PCM, leading to a faster melting rate. In essence, longer fins allow heat to flow into the PCM. Also, longer fins can conduct heat more effectively.

Table 5.3: The cell geometry variation for TSCTSU

Case	Number of cell (geometry of PCM unit)	Length of fin (mm)	Thickness of fin (mm)
E	4	47.6	1
F	6	47.6	1
G	8	47.6	1

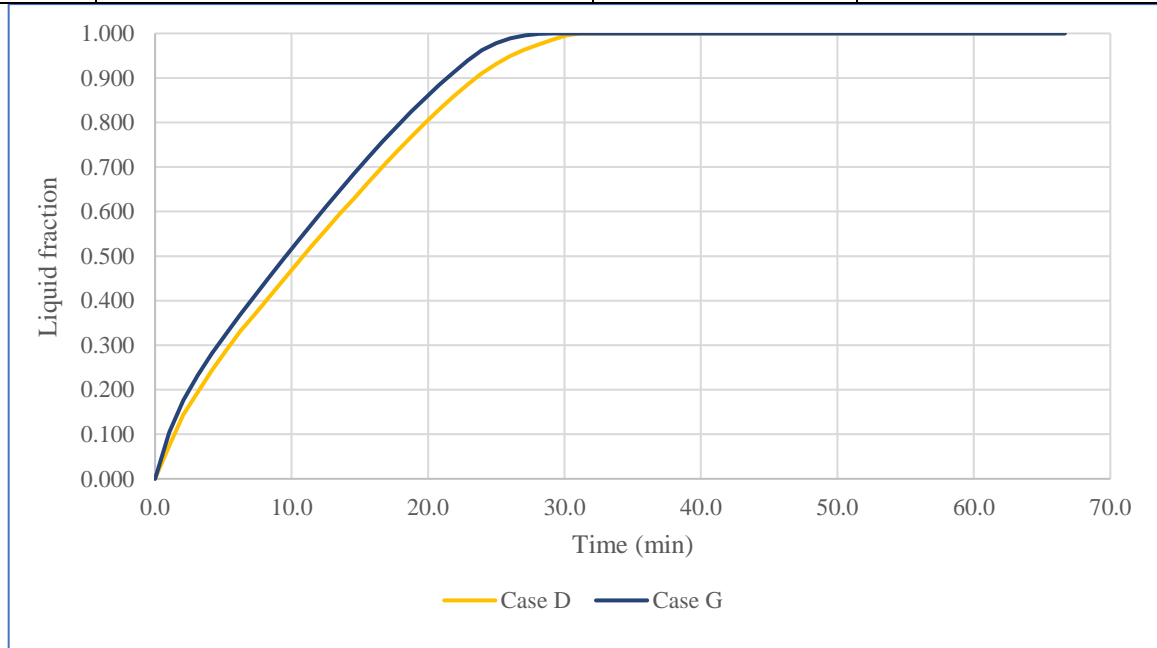


Figure 5.5: Influence of the length of fin upon the time of melting for Cases D and G to RT42 PCM with the time (min)/numerical

5.1.4 Effect of the geometry of PCM unit in TSCTSU

It is important to show the differences in the melting process and provide a more detailed representation of the temperature changes in the PCM within the TSCTSU. Following a different time step of melting aimed at a wide range of projects that required investigation is evinced in detail for all cases in Figure (5.6), and Table (5.4) also displays the improvement rates for all cases.

Conduction heat transfer took place between the channel hot wall channel and the solid surface of PCM. And, the heat transfer dominates the melting process from the beginning and creates a thin liquid layer. This layer grew

larger, and the liquid fraction increased over time; due to buoyancy-driven natural convection, the PCM's channel's upper regions were forced to contain hotter fluid, while the PCM's solid portion was forced to the bottom due to its heavier density.

The melting in various parts of the PCM was affected by natural convection as the number of fins increased, resulting in a uniform temperature distribution. Noticeably, the distribution and propagation of temperature contour lines are the same as that of the liquid mass fraction. Case G accomplished the procedure of PCM melting in just 29.2% of case A; this being regarded to be the shortest time of melting of all cases. It is reasonable to conclude that the PCM unit's geometry plays a major part into the rate of melting. And, the fins prolong the area of heat transfer as well as conduct the heat straight to the surfaces of PCM. Also, the natural convection in the unit slows down every cell melting.

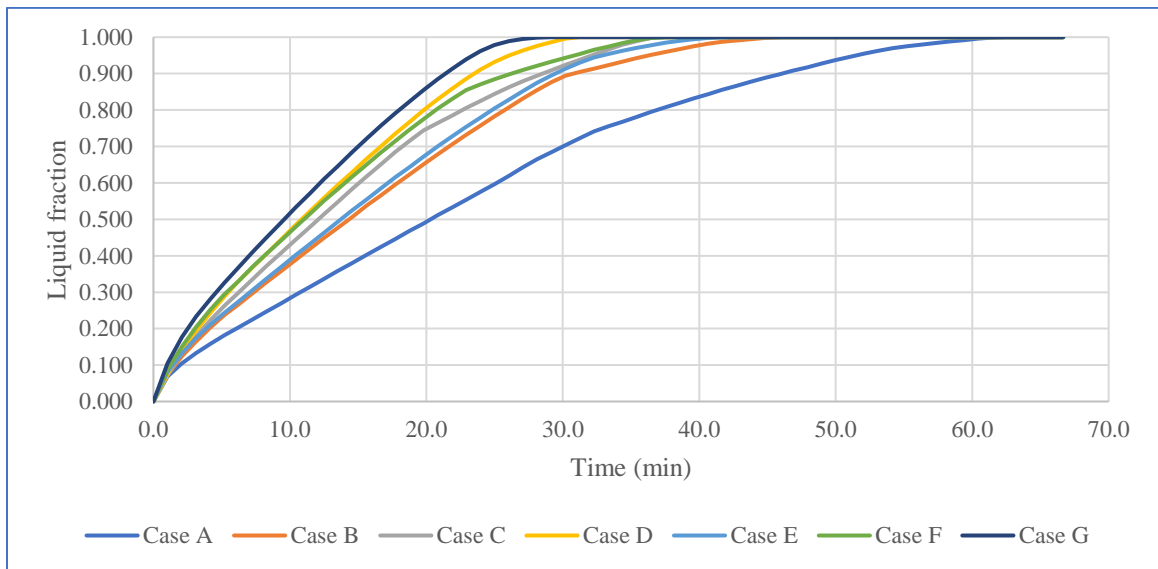


Figure 5.6: The melting fraction for RT42 PCM with melting rate for all enhancement cases / numerical.

Table 5.4: Percentage of the time of melting for various cases of TSCTSU

A	B	C	D	E	F	G
100	45.8%	37.5%	31.3%	41.7%	37.5%	29.2%

After that, the melting process is explained through a geometric PCM unit for the case of the presence and absence of fins in the following figures.

Figure (5.7) manifests the melting rate of the PCM field during (3500 s) for case (A). Without fin, the PCM initially dissolves in the region attached to the walls of HTF. And, over time, the PCM excess liquefies, creating a denser liquid film on the pooling and wall at the upper owing to free convection. Also, the PCM remains stationary in the lowest region of the system. The effect of convection continues until the melting is complete and ends at 3500 seconds.

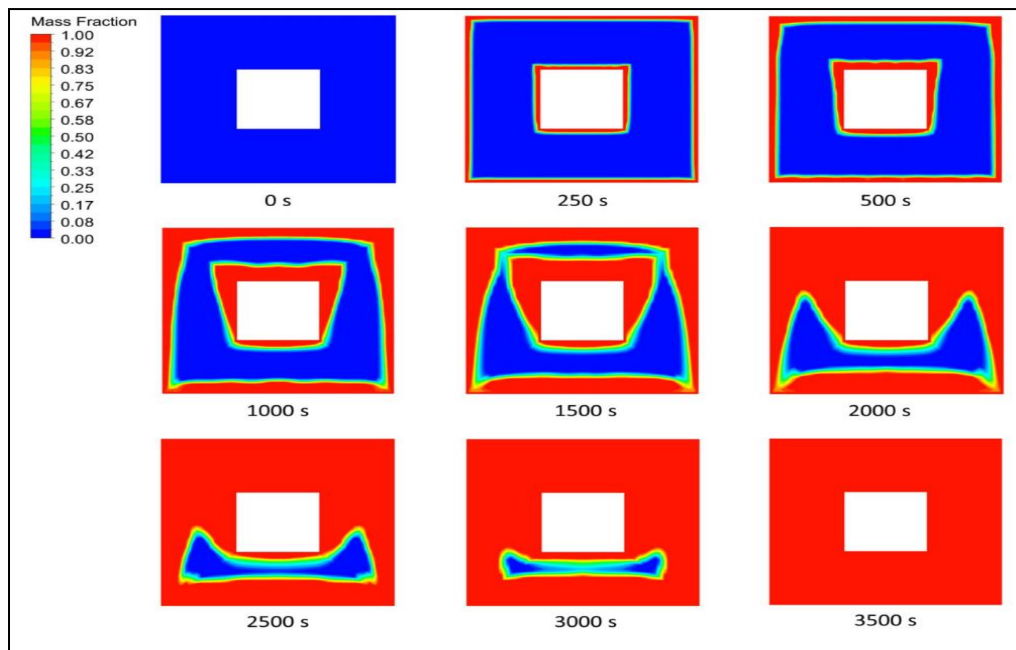


Figure 5.7: The melting fraction of RT42 PCM for case (A without fins) with melting time (numerical).

Figures (5.8 -5.10) are shown the temperature distribution of PCM field for cases (B, C, and D) in the PCM domain in (3000, 2500, and 2000) s. The fins could not heat the deep section of the PCM. Therefore, the warmth is distributed uniformly but slowly. The huge free space in the fin case helps the liquid PCM travel more easily, owing to natural convection, which is why the warmer PCM accumulates at the top, and the colder PCM gathers at the bottom.

Owing to the heat transfer's larger surface area, the longer fins, using longer fins (instance C $(480 \times 42) \text{ mm}^2$) with 6 fins) raises the unit temperature. In this instance, the movement's space is reduced substantially compared to the short fins. In 2500 seconds, the average temperature in the unit hits $66.41 \text{ }^\circ\text{C}$. As previously mentioned, the PCM constrained the space between the two neighboring fins in case D $(480 \times 42) \text{ mm}^2$ with 8 fins) by creating a little clearance between the opposing wall and the fin. And, the higher fins' surface area caused the heat to dissipate more quickly, but the fin size prevented the movement over the entire unit. The area between the two neighboring fins, however, experiences movement. In cases C and D, the mean temperature for the entire system is $66.41 \text{ }^\circ\text{C}$ and $63.89 \text{ }^\circ\text{C}$ respectively.

Most areas among the fins typically approach thermal balance with the temperature of HTF. And, the higher fins, which are absent due to the wall in the higher region, are obtained by the PCM from the lower fin, leaving a solid piece at the domain's top.

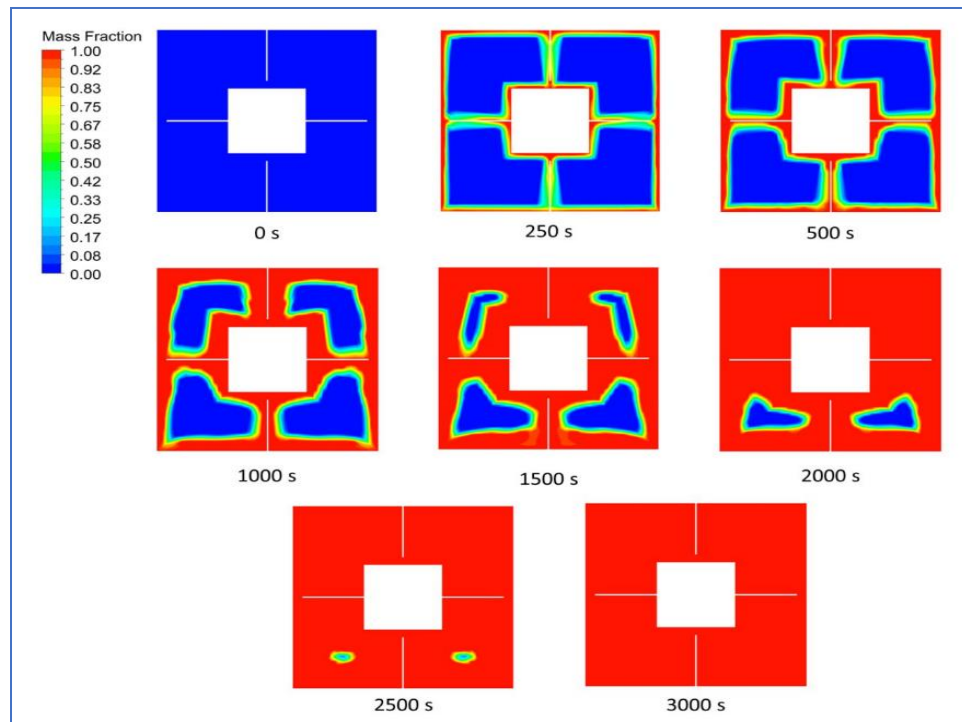


Figure 5.8: The fraction of the RT42 PCM field melting for case (B with 4 fins and length 42 mm) with melting time / numerical.

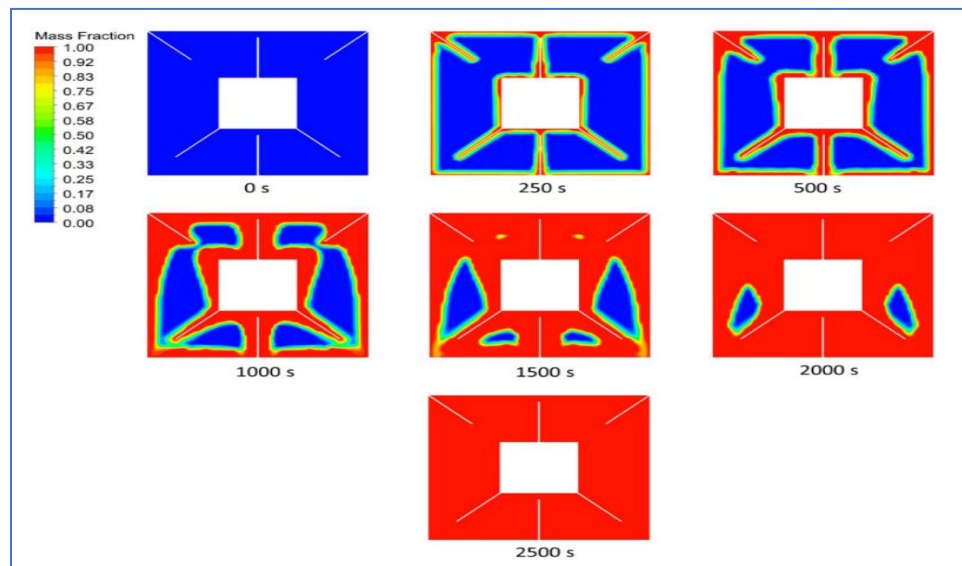


Figure 5.9: The fraction of the RT42 PCM field melting for case (C with 6 fins and L42 mm) with melting time / numerical.

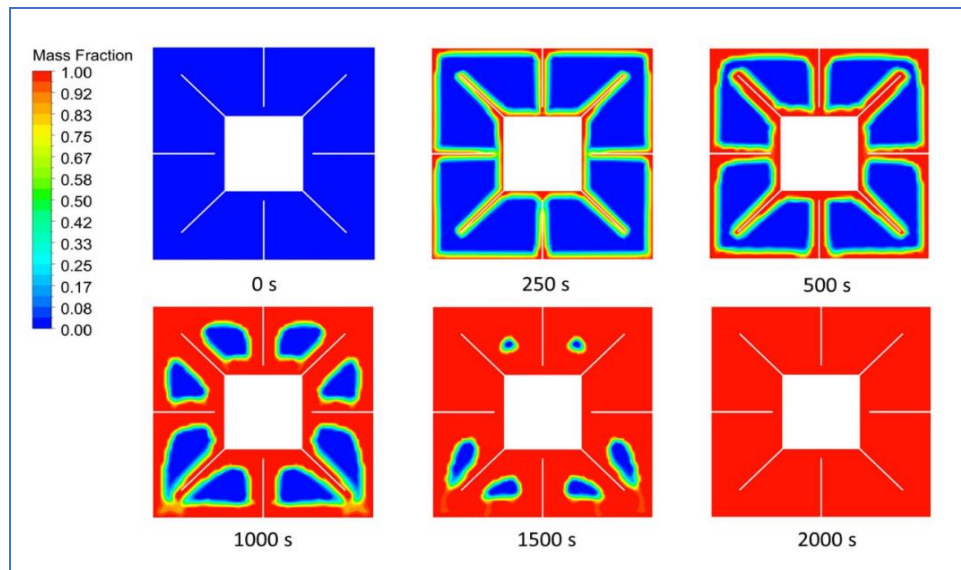


Figure 5.10: The fraction of the RT42PCM field melting for case (D with 8 fins and L42 mm) with melting time / numerical.

Figure (5.11- 5.13) elucidate the liquid fraction of PCM for the cases (E, F and G), respectively and it is clear that the number and length of fins takes a significant part into the procedure of melting, as (4, 6, and 8) fins were used for a length of 47.6 mm. It is obvious that using a larger number of fins improves the heat transfer and thus reduces the melting time. Because it provides a larger surface area and more thermal conductivity, it accelerates convection, which helps in faster melting of PCM.

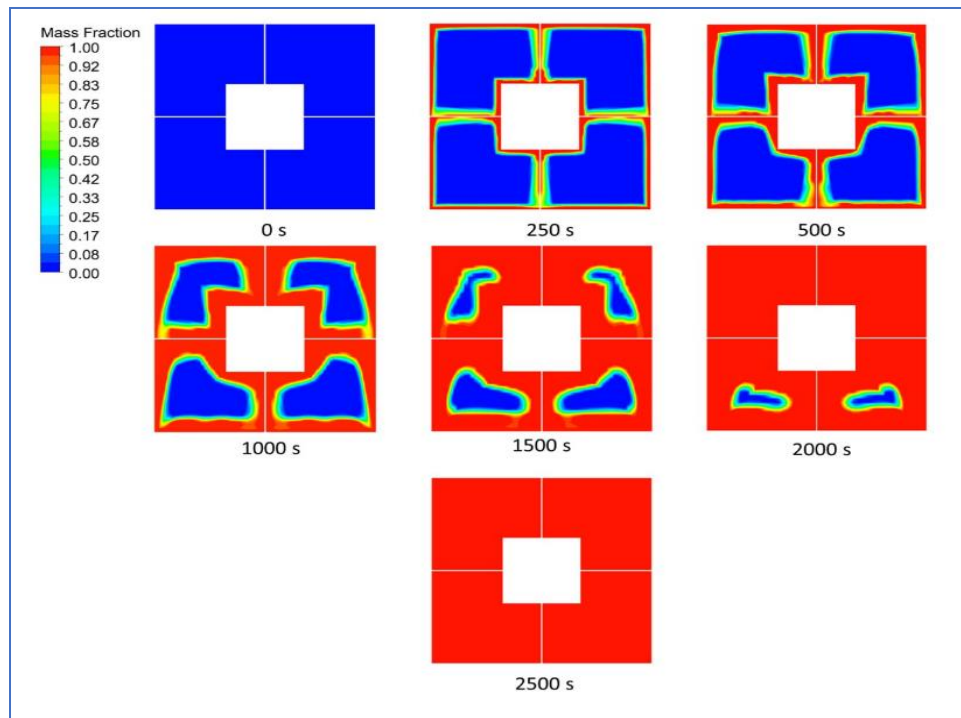


Figure 5.11: The fraction of the RT42PCM field melting for case (E with 4 fins and L 47.6 mm) with melting time/ numerical.

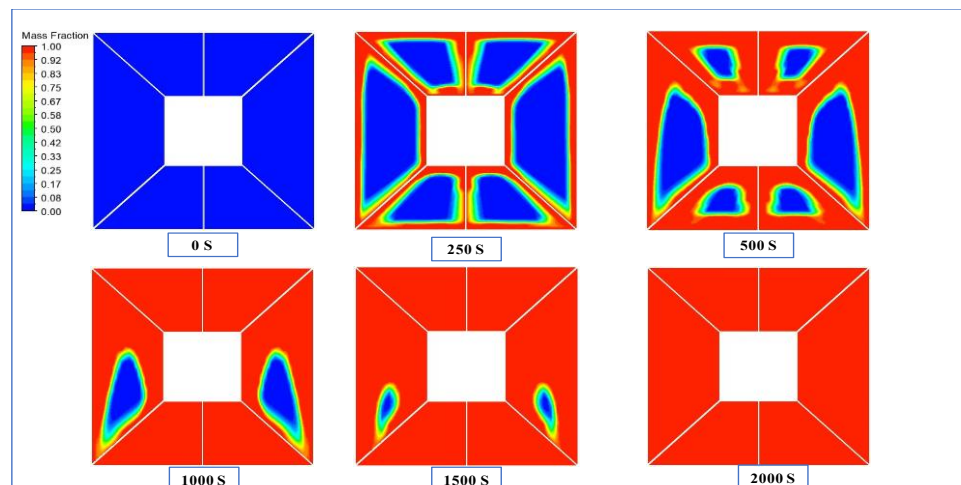


Figure 5.12: The fraction of the RT42 PCM field melting for case (F with 6 fins and L 47.6mm) melting time / numerical.

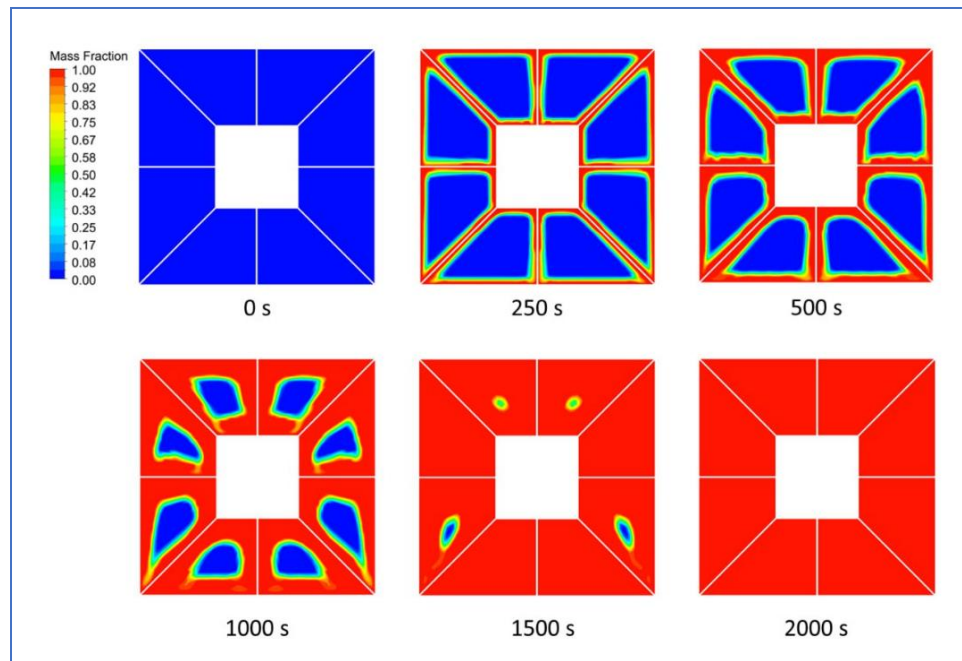


Figure 5.13: The fraction of the PCM field melting for case (G with 8 fins and L 47.6 mm) / numerical.

5.2 Optimization

After presenting the previous results, which showed the effect of the number and length of fins on reducing the melting time, it also displayed agreement with Al-Obaidi [41] in that the ideal case for fins was case G. Accordingly, in the second case, the following modifications are made:

1. The system is made of stainless steel 304 instead of copper because it is widely available in the market and easy to manufacture.
2. Using paraffin wax RT 64 instead of RT 42 to easily obtain it from Al-Doura Refinery in Baghdad -Iraq.
3. Testing the condition (G) numerically for paraffin wax RT 64 and studying it later experimentally and comparing the results. Table (5.5) represents some characteristics of wax and stainless steel 304.

Table 5.5: The properties of paraffin wax and stainless steel 304. [41]

Properties	RT64	stainless steel 304.
Density ρ (kg/m^3)	780	8030
Specific heat capacity C_p ($J/kg.K$)	2000	502.48
Thermal conductivity k ($W/m.K$)	0.2	16.27
Dynamic viscosity μ ($kg/m.s$)	0.0035	–
Thermal expansion rate β ($1/K$)	0.000545	–
Latent heat L (J/kg)	250000	–
Melting Temperature T_m (K)	337.15	–

Case Two:

1. The use of paraffin wax with a melting point of 64 °C.
2. The system was made of stainless steel 304.
3. Study the case of fins (No. 8 of fins with 47.6 mm its length). Table (5.4) above shows the properties of paraffin wax RT64 and stainless steel.

5.2.1 Effect of the volumetric flow rate of HTF and fins geometry on melting rate of PCM

The effect of various HTF volumetric rate of flow upon the procedure of PCM melting was studied numerically. For the rate of melting as well as the PCM temperature spreading, the result of flow at 80°C for the HTF for each volumetric rate in the without fins case is shown in Figures (5.14) and (5.15). The average temperature and the liquid fraction of (4, 8, 16, and 24) l/min are portrayed in these diagrams as HTF volumetric flow rates over time. Increasing the volumetric flow rate of HTF leads to an increase in the fluid velocity within the cross-section; thus, the Reynolds number and Nusselt number increase,

increasing the heat transfer coefficient and, therefore, the melting time decreases. Due to the still flow in the laminar flow, the average PCM temperature was equal for the (4, 8 and 16) l/min HTF flow rates. When the flow rate went up to 24 l/min, considered turbulent, and deemed good for heat transfer, it was apparent that an appreciable improvement was achieved. The time taken to charge was reduced by 48.41% for 16 l/min.

Thus, the results indicate that higher mass flow rates of lead to enhanced heat transfer due to increased molecules available to transfer heat to and from the PCM. These results in a higher convective heat transfer coefficient, determining the heat transfer rate between the PCM surface and the HTF.

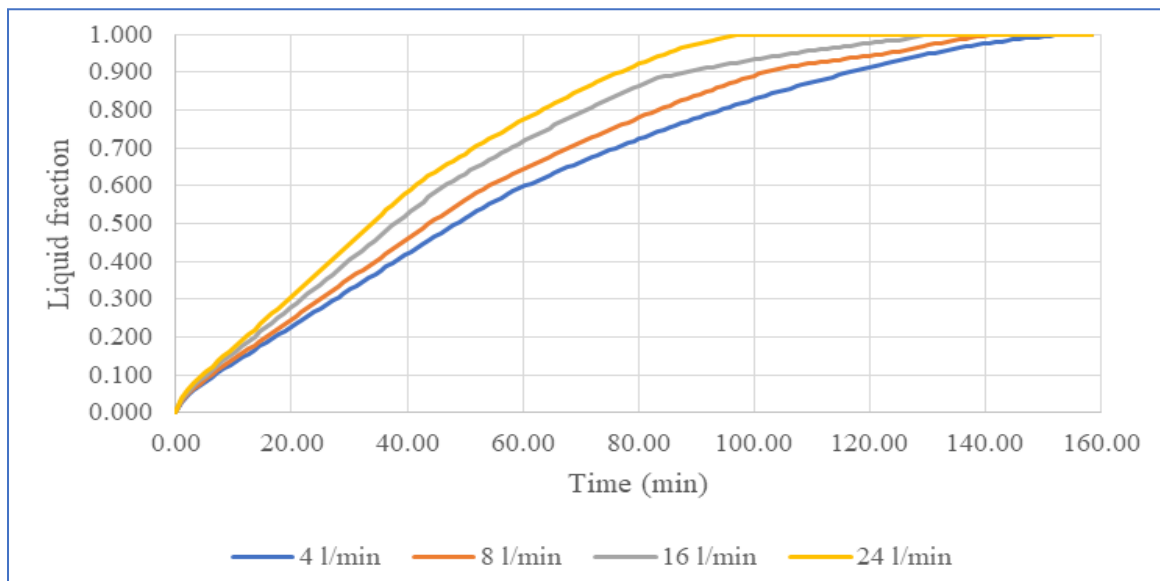


Figure 5.14: Liquid fraction of PCM RT64 vs melting time for (4, 8, 16, and 24) l/min of HTF / numerical.

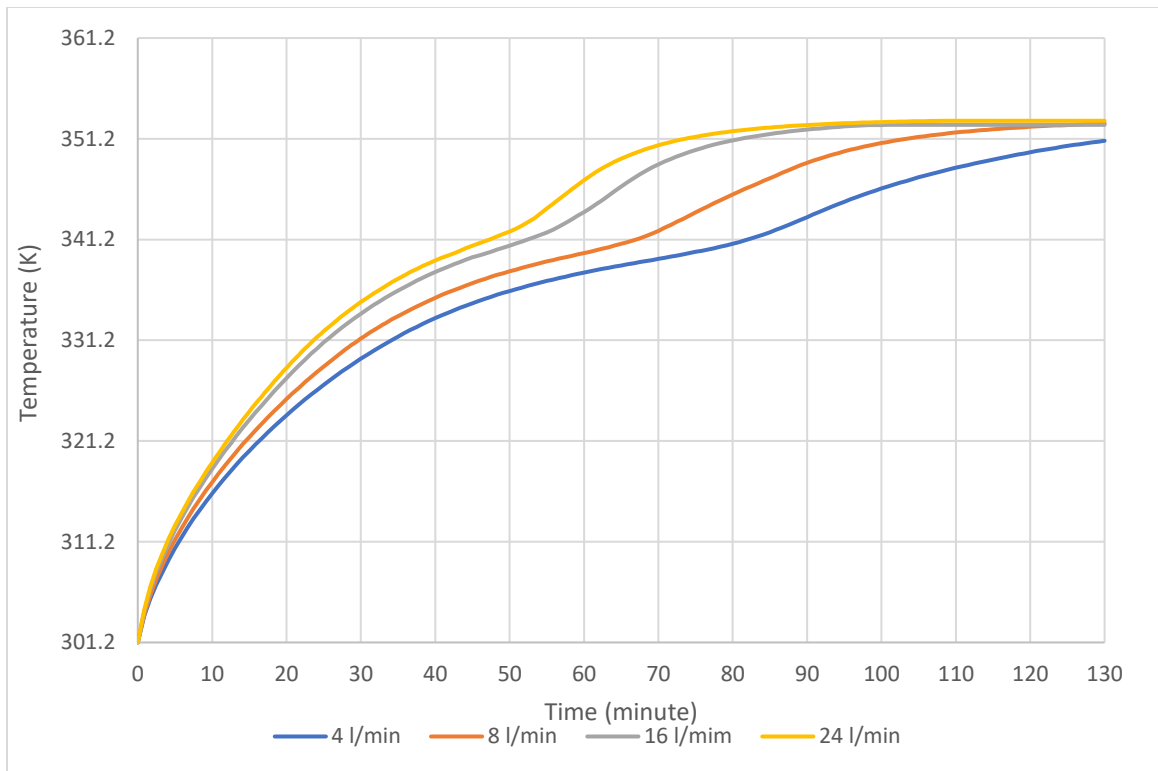


Figure 5.15: RT64 PCM temperature vs. time for (4, 8, 10 and 24) l/min of HTF / numerical.

Since symmetry boundary conditions were employed in TSCTSU geometry, storage space and solution time concerns must be made. The longitudinal YZ axis divides fluid and melting propagation and distribution behavior into two halves, as shown in Figure (5.16). Figure (5.17) displays the portions of the several case studies. Three areas of shapes were used to split a system to exhibit the melting percentage of the TSCTSU with fin in connection to time. The solid portion of each region reveals the studied planes. Both internal and exterior approaches accomplished the total process PCM melting, which would have required 60 min for a TSCTSU with eight fins due to additional heat transfer surfaces. The inner, middle, and fin walls warmed up quickly.

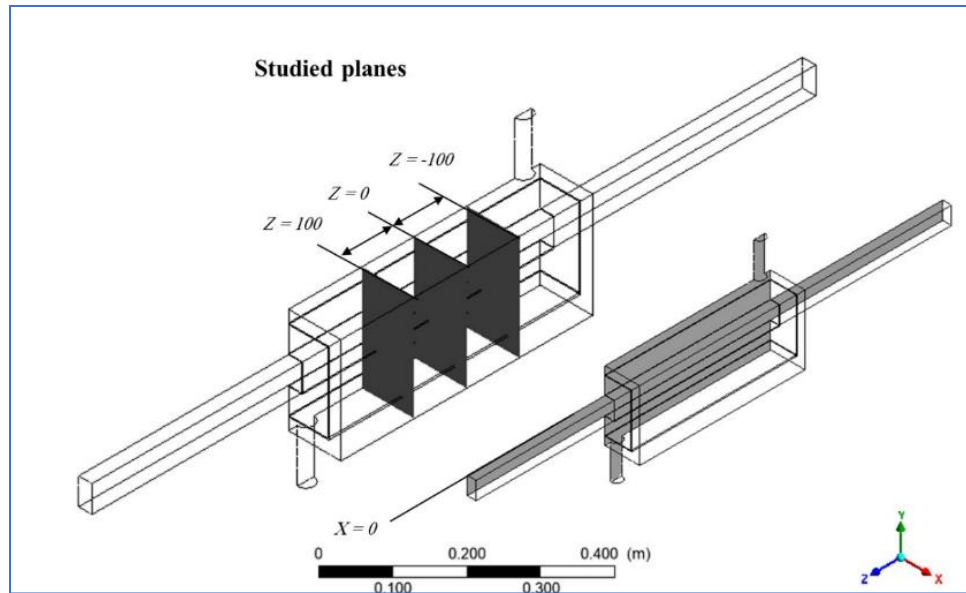


Figure 5.16: Studied planes.

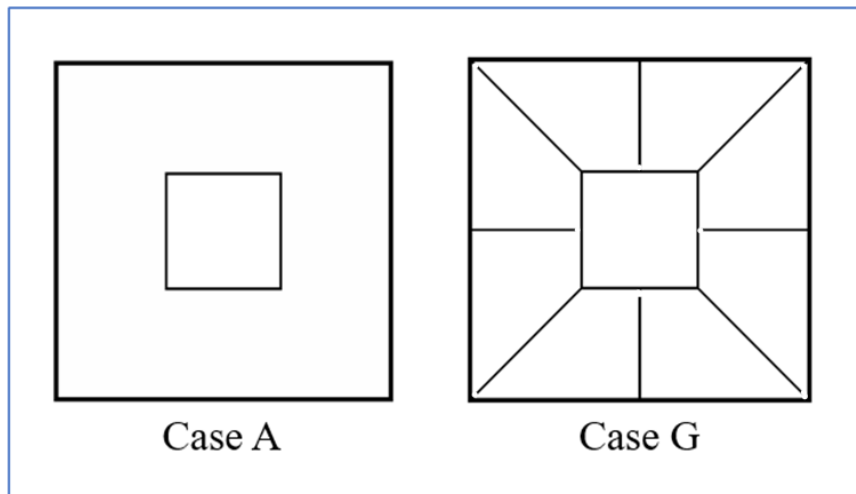


Figure 5.17: Sections of different case studies: (a) without fins, and (b) the 47.6 mm length of fins.

The final melt time of the finless case was 131.25 minutes, while the final melt time for the fins case was 67.7 minutes, reaching the final liquid state as shown in Figure (5.18). The melting rate is rapid until a specific value or a particular period, and then it starts to drop significantly as time passes when the major source of heat gain in the solid PCM is the sluggish motion caused by

gravity and buoyancy in the melt zones. The melting was influenced over time by the thermal storage's natural convection. In figure (5.18), 16 l/min flow rate will be used to demonstrate the melting rate for the finless and finned cases.

The 8 of number fins accelerate melting more effectively. As a result of the fins of the PCMs being divided into various geometric parts, there are more melts, a higher average temperature for the PCM, and a higher heat transfer surface. It is also due to the buoyancy in the lower regions that increases the heat transfer at the interface of the solid and the melt zone where RT64 is melting within each geometrical section.

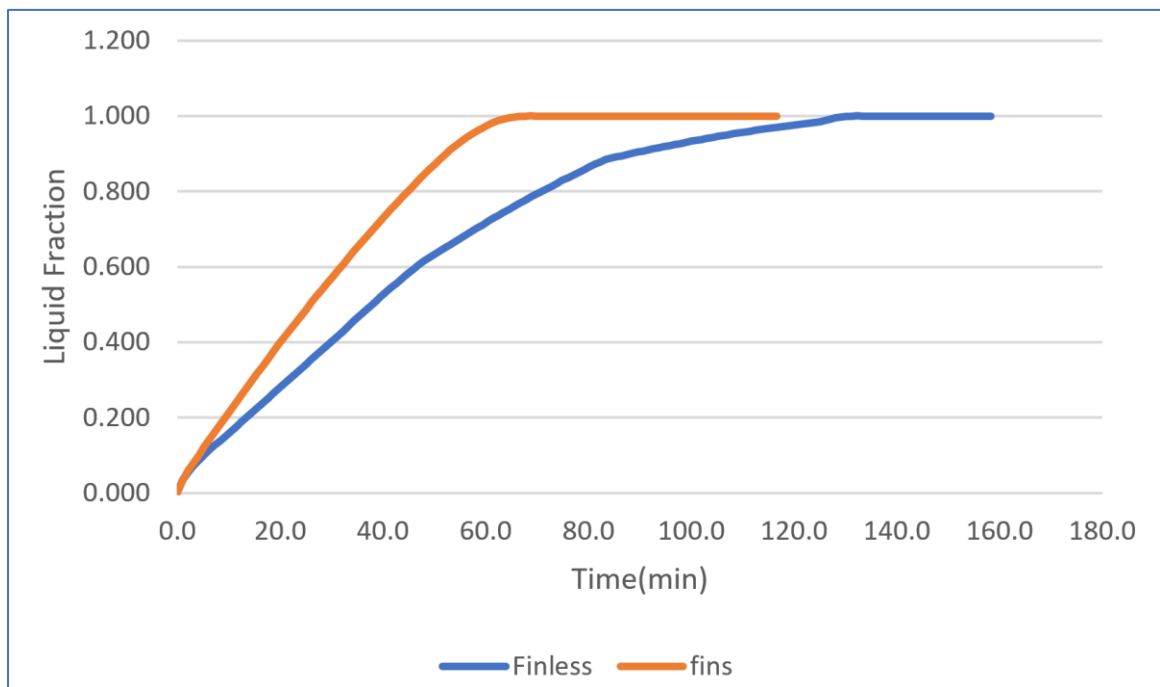


Figure 5.18: Melting rate of RT64 PCM for without fins and eight of fines cases with melting time / numerical.

Figure (5.19) depicts the connection between wax temperature and melting time at 16 l/min for with and without fins cases. The time required for the wax to liquefy decreases because the presence of blades accelerates heat transfer by convection. As a result, the intensity moving process between the

walls also accelerates. The fines liquefied in 62.5 min at a temperature of 349 K, whereas the finless case took 131.3 min to reach around 350 K. These properties were shown when the mass flow was presented, and the temperature increased.

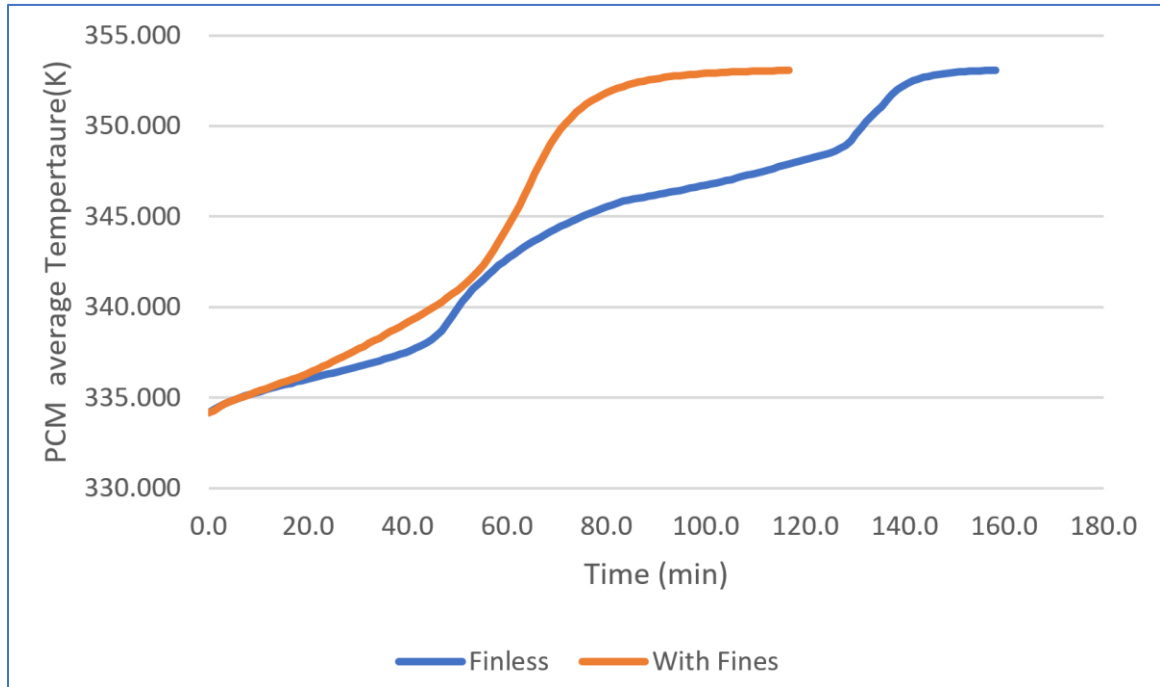


Figure 5.19: RT64 PCM average temperature until full melting with time for the with and without fines cases / numerical.

5.2.2 Effect of the PCM unit geometric in the TSCTSU

Figures (5.20) and (5.21) depict the isothermal contours of the PCM in a TSCTSU with internal-external fins at various points during the PCM melting at (125, 500, 1000, 2000, 3000, 5000, and 8000 sec). The conduction heat was transferred between both the warm walls of the channels and the hard surface of the PCM. As soon as this thermal transfer phenomenon occurred, a thick liquid layer formed, dominating the melting process. Over time, that layer expanded, and the liquid fraction grew; PCM's channels were forced to contain higher volumes of hot fluid due to buoyancy-driven natural convection in their

upper sections, while its solid part was dragged down because of increased density.

When the fins number augmented, the natural convection influenced the melting in various PCM areas, resulting in a consistent distribution of temperature. The temperature contour lines' distribution and propagation match those of the liquid mass fraction. Given that the fins increase the area of heat transfer as well as transport the heat straight to the surfaces of PCM and that the natural convection continues in the unit, which speeds up the procedure of melting in every cell, it can be inferred that the shape of PCM unit has a considerable impact upon the rate of melting.

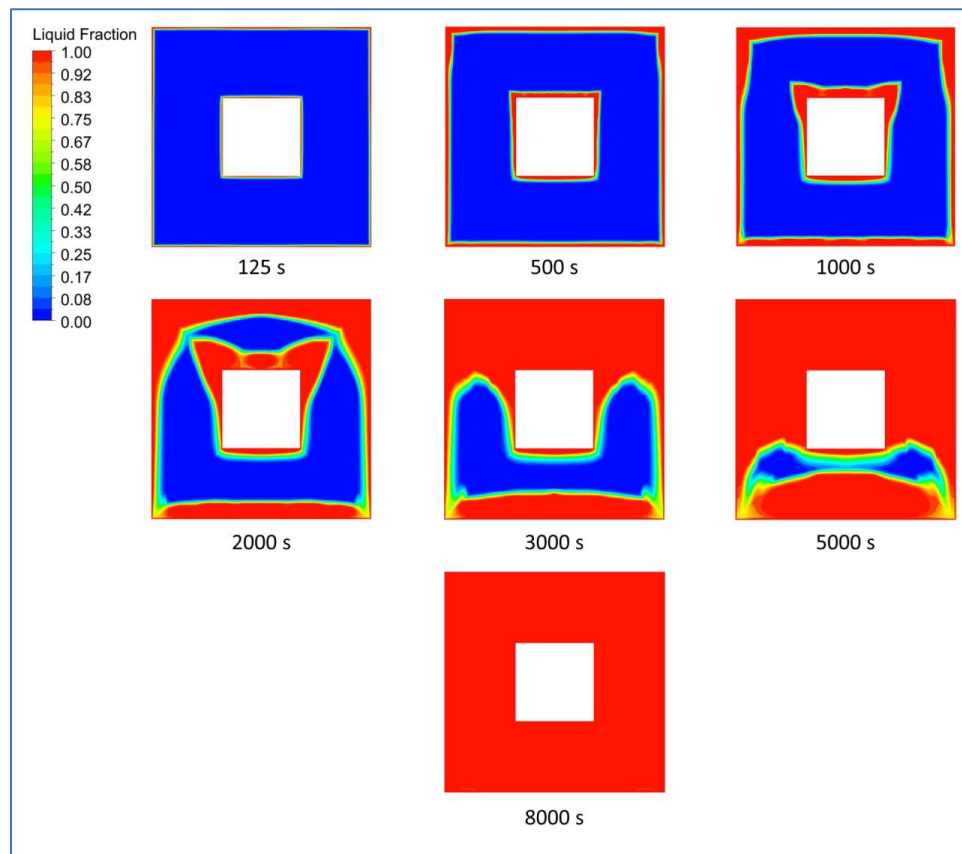


Figure 5.20: Liquid fraction for RT64 PCM with different time steps of without fins case at 16 (l/min) at $z=0$ / numerical.

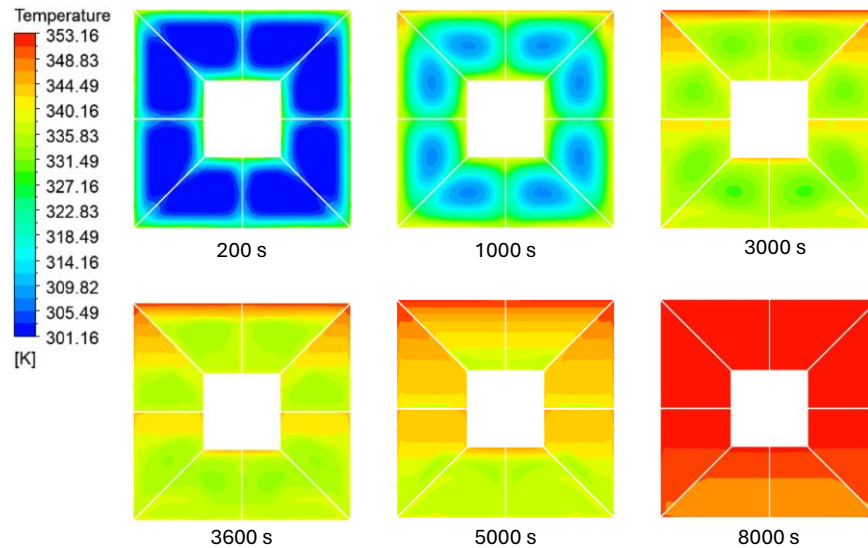
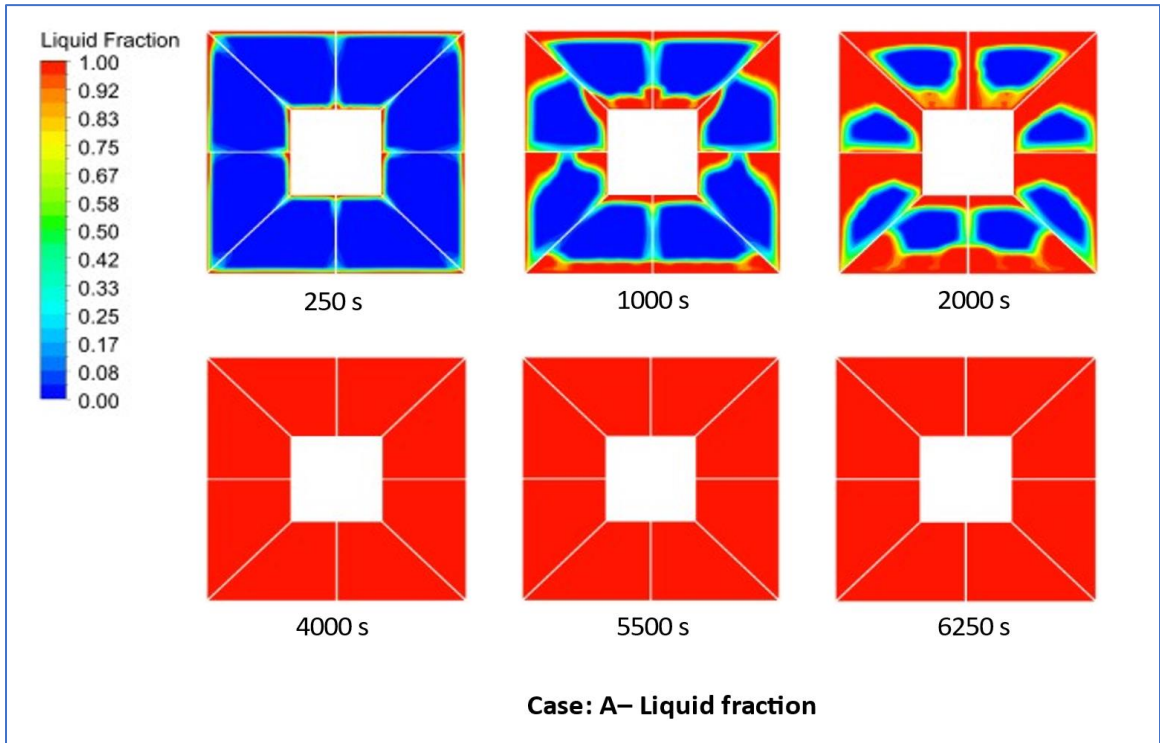


Figure 5.21: The temperature distribution of RT64 PCM with different time steps of without fins case at (16 l/min) at $z=0$ / numerical.

The evolution of the melt front and temperature field at seven different time instants while the fin length is 47.6 mm is illustrated in Figures (5.22-5.23). At the early stage of the melting process (4.16 min), it can be observed that heat is transported predominantly by conduction, resulting in a nearly uniform melting pattern adjacent to the hot channel and fins. The liquid layer also thins alongside the fins, indicating a temperature gradient between the fin base and tip. As time progresses, multiple unmelted lumps of wax furthest from the walls (thermal plumes) develop above the top surfaces of the fins due to the rising of locally hot fluid, along with four unmelted lumps of wax furthest adjacent to the vertical active hot channel. Buoyancy forces create natural convection flow patterns as more PCM is melted. With an increase in the gap between the tip of the fins and solid PCM, the hot liquid PCM ascends upward through the gap, resulting in the accumulation of more molten PCM at the top

part of the channel, while the unmelted PCM falls to the bottom until it is completely melting.



**Figure 5.22: The 47.6 mm fins case (8 RT64 PCM geometry sections)-
Liquid fraction with different time steps at $z=0$ / numerical.**

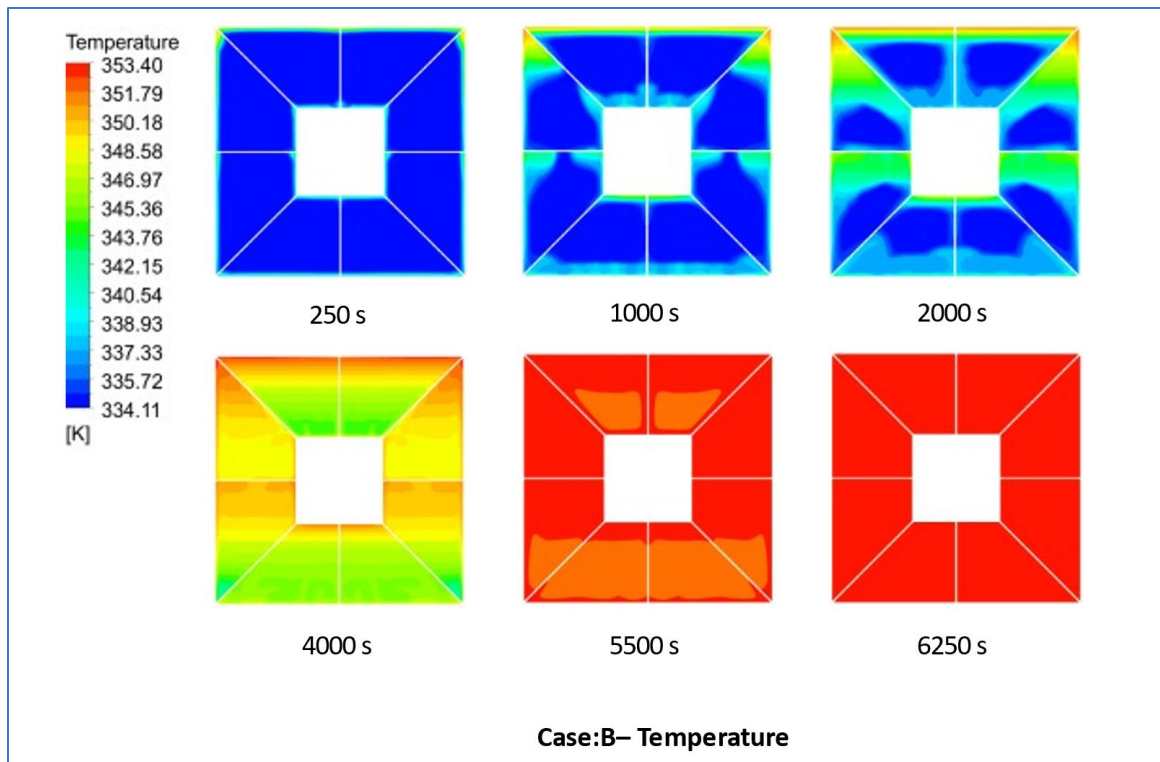


Figure 5.23: Temperature of RT64 PCM field with different time steps at $z = 0$ / numerical.

5.3 Experimental Results

The investigational results comprised the melting time measurements at various volumetric flows with and without fins.

5.3.1 Effect of Volumetric Flow rate of HTF with and without Fins

Different HTF volumetric flow rates were utilized for investigating their effects upon the melting of PCM. All experiments were performed at a constant HTF temperature (80 °C). Figure (5.24) shows the changes in the PCM temperature during the charging process without fins when the water is used as heat transfer fluid (HTF) at volumetric flow rates of (4, 8, 16, and 24) l/min. From this figure (5.24), it can be seen that for nearly all mass flow rates, the amplification rate in PCM temperature is found to be high initially due to high-temperature differences inside HTF and PCM, respectively. During the melting

process, the PCM temperature never changes but rises quickly when the liquid PCM is heated. For flow rates of (4, 8, 16, and 24) l/min, respectively, the total charging time is 166.66 minutes, 156.25 minutes, 145.25 minutes, and 102 minutes.

Figure (5.24) also, shows that the higher volumetric flow rates help maintain a larger temperature differential (temperature gradient) between the PCM and the HTF. This larger temperature differential drives a greater heat transfer rate through the convection process. Also, a higher mass flow rate can reduce the thickness of the thermal boundary layer that forms near the PCM. This boundary layer represents the fluid region with a temperature different from the bulk fluid. A thinner boundary layer allows for more efficient heat transfer by quickly bringing hotter fluid into contact with the PCM, enhancing heat transfer rates.

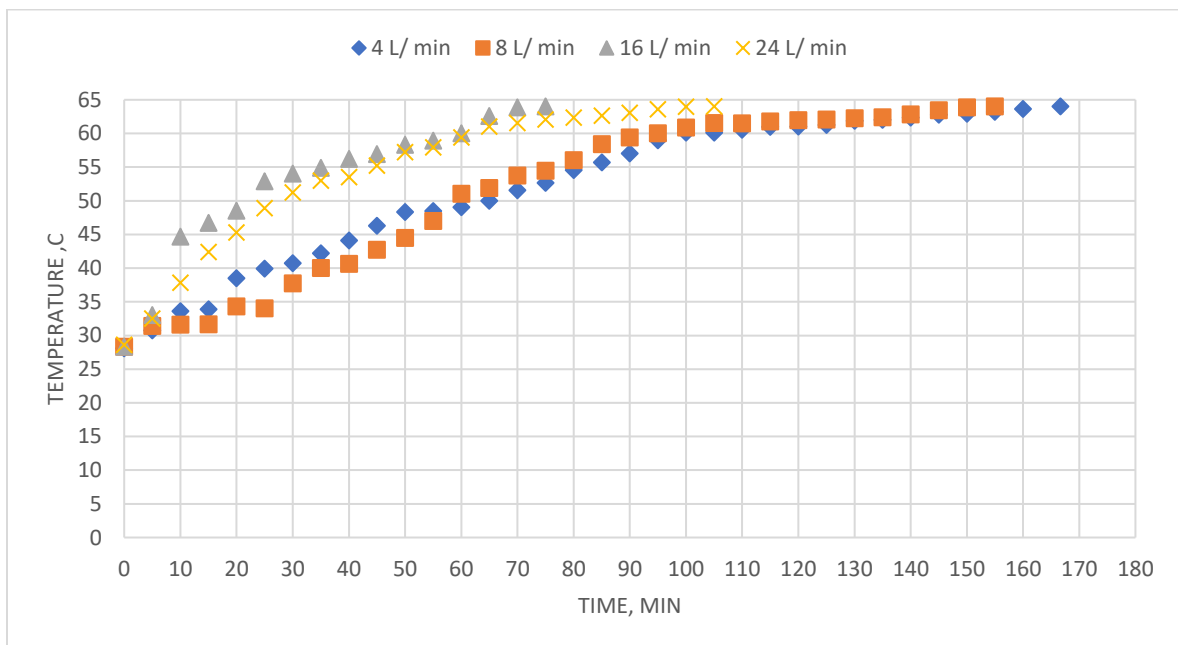


Figure 5.24: The rate of HTF volumetric flow without the influence of fins upon the time of RT64 PCM melting/ experimental

After that, the temperature differences of the PCM during the melting process in the case of the presence of fins were clarified for the same volumetric

flow values in the absence of fins, and then the improvement percentages were calculated after using the fins. Figure (5.25) explains the temperature changes during the melting process to arrive at the total melting time of paraffin wax for flow rates of (4 , 8 , 16 , and 24) l/min, respectively. The total charging time is 117.18 minutes, 98.47 minutes, 74.39 minutes, and 63.13 minutes (ignored due to the volumetric flow rate is turbulence is not in the assumptions).

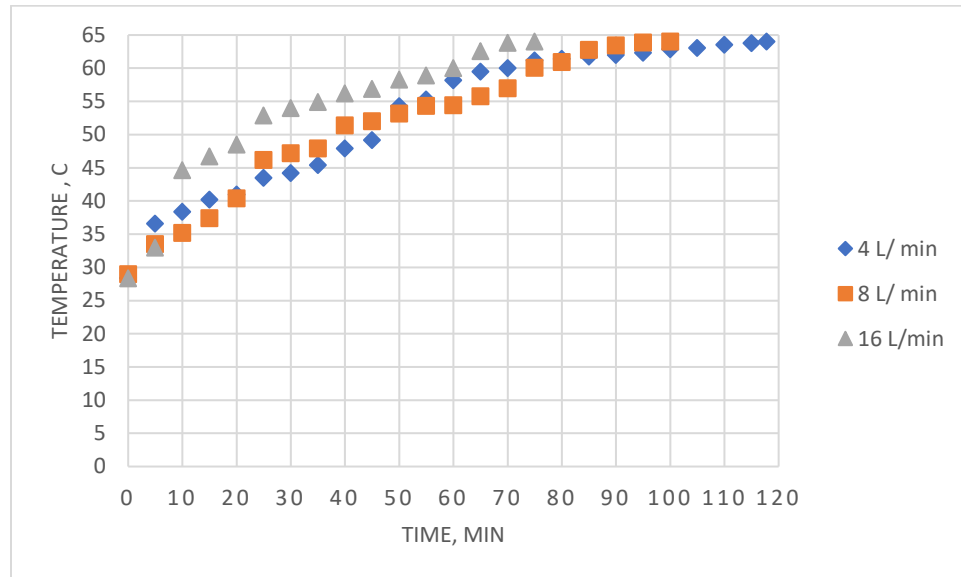


Figure 5.25: The rate of HTF mass flow without the influence of fins upon the time of PCM melting/ experimental.

The use of fins improved heat transfer during the paraffin wax melting process and thus reduced the melting time when using the same volumetric flow of (4, 8, and 16) l/min, respectively, the total enhancement of 29.68 %, 36.97%, and 48.7%. Temperature gradients within the paraffin wax can slow down the melting process. In the absence of fins, the heat may only penetrate the surface of the wax, while the fins help distribute heat more evenly, reducing these gradients and promoting uniform melting. Where the fins promote the convection currents in the surrounding air. As PCM heats up near the fins, it becomes less dense and rises, while the cooler PCM moves in to take its place.

This natural convection increases the rate at which the heat is transferred from the fins to the surrounding PCM, which, in turn, accelerates the melting process. The cumulative effect of increased surface area, enhanced heat conduction, reduced temperature gradients, and improved convection all work together to reduce the overall melting time of the paraffin wax.

The fins act as efficient heat conductors and distributors, ensuring heat penetrates the wax more quickly and uniformly.

5.4 Comparison of Numerical Results with Published Literature Results

The current numerical data were cross-referenced with the literature data, as shown in figure (5.26), which concurs with the results of the current study. External and internal fins were introduced into TTHX to increase heat transfer as a heat enhancement technique. Al-Abidi et al. [41] numerically studied the effects of various design as well as operating parameters, like length of fin and its thickness, no. of fin, geometry of PCM, material of TTHX, and Stefan no. upon the procedure of melting. According to the study outcomes, the time of the melting of the geometry of 8-cell PCM unit was decreased via (34.7%) in comparison with to the time of the melting of a triplex tube having fins, whereas in the present study with the same cases of fins but at a flow rate of 10 l/min and using RT42 instead of RT82 a reduction in charging time of 29.9% was observed.

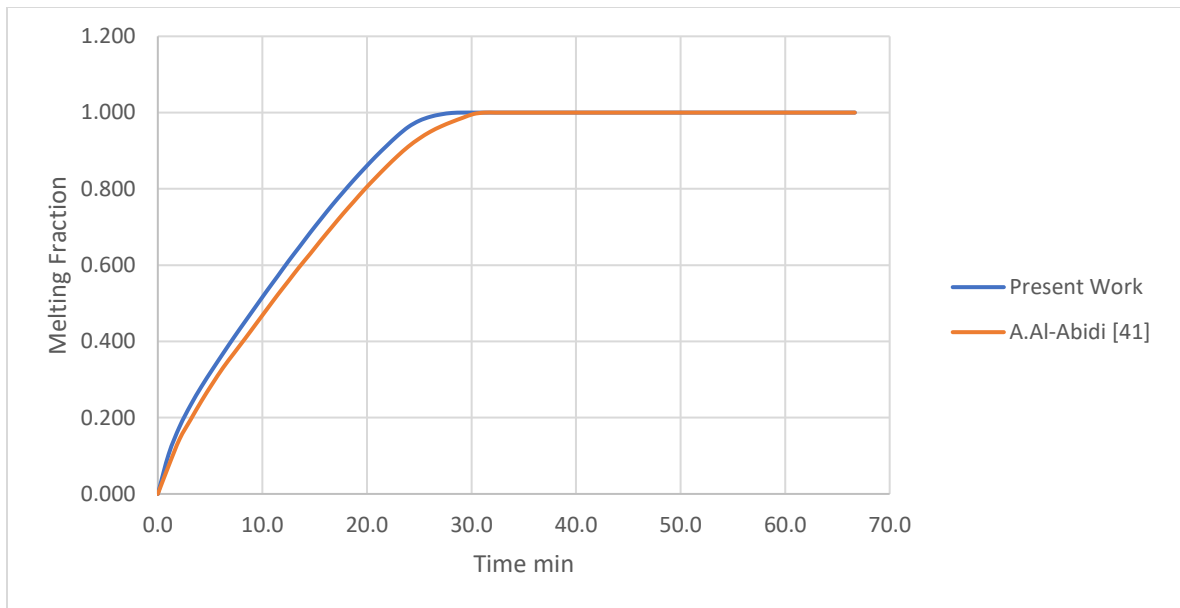


Figure 5.26: Comparison of Numerical results with Al-Abidi et al. [41] results / numerical.

Note from the figure (5.26) that the improvement is better at RT42 than at RT82, and this is because the main difference between these two waxes is their melting point and the effect of this on the melting time. Wax with a lower melting point (42°C) melt faster and at lower temperatures than wax with a higher melting point (82°C). In addition, it uses a higher mass flow at RT42 than at RT82, which speeds up the melting process and reduces the time it takes.

After that, the maximum difference was determined to identify the differences between the experimental and numerical results for the flow rates of HTF (4,8, and16) l/ min which were (4, 8, and 9) %, so the maximum difference was 9% for flow rate 16 l/ min. Figure (5.27) show the comparison of numerical and experimental results for the present work with and without fins.

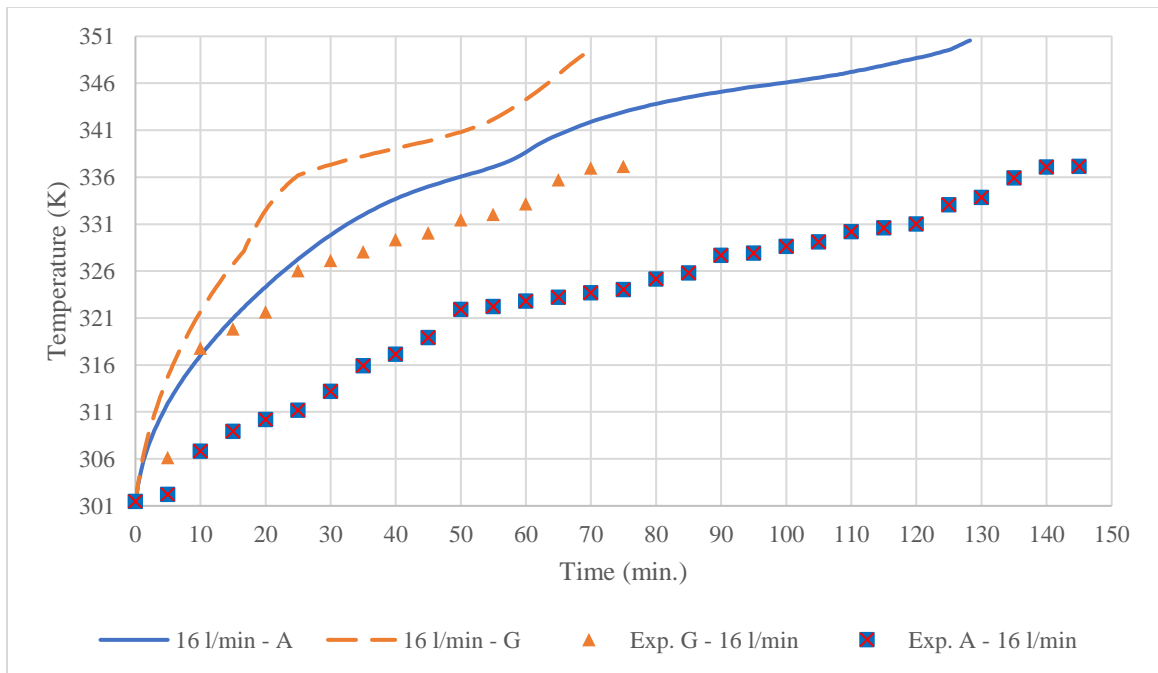


Figure 5.27: Comparison of experimental and numerical results for the present work without and with using fins for flow rate 16 l/ min.

figure (5.27) above manifests the percentages of improvement in melting time after using the fins in the work. The results indicate the difference between the numerical results and the practical results for the following reasons:

- Numerical results often rely on theoretical models that make simplifications and assumptions to describe real-world phenomena. These idealizations may not perfectly capture a practical system's complexities and nuances. Real-world systems can have imperfections, non-linear behavior, or other factors that theoretical models may not account for accurately.
- In practical experiments, measurements are subjected to error. Instruments used to collect data may have accuracy, precision, or

calibration limitations. These errors can introduce discrepancies between expected and observed results.

- Practical experiments are conducted in real-world environments, which can introduce variability that theoretical models may not consider. Factors, such as temperature fluctuations, humidity, and ambient conditions can influence the experimental outcomes.
- Theoretical models often rely on specific assumptions and boundary conditions that may not perfectly match the real-world scenario. Deviations from these assumptions can lead to differences between theoretical and practical results.
 - Human error can play a significant role in experimental settings. Errors in setup, execution, or data recording can affect practical results.

Chapter Six: Conclusions And Future Work

6.1 Conclusions

Numerical and experimental analysis on melting paraffin wax in a TSCTSU with triple-square channel heat exchanger, investigating heat transfer enhancement with and without fins, supported by ANSYS FLUENT simulations and Al-Abidi publication [41]. Examined design and operational factors include charging time, mass flow rate fluctuation, temperature changes, fin length, number, shape, and solid-liquid interface proportion visualization.:

1. Heat transfer in triplex-square channel exchanger was better than a triplex-tube HE about 13.8 %.
2. Heat transfer enhancement for a triplex square channel thermal energy unit via utilizing interior and exterior fins for accelerating the rate of RT42 melting as a phase change material was numerically studied; the various factors design and working comprise length of fin, fins no., and geometry of PCM unit were scrutinized. And, the study was carried out in various cases, and in accordance with the findings, Case G reached the whole time of melting earlier than the else cases about 29.2%.
3. In a finned TTHX, the rates of melting as well as the heat transmission considerably augmented if the fins were linked to the exterior and interior channels.
4. The findings manifested that the time of melting reduced via increasing the fins number.

5. The phenomena of heat transfer through conduction and natural convection during charging are documented, and a numerical model for simulating it is validated.
6. Investigating the simultaneous effects as a result of change in latent heat and heat transfer due to the addition of fins in LHS.
7. Comparing the strengths and limits of the heat transfer enhancement techniques in PCM, it was found that relatively adding fins is the most effective solution.

6.2 Recommendations for Future Research

This study brings to light a number of areas for future study, as mentioned below.

1. Study the solidification rate and the energy storage rate of the TSCTSU.
2. Using other type of fins and increasing the heat transfer enhancement with nanofluid.
3. By combining the metal nanoparticles that come with PCM, it is possible to increase the rate of heat transmission.

References

- [1] R. Qaiser and M. Khan, *Heat Transfer Enhancement of Latent Thermal Energy Storage System Using Multiple Tubes and Modified Shell Designs*. 2020.
- [2] N. Zhang, Y. Yuan, X. Cao, Y. Du, Z. Zhang, and Y. Gui, “Latent heat thermal energy storage systems with solid–liquid phase change materials: a review,” *Adv. Eng. Mater.*, vol. 20, no. 6, p. 1700753, 2018.
- [3] A. Sarı and A. Karaipekli, “Thermal conductivity and latent heat thermal energy storage characteristics of paraffin/expanded graphite composite as phase change material,” *Appl. Therm. Eng.*, vol. 27, no. 8–9, pp. 1271–1277, 2007.
- [4] A. I. Fernandez, C. Barreneche, M. Belusko, M. Segarra, F. Bruno, and L. F. Cabeza, “Considerations for the use of metal alloys as phase change materials for high temperature applications,” *Sol. Energy Mater. Sol. Cells*, vol. 171, pp. 275–281, 2017.
- [5] K. Kavitha, “Design construction and modeling studies of paraffin and its composites as pcm s in solar water heater applications”.
- [6] R. Palanichamy, “Heat transfer analysis in a circular tube with internal fin by numerical method”.
- [7] W. A. Vishwanath, “Heat transfer enhancement in Phase change material for thermal energy storage system”.

- [8] P. C. M. Kumar and V. Hariprasath, "A review on triple tube heat exchangers," *Mater. Today Proc.*, vol. 21, pp. 584–587, 2020.
- [9] I. Sarbu and C. Sebarchievici, "A comprehensive review of thermal energy storage," *Sustainability*, vol. 10, no. 1, p. 191, 2018.
- [10] J. Jeon, J.-H. Lee, J. Seo, S.-G. Jeong, and S. Kim, "Application of PCM thermal energy storage system to reduce building energy consumption," *J. Therm. Anal. Calorim.*, vol. 111, pp. 279–288, 2013.
- [11] A. Wazeer, A. Das, and S. Vidya, "Phase Change Materials for Solar Energy Applications," *Trans. Indian Inst. Met.*, vol. 76, no. 5, pp. 1155–1163, 2023.
- [12] P. K. Kushwaha, N. K. Sharma, A. Kumar, and C. S. Meena, "Recent Advancements in Augmentation of Solar Water Heaters Using Nanocomposites with PCM: Past, Present, and Future. Buildings 2023, 13, 79." 2022.
- [13] S. Seddegh, X. Wang, and A. D. Henderson, "A comparative study of thermal behaviour of a horizontal and vertical shell-and-tube energy storage using phase change materials," *Appl. Therm. Eng.*, vol. 93, pp. 348–358, 2016.
- [14] Y. Hong, W.-B. Ye, S.-M. Huang, M. Yang, and J. Du, "Thermal storage characteristics for rectangular cavity with partially active walls," *Int. J. Heat Mass Transf.*, vol. 126, pp. 683–702, 2018.
- [15] H. Eslamnezhad and A. B. Rahimi, "Enhance heat transfer for phase-change materials in triplex tube heat exchanger with selected arrangements of fins,"

- Appl. Therm. Eng.*, vol. 113, pp. 813–821, 2017.
- [16] A. M. Saeed *et al.*, “A numerical investigation of a heat transfer augmentation finned pear-shaped thermal energy storage system with nano-enhanced phase change materials,” *J. Energy Storage*, vol. 53, p. 105172, 2022.
- [17] N. Boulaktout, E. H. Mezaache, and A. Laouer, “Study of Thermal Behavior of a Horizontal Two Fins Annular Tube Heat Exchanger with Melting Phase Change Material: Fins Orientation Effects.,” in *Annales de Chimie Science des Matériaux*, 2021, vol. 45, no. 2.
- [18] S. Ahmed *et al.*, “Melting enhancement of PCM in a finned tube latent heat thermal energy storage,” *Sci. Rep.*, vol. 12, no. 1, p. 11521, 2022.
- [19] K. Hosseinzadeh, E. Montazer, M. B. Shafii, and A. R. D. Ganji, “Solidification enhancement in triplex thermal energy storage system via triplets fins configuration and hybrid nanoparticles,” *J. Energy Storage*, vol. 34, p. 102177, 2021.
- [20] A. Maneengam *et al.*, “Numerical study of heat transfer enhancement within confined shell and tube latent heat thermal storage microsystem using hexagonal PCMs,” *Micromachines*, vol. 13, no. 7, p. 1062, 2022.
- [21] X. Sun *et al.*, “Investigation of heat transfer enhancement in a triple TUBE latent heat storage system using circular fins with inline and staggered arrangements,” *Nanomaterials*, vol. 11, no. 10, p. 2647, 2021.
- [22] X. Huang and S. Yao, “Solidification performance of new trapezoidal

- longitudinal fins in latent heat thermal energy storage,” *Case Stud. Therm. Eng.*, vol. 26, p. 101110, 2021.
- [23] M. Ghalambaz, S. A. M. Mehryan, M. Mahdavi, O. Younis, and M. A. Alim, “Evaluation of the Melting Performance in a Conical Latent Heat Thermal Unit Having Variable Length Fins. *Sustainability* 2021, 13, 2667.” s Note: MDPI stays neutral with regard to jurisdictional claims in published ..., 2021.
- [24] M. J. Zarei, H. Bazai, M. Sharifpur, O. Mahian, and B. Shabani, “The effects of fin parameters on the solidification of PCMs in a fin-enhanced thermal energy storage system,” *Energies*, vol. 13, no. 1, p. 198, 2020.
- [25] V. Pandiyarajan, M. C. Pandian, E. Malan, R. Velraj, and R. V Seeniraj, “Experimental investigation on heat recovery from diesel engine exhaust using finned shell and tube heat exchanger and thermal storage system,” *Appl. Energy*, vol. 88, no. 1, pp. 77–87, 2011.
- [26] N. Modi, X. Wang, and M. Negnevitsky, “Experimental investigation of the effects of inclination, fin height, and perforation on the thermal performance of a longitudinal finned latent heat thermal energy storage,” *Energy*, vol. 274, p. 127327, 2023.
- [27] R. Karami and B. Kamkari, “Experimental investigation of the effect of perforated fins on thermal performance enhancement of vertical shell and tube latent heat energy storage systems,” *Energy Convers. Manag.*, vol. 210, p. 112679, 2020.

- [28] U. V. Awasarmol and A. T. Pise, "An experimental investigation of natural convection heat transfer enhancement from perforated rectangular fins array at different inclinations," *Exp. Therm. Fluid Sci.*, vol. 68, pp. 145–154, 2015.
- [29] B. Kamkari and H. Shokouhmand, "Experimental investigation of phase change material melting in rectangular enclosures with horizontal partial fins," *Int. J. Heat Mass Transf.*, vol. 78, pp. 839–851, 2014.
- [30] B. Kamkari and D. Groulx, "Experimental investigation of melting behaviour of phase change material in finned rectangular enclosures under different inclination angles," *Exp. Therm. Fluid Sci.*, vol. 97, pp. 94–108, 2018.
- [31] B. Kamkari, H. Shokouhmand, and F. Bruno, "Experimental investigation of the effect of inclination angle on convection-driven melting of phase change material in a rectangular enclosure," *Int. J. Heat Mass Transf.*, vol. 72, pp. 186–200, 2014.
- [32] M. R. Salem, M. N. Owyed, and R. K. Ali, "Experimental investigation of the performance attributes of a thermal energy storage unit using different system configurations," *Appl. Therm. Eng.*, vol. 230, p. 120678, 2023.
- [33] L. Lv *et al.*, "Experimental study on a pilot-scale medium-temperature latent heat storage system with various fins," *Renew. Energy*, vol. 205, pp. 499–508, 2023.
- [34] J. Zou, F. He, Y. Qi, X. Meng, and W. Ma, "Thermal performance improvement of thermal energy storage systems by employing a contrastive

- experiment,” *Case Stud. Therm. Eng.*, vol. 41, p. 102647, 2023.
- [35] J. Majeed, J. Abdulateef, and M. Zych, “Thermal Performance Enhancement of Triplex Tube Heat Storage Using Metal Foam,” *Diyala J. Eng. Sci.*, pp. 62–71, 2022.
- [36] J. Vogel and A. Thess, “Validation of a numerical model with a benchmark experiment for melting governed by natural convection in latent thermal energy storage,” *Appl. Therm. Eng.*, vol. 148, pp. 147–159, 2019.
- [37] R. Kumar and P. Verma, “An experimental and numerical study on effect of longitudinal finned tube eccentric configuration on melting behaviour of lauric acid in a horizontal tube-in-shell storage unit,” *J. Energy Storage*, vol. 30, p. 101396, 2020.
- [38] R. Qaiser, M. M. Khan, L. A. Khan, and M. Irfan, “Melting performance enhancement of PCM based thermal energy storage system using multiple tubes and modified shell designs,” *J. Energy Storage*, vol. 33, p. 102161, 2021.
- [39] M. Z. Mahmoud *et al.*, “Melting enhancement in a triple-tube latent heat storage system with sloped fins,” *Nanomaterials*, vol. 11, no. 11, p. 3153, 2021.
- [40] A. Joulin, Z. Younsi, L. Zalewski, S. Lassue, D. R. Rousse, and J.-P. Cavrot, “Experimental and numerical investigation of a phase change material: Thermal-energy storage and release,” *Appl. Energy*, vol. 88, no. 7, pp. 2454–2462, 2011.

- [41] A. A. Al-Abidi, S. Mat, K. Sopian, M. Y. Sulaiman, and A. T. Mohammad, "Internal and external fin heat transfer enhancement technique for latent heat thermal energy storage in triplex tube heat exchangers," *Appl. Therm. Eng.*, vol. 53, no. 1, pp. 147–156, 2013.
- [42] Y. Muhammad, P. Saini, K. Knobloch, H. L. Frandsen, and K. Engelbrecht, "Rock bed thermal energy storage coupled with solar thermal collectors in an industrial application: Simulation, experimental and parametric analysis," *J. Energy Storage*, vol. 67, p. 107349, 2023.
- [43] S. Liu, H. Peng, Z. Hu, X. Ling, and J. Huang, "Solidification performance of a latent heat storage unit with innovative longitudinal triangular fins," *Int. J. Heat Mass Transf.*, vol. 138, pp. 667–676, 2019.
- [44] A. M. Abdulateef, S. Mat, J. Abdulateef, K. Sopian, and A. A. Al-Abidi, "Thermal performance enhancement of triplex tube latent thermal storage using fins-nano-phase change material technique," *Heat Transf. Eng.*, vol. 39, no. 12, pp. 1067–1080, 2018.
- [45] F. L. Rashid *et al.*, "Solidification enhancement of phase change materials using fins and nanoparticles in a triplex-tube thermal energy storage unit: Recent advances and development," *Int. Commun. Heat Mass Transf.*, vol. 147, p. 106922, 2023.
- [46] M. W. Aljibory, F. L. Rashid, and S. M. A. Alais, "An Experimental and numerical investigation of heat transfer enhancement using annular ribs in a

- tube,” in *IOP conference series: materials science and engineering*, 2018, vol. 433, no. 1, p. 12057.
- [47] A. R. Darzi, M. Farhadi, and K. Sedighi, “Numerical study of melting inside concentric and eccentric horizontal annulus,” *Appl. Math. Model.*, vol. 36, no. 9, pp. 4080–4086, 2012.
- [48] S. Seddegh, M. M. Joybari, X. Wang, and F. Haghghat, “Experimental and numerical characterization of natural convection in a vertical shell-and-tube latent thermal energy storage system,” *Sustain. cities Soc.*, vol. 35, pp. 13–24, 2017.
- [49] W. Xiong, “Numerical and Experimental Study of the Melting Process of a Phase Change Material in a Partially Filled Spherical Shell.” Lehigh University, 2017.
- [50] V. R. Voller and C. Prakash, “A fixed grid numerical modelling methodology for convection-diffusion mushy region phase-change problems,” *Int. J. Heat Mass Transf.*, vol. 30, no. 8, pp. 1709–1719, 1987.
- [51] A. A. Al-Abidi, S. Mat, K. Sopian, M. Y. Sulaiman, and A. T. Mohammad, “Experimental study of PCM melting in triplex tube thermal energy storage for liquid desiccant air conditioning system,” *Energy Build.*, vol. 60, pp. 270–279, 2013.
- [52] M. F. Al-Saleh and A. E. Yousif, “Properties of the standard deviation that are rarely mentioned in classrooms,” *Austrian J. Stat.*, vol. 38, no. 3, pp. 193–202, 2009.

Appendices

Appendix-A

Details of ANSYS FLUENT program

This appendix is devoted to illustrating the steps of the numerical simulation using Fluent. The steps from importing geometry to Design Modeler, to the start of the run are shown, the methods of solution are illustrated as well.

1. Workbench and Component Systems

Open Ansys Workbench, from the list of *Component Systems* drag and drop the *Geometry*, *Mesh*, *Fluent* and *Results (CFD Post)* components, link A2 to B1, B3 to C2 and C3 to D2¹, as shown in the following figure.

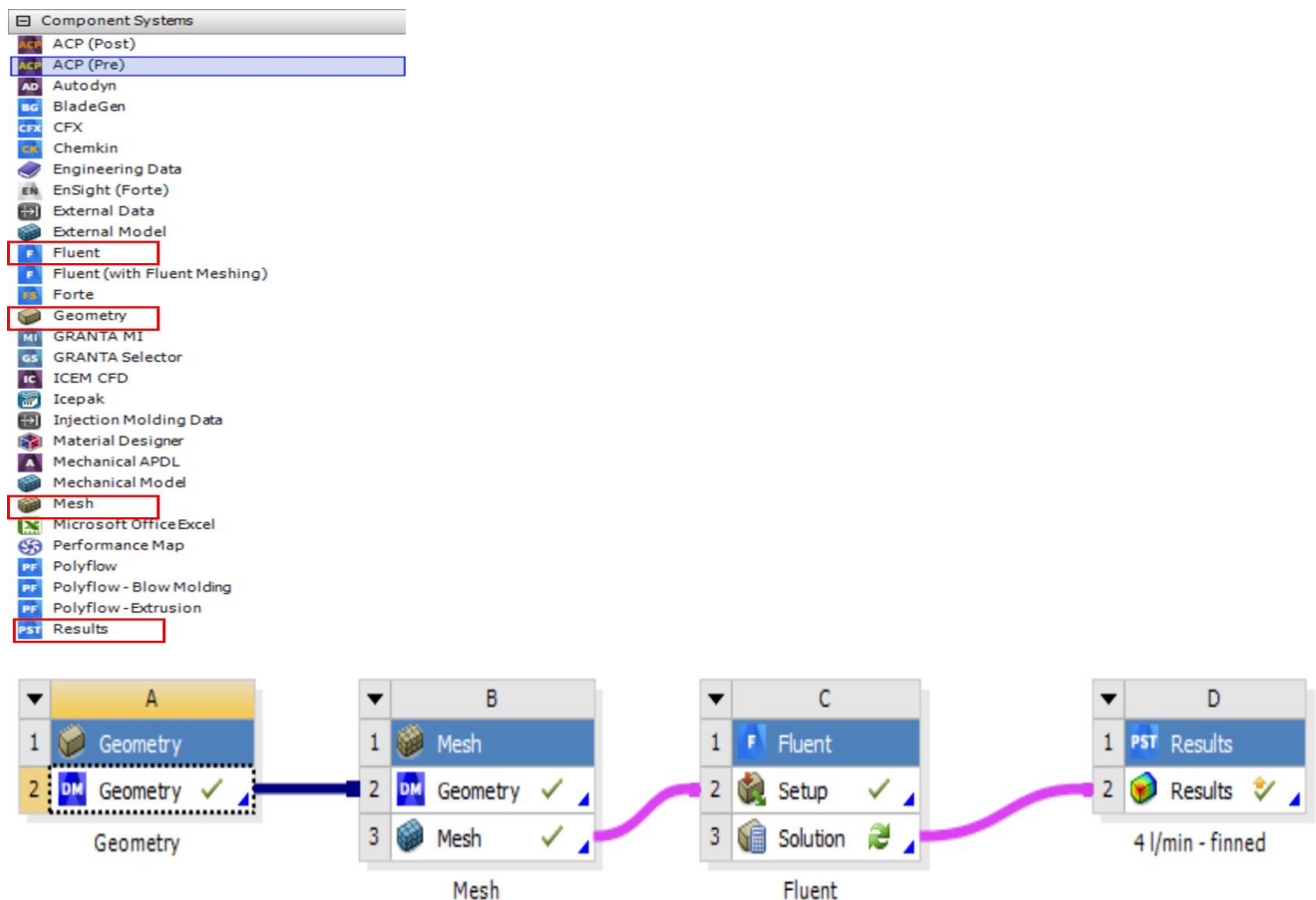


Figure A.1: System Components and Scheme of Analysis.

¹ Note that these letters A, B, C, ... may change with the order of the component in the workbench interface.

2. Geometry preparation

Open Design Modeler. From *File* chose *Import External Geometry File...* Select file (ex: *file_name.sldprt*) and click on *Open*. Make sure that model's base plane is XY plane, i.e. the longitudinal axis is Z.

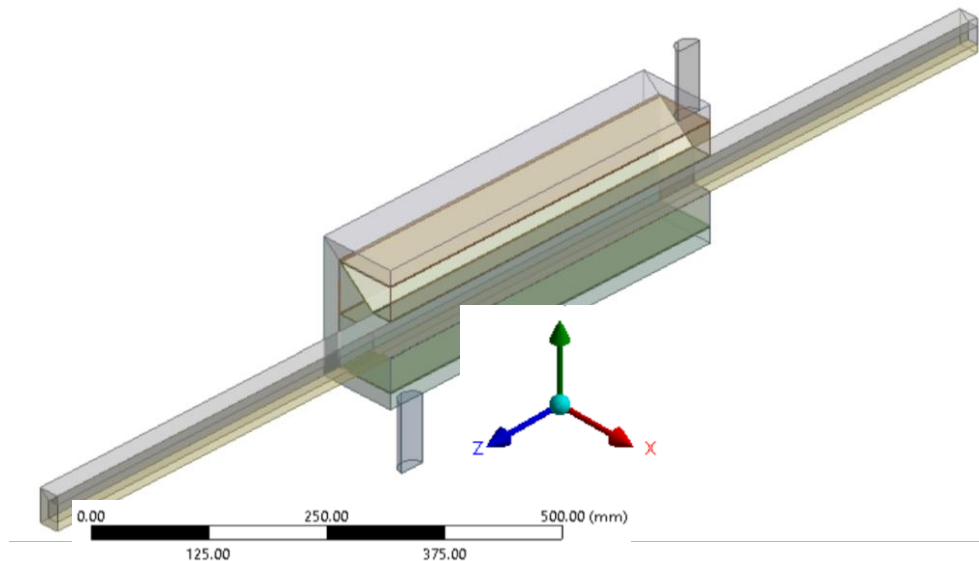


Figure A.2: The Imported Geometry.

Create planes with 45 degrees with X and Y axes. Select *Slice* command, select *Slice by Plane* and slice the body according to the position and length of fins to ease the creation of structured hexahedral mesh in the step of meshing.

Combine the sliced bodies. Chose the bodies of the PCM domain right click, then hit *Form New Part* (see Figure 2). Repeat this to group the bodies of inner HTF, outer HTF, the inner tube and the middle tube, each group separately. This will guarantee that each group will be treated as a single body (domain) in the solver.

From *File* chose *Save Project*, name the file (ex: *pcm_simulation.wbpj*) and hit *Save*. This will save the working files in the destination (or path) you prefer. Make sure you switched the type of each group of bodies to *Fluid* (for PCM, inner HTF and outer HTF), or keep as *Solid* for tubes by left clicking on the group from *Details View* panel.

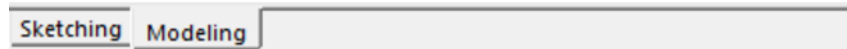
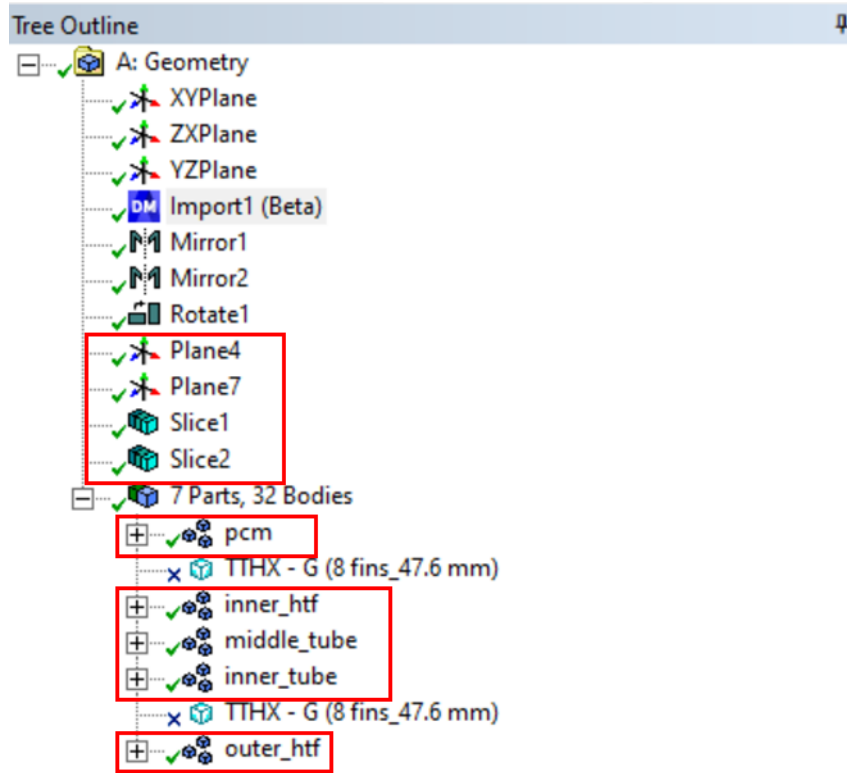


Figure A.3: Model Tree Outline.

Details of pcm	
Part	pcm
Volume	4.6086e+06 mm ³
Surface Area	4.3399e+05 mm ²
Bodies	4
Faces	24
Edges	48
Vertices	32
Fluid/Solid	Fluid
Shared Topology Method	Automatic

Figure A.4: Details of The PCM (as an Example).

3. Mesh generation

Open Ansys Mesh component, review the connections (*Outline > Contacts > Connections*). Or better if contacts are defined on your own. These contacts are four contacts, namely, (1) inner HTF – inner wall of the inner tube, (2) outer wall of the inner tube – PCM inner wall, (3) PCM outer wall – middle tube inner wall and (4) middle tube outer wall – outer HTF inner wall.

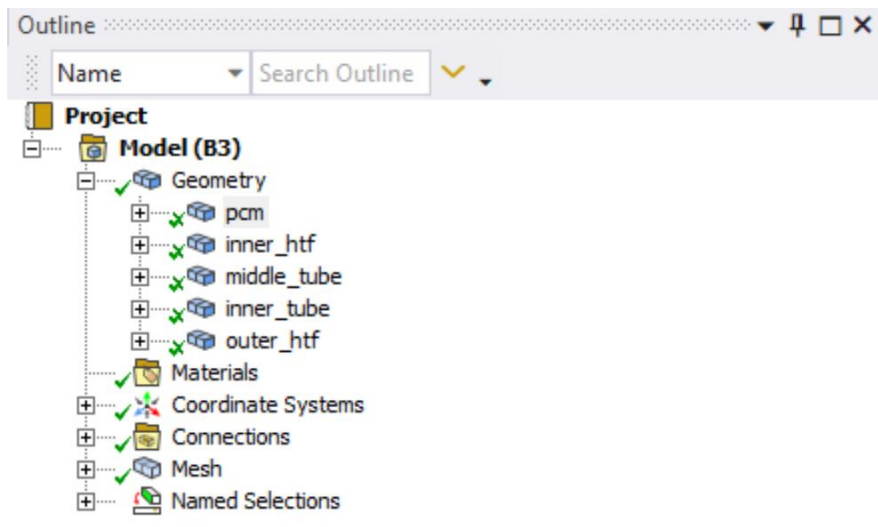


Figure A.5: Mesh Outline.

Lift clicks on *Mesh* and select the edges individually or similar edges together and apply an adequate *Edge Sizing* on the edges. Apply an adequate *Bias Type* if required to count for near wall refinement. Apply *Multizone* mesh method to the inlet and outlet tubes of the outer HTF and the tubes to help in structuring the mesh cells. Click *Generate* from *Mesh* panel to generate the mesh.

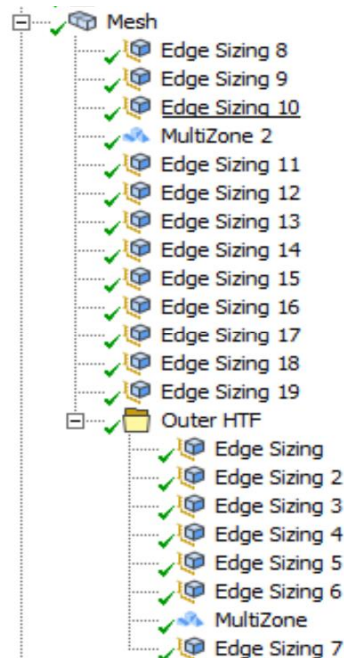


Figure A. 6: Mesh of Edges And Bodies.

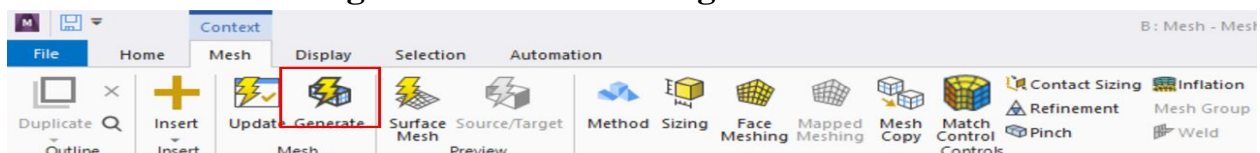


Figure A.7: Mesh panel.

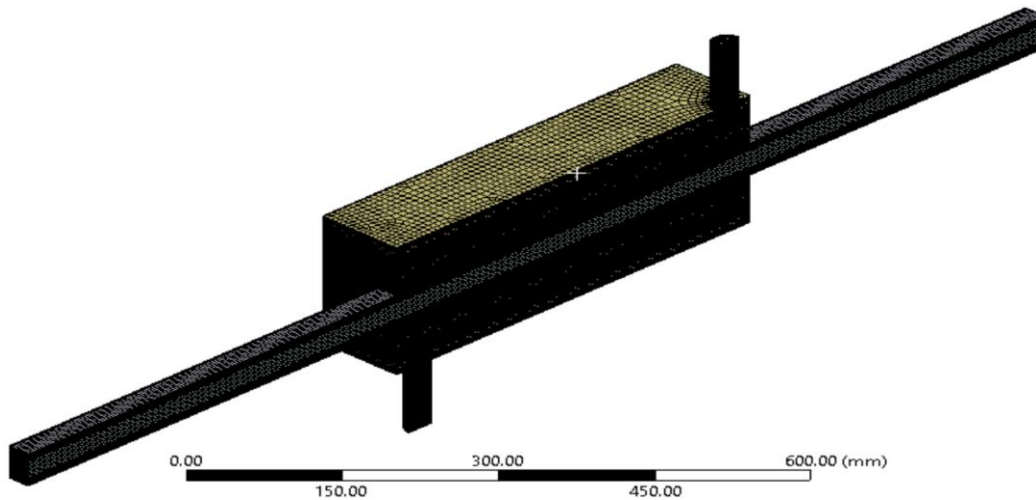


Figure A.8: Mesh After Generation.

Select the boundaries of the model (ex: inlet, outlet, walls, PCM domain² etc.) separately, then right click and select *Create Named Selection...*, name each boundary and hit *OK* to define the boundaries at which boundary conditions will be assigned.

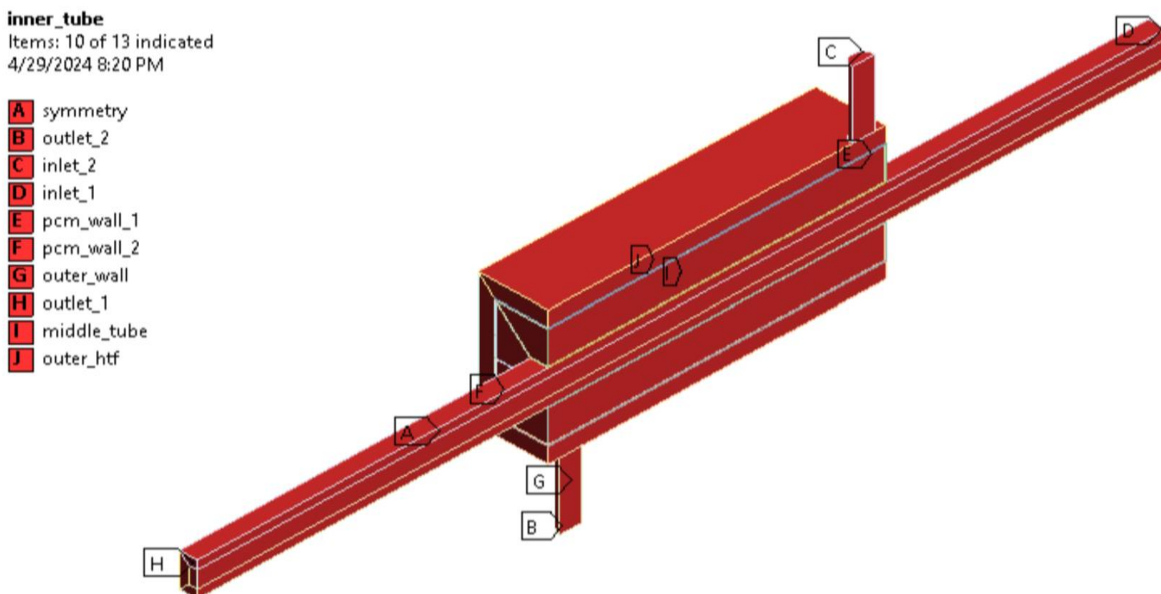


Figure A.9: Named Selections of The Boundaries.

4. Solver setup

Close *Mesh*. Double click on *Setup* (or right click and hit *Edit...*). A dialog box will appear called *Fluent Launcher*. Tick *Double Precision* and select an adequate number of cores according to your machine's specifications.

² Body named selection will be defined as interior type boundary condition in Fluent.

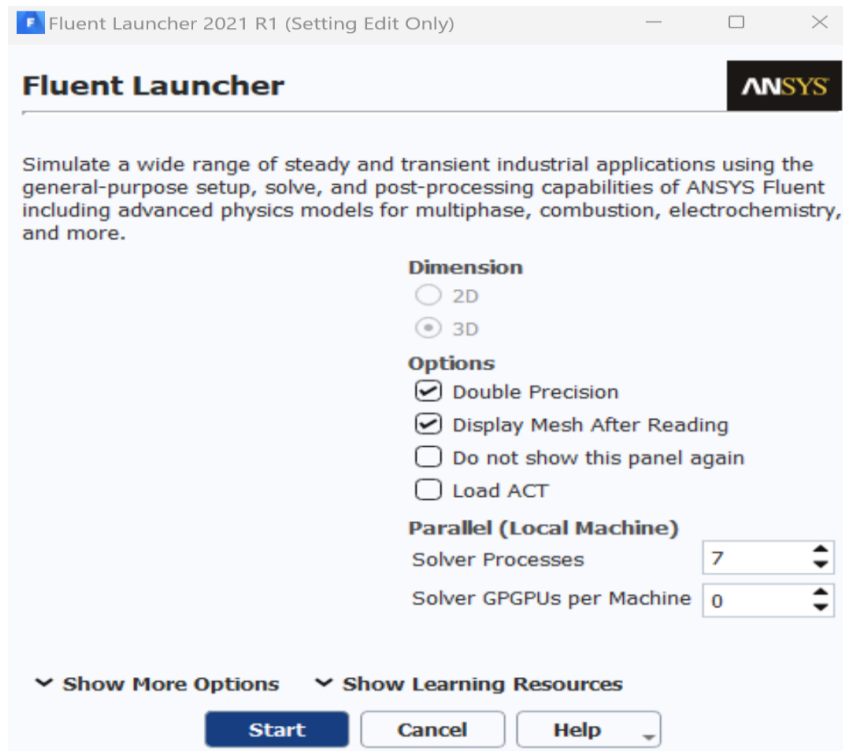


Figure A.10: Fluent Launcher settings.

When the interface of Fluent is open, from *General*, keep *Type* as *Pressure-Based* and *Velocity Formulation* as *Absolute*. For *Time* select *Transient*. Tick *Gravity* and enter the gravitational acceleration as -9.81 m/s^2 in Y direction (see Figure 11).

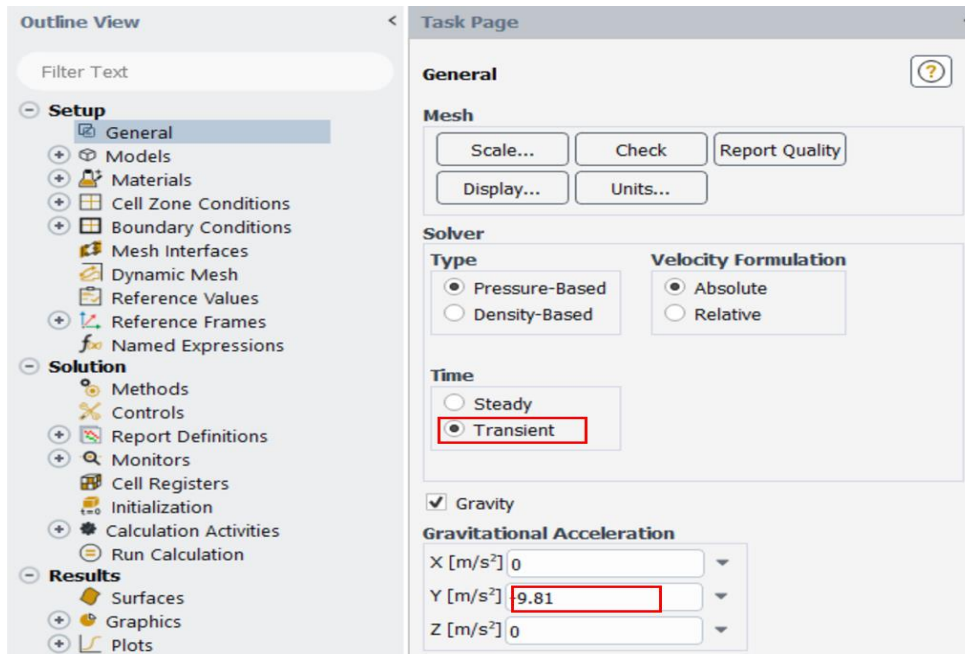


Figure A.11: General task page settings.

Under *Models* double click on *Energy* and tick *ON*. Double click on *Viscous* and select *Laminar* or *k- ω SST with Low-Re Corrections* according to the Reynolds number of the HTF. Under *Solidification & Melting* tick *ON* and keep the *Mushy Zone Parameter* as default.

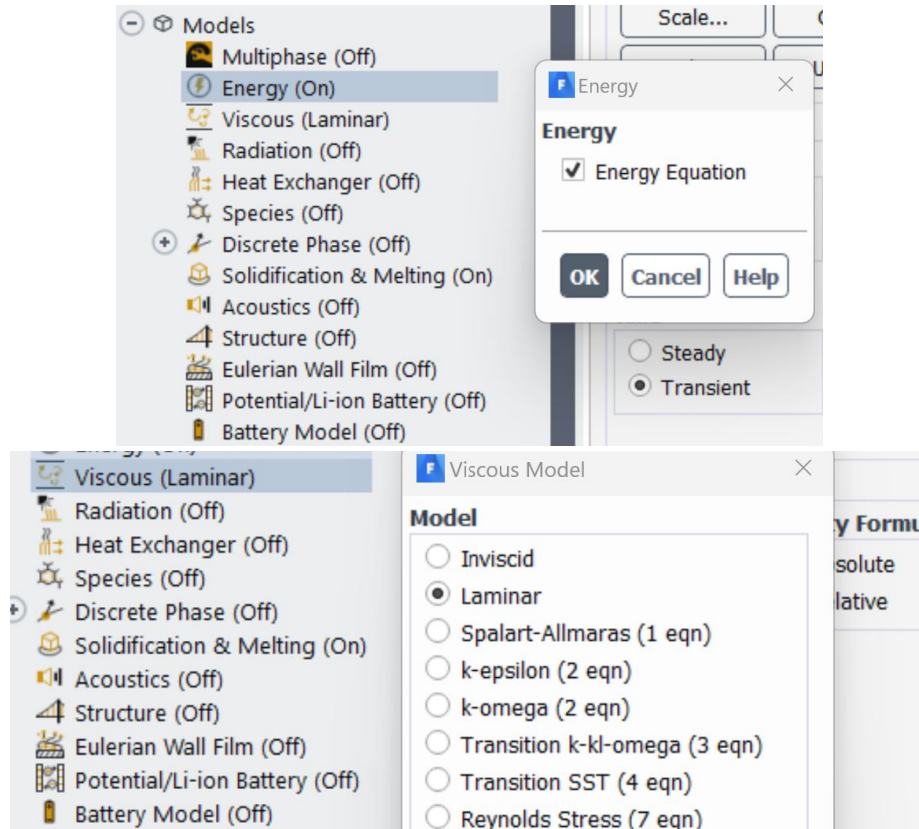


Figure A.12: Energy and Viscous settings.

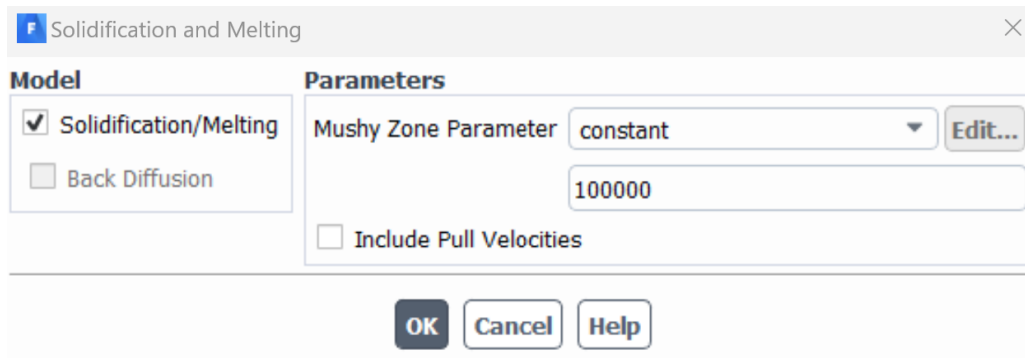


Figure A.13: Solidification and Melting settings.

Under *Materials* > *Fluid*, rename default material (air) under *Name* (ex: beeswax, RT42, etc.). change *Density* to *boussinesq*, enter the data of the PCM and hit *Change/Create*.

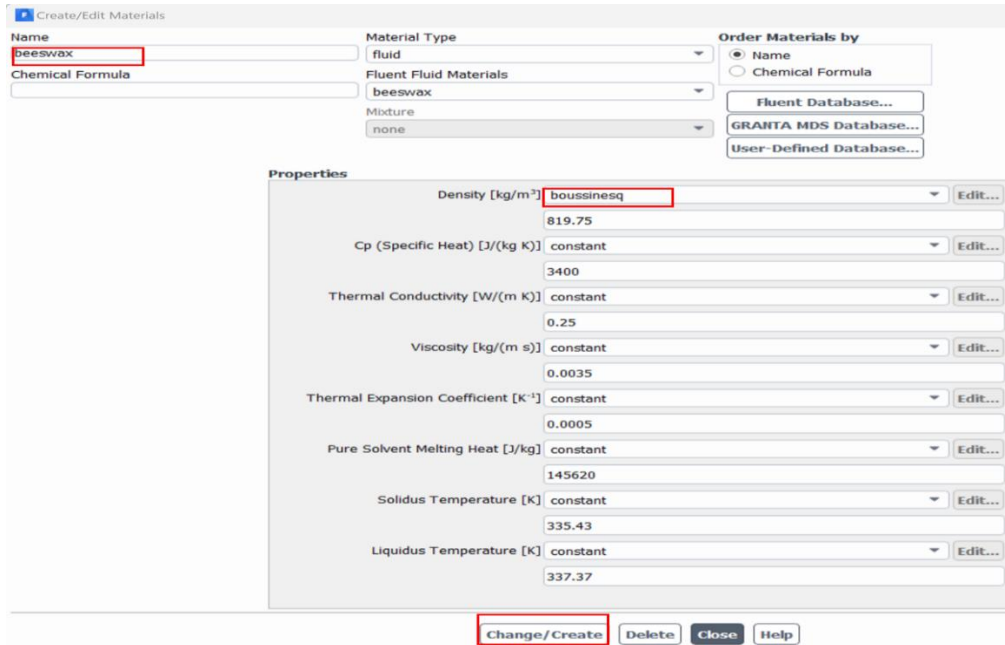


Figure A.14: PCM Material Insertion.

Similarly, change the material of the solids present.

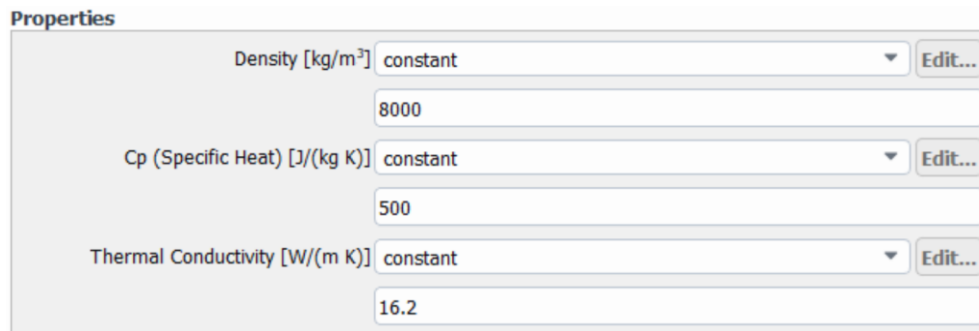


Figure A.15: Solid Material Properties.

Under *Cell Zone Conditions* you will find inner and outer HTF and PCM are under *Fluid* (if materials of inner and outer HTF and PCM are changed as in Section 2 in geometry step, otherwise define them by right clicking the cell zone and changing *Material Name* to the name of the fluid, namely, water for HTF and the PCM material for PCM, then click *Apply*). However, you must change the material to specify both HTF and PCM materials. If more than a material is used for solids, do the same to specify the correct material per zone as well.

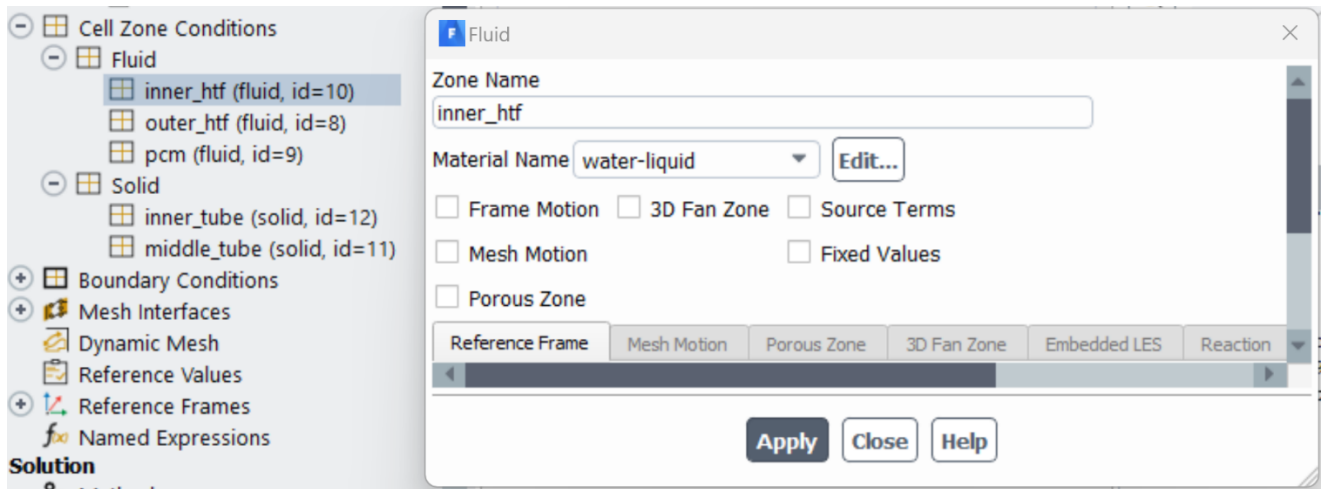


Figure A.16: Setting Up Cell Zones.

For *Boundary Conditions*, the only boundary conditions of interest are the two inlets and outlets, the outer wall of the outer HTF and the coupled walls. Set inlet to *mass-flow-inlet* and outlet as *outflow*. If the boundary condition type was *velocity-inlet* and *pressure-outlet* for example, right click the boundary and then select *mass-flow-inlet* and *outflow* from the list. Check that coupled walls have shadow walls. These walls are the walls through them heat transfer occurs between solids and fluids, i.e. their boundary values are dependent. Keep the outer wall of the outer HTF as a no slip, zero heat flux wall. For inlet, enter the value of *Mass Flow Rate* in *Momentum* panel and switch to *Thermal* panel and enter the stream *Total Temperature*.

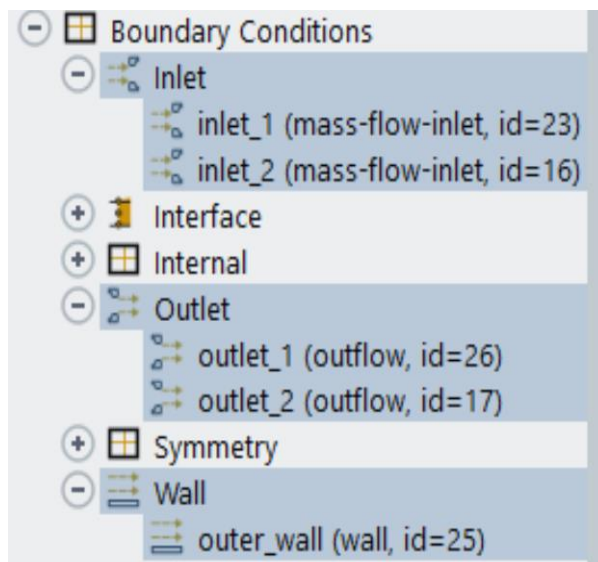


Figure A.17: Boundaries Of Interest.

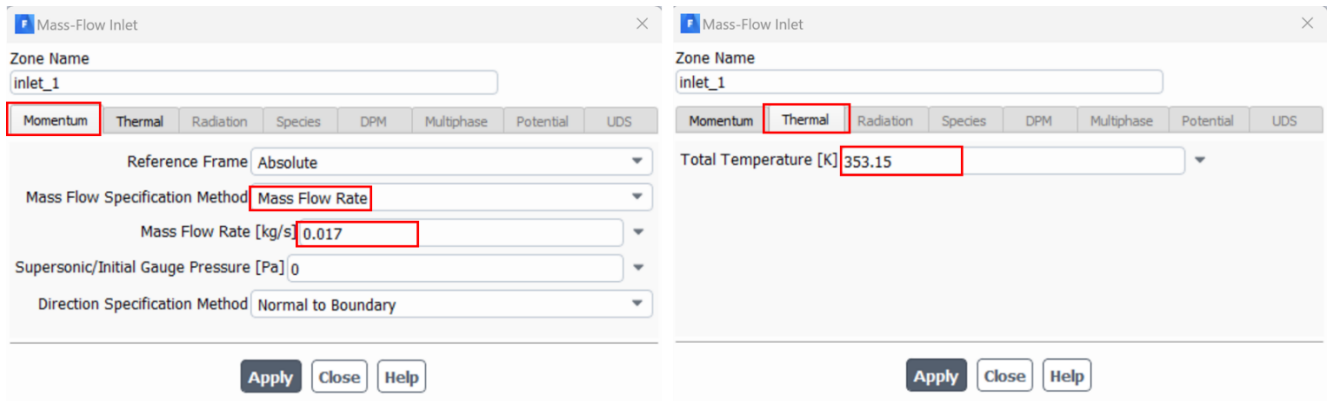


Figure A.18: Inlet Boundary Condition Settings.

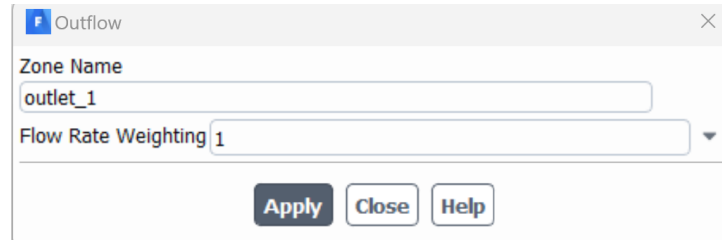


Figure A.19: Pressure Outlet Boundary Condition Settings.

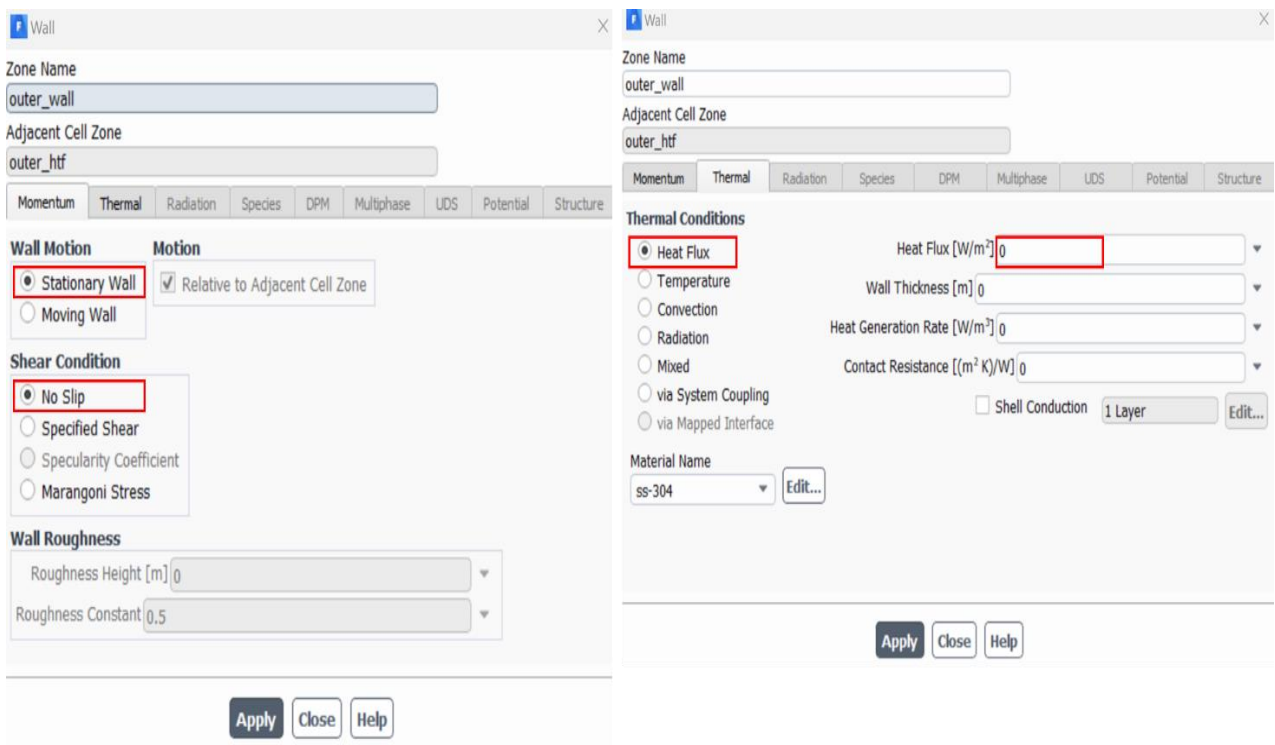


Figure A.20: Outer Wall of The Outer HTF Settings.

On *Methods* task page, under *Scheme* select *Simple*. Under *Spatial Discretization* select *PRESTO!* for *Pressure*, *QUICK* for *Momentum* and *Second Order Upwind* for *Energy*. Tick *Higher Order Term Relaxation*.

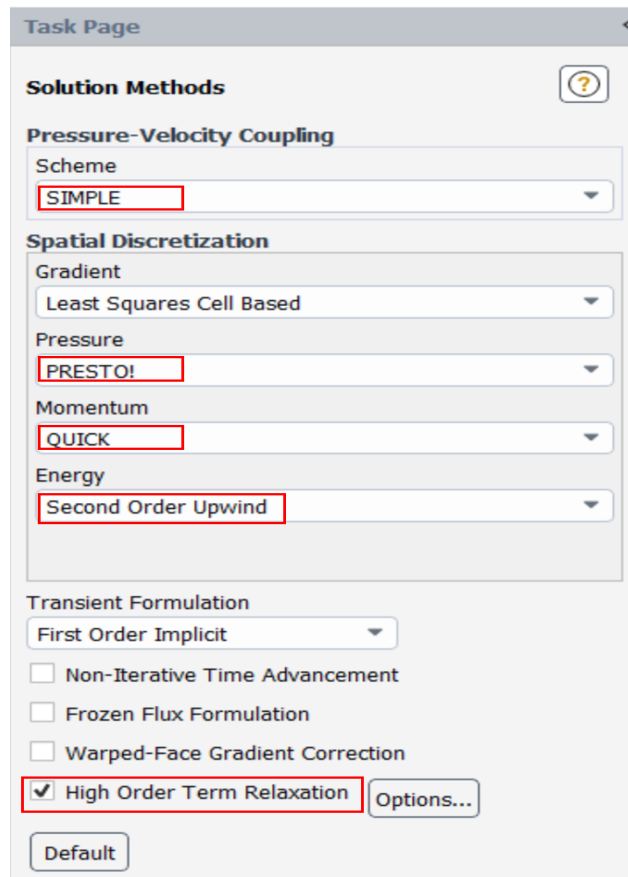


Figure A.21: Solution Methods Settings.

On *Report Definitions*, right click, select *New > Volume-Average*. Give a name to the report under *Name*, tick *Report Plot* and *Report File*, and specify the interval (number of timesteps) to update the report and plot. We need two report plots and files, one for liquid fraction and the other for temperature. For liquid fraction reports (Figure 23) select *Solidification/Melting... > Liquid Fraction* under *Field Variable* then hit *OK*. Under *Cell Zone* select PCM zone. The same is done for temperature reports (Figure 24). Give the report a name, select *Volume-Average* under *Report Type*. select *Temperature > Total Temperature*.

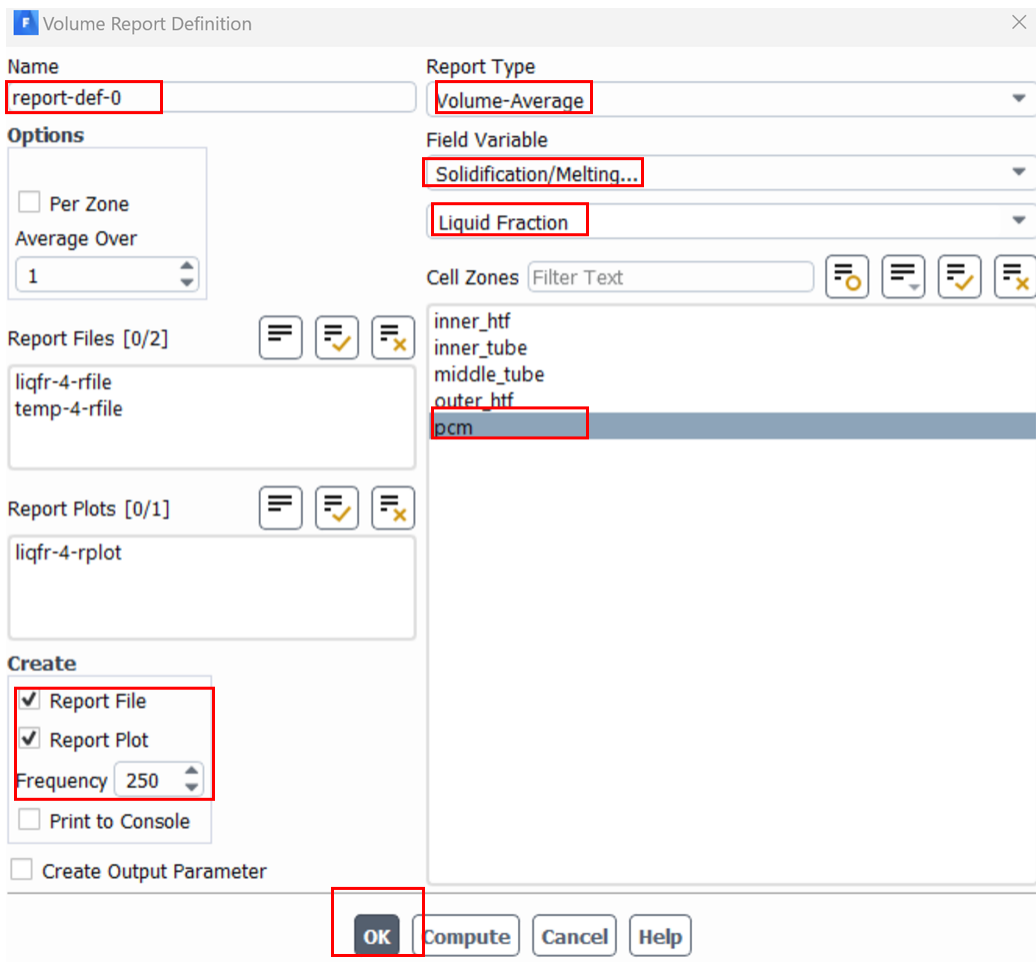


Figure A.22: Creating a Report Definition.

The screenshot shows the 'Volume Report Definition' dialog box. The 'Name' field is 'liqfr-4'. The 'Report Type' is 'Volume-Average'. The 'Field Variable' is 'Solidification/Melting...' and the 'Cell Variable' is 'Liquid Fraction'. The 'Average Over' is set to '1'. The 'Cell Zones' list includes 'inner_htf', 'inner_tube', 'middle_tube', 'outer_htf', and 'pcm', with 'pcm' selected. The 'Report Files' list includes 'liqfr-4-rfile' and 'temp-4-rfile'. The 'Report Plots' list includes 'liqfr-4-rplot'. There are buttons for 'OK', 'Compute', 'Cancel', and 'Help' at the bottom.

Figure A.23: Report Definition of Liquid Fraction.

The screenshot shows the 'Volume Report Definition' dialog box. The 'Name' field is 'temp-4'. The 'Report Type' is 'Volume-Average'. The 'Field Variable' is 'Temperature...' and the 'Cell Variable' is 'Total Temperature'. The 'Average Over' is set to '1'. The 'Cell Zones' list includes 'inner_htf', 'inner_tube', 'middle_tube', 'outer_htf', and 'pcm', with 'pcm' selected. The 'Report Files' list includes 'liqfr-4-rfile' and 'temp-4-rfile'. The 'Report Plots' list includes 'temp-4-rplot'. There are buttons for 'OK', 'Compute', 'Cancel', and 'Help' at the bottom.

Figure A.24: Report Definition of Temperature.

Set the residuals as in Figure 25 below (0.001 for continuity, x-velocity, y-velocity and z-velocity, k and omega if present and 0.00001 for Energy).

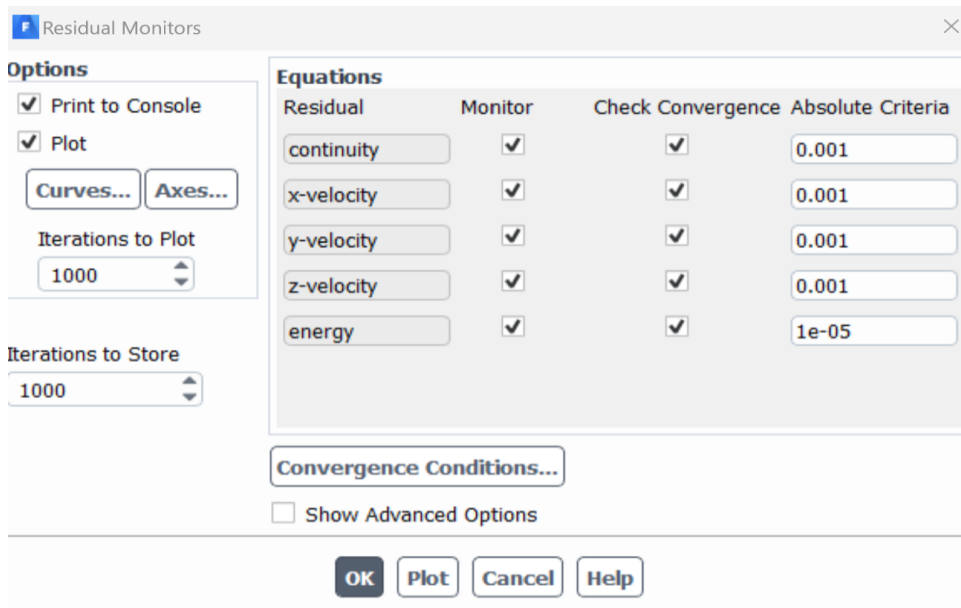


Figure A.25: Solution Residual Monitors.

For *Initialization*, select *Hybrid Initialization*, then hit *Patch* and assign *Temperature* to the inlet temperature for HTFs and the starting initial temperature (say 292 K) for the tubes and PCM.

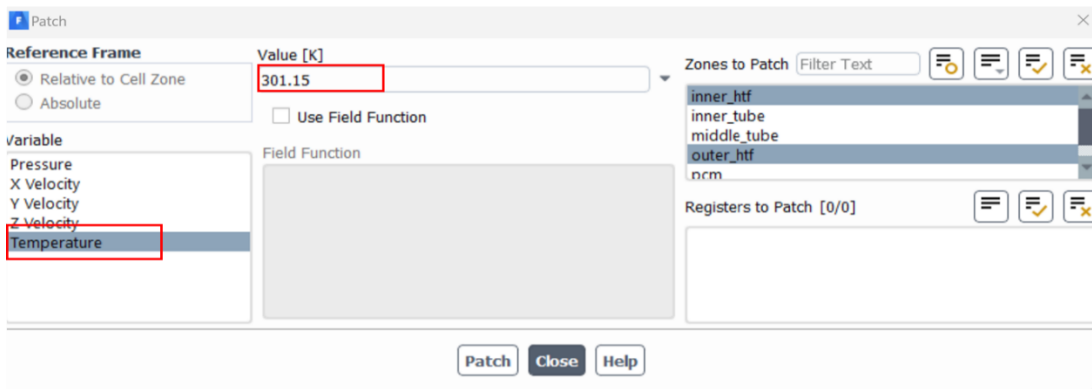
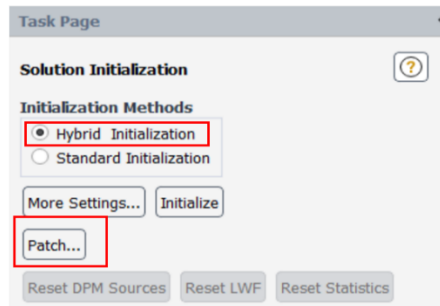


Figure A.26: Initialization Process.

On Calculation Activities task page autosave after a suitable number of timesteps (say 1000 timesteps).

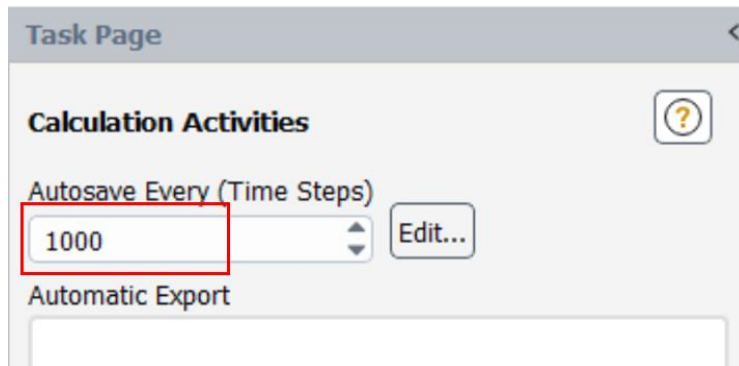


Figure A.27: Autosave of The Solution.

To start the calculation, on *Run Calculation* task page, enter a suitable number of timesteps to the problem, a suitable timestep and number of iterations per each step, then hit *Calculate* (see Figure 28).

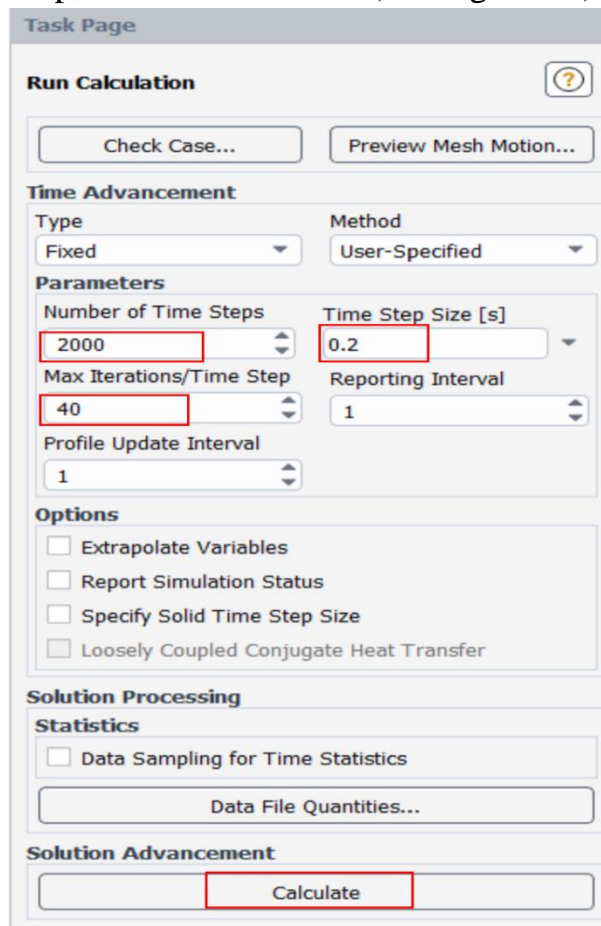


Figure A.28: Running The Calculation Step.

Appendix -B

Calibration of Instruments

Calibration of tools refers to procedures and operations aimed at adjusting and correcting standard tools, electronic devices, or scientific instruments to ensure their accuracy and the precision of their readings. The Renewable Energy Directorate of the Ministry of Science and Technology as well as the Central Organization for Standardization and Quality Control Metrology/Physics Section calibrated the following measuring equipment:

- Thermometer type Lutron BTM-4208SD.
- Thermocouples.



Calibration Certificate
Central Organization for Standardization and Quality Control
(COSQC)

Metrology Department - Physics Section
P.O. Box13032 Aljadriya street , Baghdad , Tel:7785180 , E-Mail : metrology.cos@cosqc.gov.iq

Certificate No.: PHT 888/2023 (QF - 7.8 - 01) Date of issue : 04/07/2023

Customer			
Name:	جامعة كربلاء / كلية الهندسة / قسم الهندسة الميكانيكية / طالب الدراسات العليا أمين محمد رحمان منصور / ماجستير		
Address	العراق - كربلاء المقدسة		
Item under calibration			
Description:	12 Channel Temperature Recorder With TC Type (K)	Res. :	0.1 ° C
Manufacturer:	Lutron	Model :	BTM - 4208SD
Other identification:	(-200 --- 1370)°C	Serial number:	TP-01
Date of reception:	13/06/2023	Order No. :	345
Condition of reception:	As Found		
Standard(s) used in the calibration			
Description:	Agilent Model (34420A) With PT100 (S. NO. : 3)		
Calibration information			
Date of calibration:	26/06/2023	Validation :	One Year
Place of calibration:	PH Lab (1)	Calibration quantity :	Temperature ° C
Method(s) of calibration:	Calibration method using : QP-7.2-01-C		
Measurement uncertainty:	The reported expanded uncertainty is based on UKAS M3003 Standard and the standard Uncertainty multiplied by coverage factor k=2 to give confidence level of 95%		
Metrological traceability:	The traceability of measurement results to the SI units is assured by the National standard maintained at Central Organization for standardization and Quality Control through calibration at :- UME (G1KS-0248)		
Environmental conditions	Temp. : 30.38° C	RH % :	24.6%

Results

Set. Value °C	Ref. (R) °C	UUC (M) °C	Error (M - R) °C	Uncertainty ± °C
150.0	150.4	151.3	0.9	1.08
Observations, opinions or recommendations:		The Results in the table should be taken in to consideration according to your decision rule		

Calibration Specialist :
Khalid Naser
04/07/2023

Revised by :
Alyaa Farhan
04/07/2023

Approved by :
Head Of Physics Section
Hanaa Mohamined
04/07/2023

This certificate is issued in accordance with the laboratory accreditation requirements. It provides traceability of measurement to recognized national standards, and to the units of measurement realized at the COSQC or other recognized national standards laboratories. This certificate may not be reproduced other than in full by photographic process. This certificate refers only to the particular item submitted for calibration

Appendix- C

Uncertainty analysis

This aspect summarizes the method of calculating the inaccuracy of measured data obtained from practical experiments, as it divides the error rate into three groups: Calibration errors, data collection, and data reduction. The data are measured with devices, such as temperature and flow rate.

- **Flow meter**

The Root Square Sum formula may be used to get the overall uncertainty of the Heat Transfer flow (water) rate, which is equal to the uncertainties of the curve fitting [52]:

$$U_{F,ov} = \pm \sqrt{(U_{F,c-f})^2}$$

Where, $U_{F,ov}$, is the overall uncertainty in the flow rate measurement, and $U_{F,c-f}$ is the curve fitting uncertainty. The statistical calculation of the curve fitting uncertainty is shown in Table (C-1).

Table C-1: Uncertainty in flow rate measurement

Data point	Flow meter reading (L/min)	Measured flow rate (L/min)	Curve fitting equation $Y=0.993X+0.27$	Deviation squared = (flow rate reading- Y)
1	1	1.2	1.263	0.263
2	1.5	1.7	1.7595	0.2595
3	2	2.2	2.256	0.256
4	2.5	2.75	2.7525	0.2526
5	3	3.27	3.249	0.249
6	3.5	3.57	3.7455	0.07
7	4	4.2	4.242	0.242
8	4.5	4.55	4.7185	0.218

9	5	5.25	5.215	0.215
10	5.5	5.52	5.7115	0.2115
11	6	6.21	6.208	0.208
12	6.5	6.62	6.7045	0.2045
13	7	7.21	7.201	0.201
Sum = 2.85				
Degree of freedom (n-1) = 12				
Standard deviation = $\sqrt{\frac{\sum \text{Divation squar}}{n-1}} = 0.483$				
$U_{F,c-f} = \pm 0.483 \text{ l/min} = U_{F,ov}$				

To calculate the Repeatability of the experimental results, the following parameter are concerned [52]:

1. The mean value of the variable x calculated as: $X^{mean} = X_{average} = \frac{\sum_i^n x_i}{n}$
2. The standard deviation of x , given by: $\sigma = \sqrt{\frac{\sum_{i=1}^n (x_i - \bar{x})^2}{n-1}}$



Appendix- D
Published Research

D-1: Published Research in 6th International Conference On Engineering Sciences-ICES” which was held from 18 to 22 December,2022.

The paper was accepted for presentation and publication in the ICES conference proceedings.



D-2: Published Research in 7th International Conference On Engineering Sciences-ICES” which was held from 13 to 14 December,2023.

The paper was accepted for presentation and publication in the ICES conference proceedings.



*Certificate of Participation
Presented to*

I, hereby, certify that **Zainab Abdul Karim Alkhekany,
Mohammed Wahhab Aljibory & Farhan Lafta Rashid**

submitted the paper entitled

**Impact of Modified Fin Geometry on Triple-Square Channel Thermal
Energy Storage Unit Performance**

to the “7thInternational Conference On Engineering Sciences - ICES”

which was held from 13 to 14 December, 2023

The paper was accepted for presentation and publication
in the conference proceedings.


Prof. Dr. Basim Khalil Nile
President of University of Kerbala
Chair of the Scientific Committee of ICES



الخلاصة

في نظام تخزين الطاقة ، اعتبرت أن الطاقة الحرارية الحرارية الكامنة مهمة للغاية من الطاقة المعقولة بسبب كثافتها الكبيرة من طاقة التخزين في وحدة كتلة عند طاقة حرارية ثابتة تقريبا. يستخدم العمل الأخير زعانف داخلية وخارجية لمناقشة تقنية لتعزيز نقل الحرارة أثناء ذوبان مواد تغيير الطور (PCM) في مبادل حراري ثلاثي القناة. (TSCHE) تم تطوير نموذج رقمي ثلاثي الأبعاد باستخدام برنامج FLUENT 2021. يتم النظر في التوصيل النقي والحمل الحراري الطبيعي في المحاكاة. في الحالة الأولى من العمل ، تمت دراسته عدديا باستخدام شمع البارافين RT42 ، مع قناة نحاسية ثلاثية المربعه. إن العثور على عدد الزعانف وطول الزعنفة ومعدلات تدفق الكتلة وهندسة مادة تغيير الطور (PCM) في TSCHE هو دراسة تأثير الوقت لذوبان PCM الشامل. ركزت الدراسة على حالات الزعانف ، وتحديد الحالة A (بدون زعانف) ، والحالة B (مع 4 زعانف) ، والحالة C (6 زعانف) ، والحالة D (8 زعانف) ، وجميعها يبلغ طولها 42 ملم. أيضا ، يبلغ طول الحالة E (4 زعانف) والحالة F (6 زعانف) والحالة G (8 زعانف) 47.6 مم ، وأظهرت النتائج الحسابية أن الحالة G (هندسة PCM المكونة من 8 خلايا) أدت وقتا أقصر لإكمال ذوبان PCM ، مع تقليل وقت الانصهار الإجمالي إلى 29.2٪. في الحالة الثانية ، أجريت الدراسة عدديا وتجريبيا: يتم استخدام شمع البارافين RT64 ، وكان النظام مصنوعا من الفولاذ المقاوم للصدأ 304 ، وتأثير معدل تدفق الكتلة ، بدون ومع استخدام زعنفة. للتحقق من صحة النموذج المقترح ، أجريت التجارب. تتطابق نتائج المحاكاة مع نتائج الجزء التجريبي. أدى استخدام الزعانف إلى تحسين انتقال الحرارة أثناء عملية ذوبان شمع البارافين وبالتالي تقليل وقت الانصهار عند استخدام نفس التدفق الحجمي (4 و 8 و 16) لتر / دقيقة على التوالي ، وبلغ إجمالي التحسين 29.68٪ و 36.97٪ و 48.7٪. بعد ذلك تم تحديد الفرق الأقصى لتحديد الفروق بين النتائج التجريبية والعددية لمعدلات تدفق HTF (4,8,16) لتر/دقيقة والتي كانت (4، 8، 9)٪، وبذلك كان الفرق الأقصى 9٪ لمعدل التدفق 16 لتر/دقيقة.



جمهورية العراق
وزارة التعليم العالي و البحث العلمي
جامعة كربلاء
كلية الهندسة
قسم الهندسة الميكانيكه

دراسة تأثير هندسة الزعانف المعدلة على أداء وحدة التخزين الحراري ثلاثية القنوات المربعة

رسالة مقدمة الى مجلس كلية الهندسة / جامعة كربلاء وهي جزء من متطلبات نيل درجة الماجستير في
علوم الهندسة الميكانيكية

المؤلف:

اسم الطالب

زينب عبد الكريم سالم

بإشراف :

اسماء المشرفين

ا. م.د. فرحان لفته رشيد

ا.د. محمد وهاب الجبوري